Spring 5-2010

Towards Multiplexed Electrogenerated Chemiluminescent Detection

Shijun Wang
University of Southern Mississippi

The University of Southern Mississippi

TOWARDS MULTIPLEXED ELECTROGENERATED CHEMILUMINESCENT DETECTION

by

Shijun Wang

Abstract of a Dissertation
Submitted to the Graduate School
of The University of Southern Mississippi
in Partial Fulfillment of the Requirements
for the Degree of Doctor of Philosophy

May 2010

ABSTRACT

TOWARD MULTIPLEXED

ELECTROGENERATED CHEMILUMINESCENT DETECTION

by Shijun Wang

May 2010

The main objective of this dissertation is to understand and study the principle of electrogenerated chemiluminescence (ECL) and its applications to detect biomolecules simultaneously. Four aspects of ECL were studied. In order to carry out multiplexed ECL detection, both classical and several novel ECL systems have been investigated.

In the first aspect, significant effect of chloride ions on the ECL behavior of the tris(2,2′-bipyridyl) ruthenium(II) ($Ru(bpy)_3^{2+}$)/tri-*n*-propylamine (TPrA) system at Au electrode was investigated. At low concentrations (e.g., $[Cl^-] < 5$ mM), the ECL was enhanced; at relatively high concentrations, however, the ECL intensity decreased with the increase of the $[Cl^-]$. At $[Cl^-] = 90$ mM, ~ 50% and 100% ECL inhibition was observed for the first and the second ECL wave, respectively. The electrogenerated chloroaurate anions ($AuCl_2^-$ and $AuCl_4^-$) which were verified using an electrochemical quartz-crystal microbalance (EQCM) method were found to be responsible for the ECL inhibition. This study suggests that care must be taken when Au working electrode is used for ECL studies in chloride-containing buffer solutions (widely used in DNA probes) and/or with the commonly used chloride-containing reference electrodes since in these cases the ECL behavior may significantly disagree with that obtained using other electrodes and reaction media.

In the second aspect, the electrochemical behavior of a trinuclear ruthenium(II)-containing complex, $[((phen)_2Ru(dpp))_2RhCl_2]^{5+}$ (where phen = 1,10-phenanthroline, dpp

= 2,3-bis-2-pyridylpyrazine), was studied in acetonitrile (MeCN) and aqueous solutions. In MeCN containing 0.10 M tetra-*n*-butylammonium perchlorate (TBAP), the complex displayed a reversible, overlapping $Ru^{II/III}$ redox process with $E_{1/2}$ = +1.21 V vs Ag/Ag^{+} (10 mM), an irreversible reduction of $Rh^{III/I}$ at -0.73 V vs Ag/Ag^{+}, and two quasi-reversible dpp/dpp^{-} couples with $E_{1/2}$ = -1.11 V and -1.36 V vs Ag/Ag^{+} at a Pt electrode with a scan rate of 50 mV s^{-1}. In 0.20 M Tris buffer solution (pH 7.4), an irreversible, overlapping $Ru^{II/III}$ oxidation at +1.48 V vs Ag/AgCl (3 M KCl), and an irreversible reduction of $Rh^{III/II}$ at -0.78 V vs Ag/AgCl were observed at a glassy carbon electrode with a scan rate of 50 mV/s.

Investigations on the ECL of the complex revealed that 2-(dibutylamino) ethanol (DBAE) was superior to TPrA as an ECL coreactant within their entire concentration range of 10-100 mM in MeCN, and in aqueous media, as low as 1.0 nM of the complex could be detected using TPrA coreactant ECL. A maximum ECL emission of 640 nm, which is about 55 nm blue-shifted with respect to its fluorescence peak, was observed in MeCN with DBAE as a coreactant.

Interactions of the complex with calf thymus DNA (ctDNA) were conducted with a flow-cell based QCM, and a binding constant of 2.5×10^{5} M^{-1} was calculated on the basis of the Langmuir isotherm equation.

In the third aspect, ECL behavior of core/shell semiconductor CdSe/ZnS nanocrystals coated with a carboxyl polymer layer (quantum dot, Qdot, or QDs) was studied in aqueous solutions using TPrA and DBAE as ECL coreactant. Upon the anodic potential scanning, strong ECL emissions were observed at glassy carbon (GC) electrode within the potential range of ~0.75 to 1.5 V vs Ag/AgCl (3.0 M KCl) when DBAE was

used as the coreactant. The ECL behavior of the Qdot was found to be strongly dependent on the types and concentrations of ECL coreactants as well as the nature of the working electrode. The ECL emission measured with the Qdot/DBAE/GC electrode system has a peak value of ~625 nm, which matched well with its fluorescence. The Qdot as a label for ECL-based C-reactive protein (CRP) immunoassays was realized by covalent binding of avidin on its surface, which allowed biotinalyted antibodies to be attached and interacted with antigens and the antibodies linked to micro-sized magnetic beads. The newly formed sandwich type aggregates were separated magnetically from the solution matrix, followed by the ECL generation in the presence of the coreactant DBAE. ECL experiments were carried out with a potential scan from 0 to 1.5 V vs Ag/AgCl at partially transparent Au/CD electrodes, and the integrated ECL intensity was found to be linearly proportional to the CRP concentration over the range of 1.0-10.0 μg/mL.

In the fourth aspect, the ECL behavior of $Ru(bpy)_3^{2+}$, 9,10-diphenylanthracene (DPA), and rubrene (RUB) with DBAE or TPrA as the coreactant was studied in acetonitrile solution. The ECL emission spectra of the mixed solution including the above three ECL labels were investigated. The ECL maximum emissions at ~440 nm for DPA, ~560 nm for RUB, and ~630 nm for $Ru(bpy)_3^{2+}$ were linearly proportional to the concentration of each individual ECL labels in mixed solutions, suggesting that multiplexing detection and quantification of biomolecules with ECL technology is feasible.

ACKNOWLEDGEMENTS

First of all, I would like to thank my advisor, Dr. Wujian Miao, for his guidance, patience, direction, encouragement, irrepressible enthusiasm, understanding and financial support during my tenure as a graduate student. I would also like to thank Dr. Douglas Masterson, Dr. Hans Schanz, Dr. Faqing Huang, Dr. Karl Wallace, and Dr. Milka Neshkova (Bulgarian Academy of Sciences) for their advice and support. I would like to thank Dr. Robert Bateman for his advice and leadership.

Secondly, I would also like to thank Dr. Alvin Holder for synthesizing the tri-nuclear compound $[((phen)_2Ru(dpp))_2RhCl_2]^{5+}$. I would like to thank Dr. Gordon Cannon for his guidance. I would like to thank my group members Tommie Pittman, Suman Parajuli, Jenifer Milam, Amma Harris and Tommy Maestri for their unlimited support and friendship.

Financially, I would like to thank USM Materials Research Science and Engineering Center (MRSEC), NSF-OISE0535467, and the Department of Chemistry and Biochemistry at USM for support.

Finally, many thanks go to my family, my grandmother, my mother, Guangzhi Wang, my father, Xuecheng Lu, my wife, Qun Zhu and my son, Ryan Wang for their selfless, long-term support and patience.

TABLE OF CONTENTS

LIST OF SCHEMES

Scheme

LIST OF ILLUSTRATIONS

Figure

LIST OF TABLES

Table

LIST OF EQUATIONS

Equation

4.5. $(CdSe/ZnS/PEG)^{\bullet+} + (CdSe/ZnS/PEG)^{\bullet-} \rightarrow (CdSe/ZnS/PEG)^{*} + CdSe/ZnS/PEG$ …..……..…...100

4.6. $(CdSe/ZnS/PEG)^{\bullet+} + DBAE^{\bullet} \rightarrow (CdSe/ZnS/PEG)^{*} + P1$……...……100

4.7a. $(CdSe/ZnS/PEG)^{*}_{well\text{-}passivated} \rightarrow CdSe/ZnS/PEG + h\nu\ (\sim 625\ nm)$ ……..….100

4.7b. $(CdSe/ZnS/PEG)^{*}_{partially\text{-}passivated} \rightarrow CdSe/ZnS/PEG + h\nu\ (\sim 695\ nm)$ ……...100

CHAPTER I

INTRODUCTION AND OVERVIEW OF ELECTROCHEMICAL TECHNIQUES

The main scope of this dissertation is to investigate some fundamental aspects of electrogenerated chemiluminescence (ECL) for both classical (e.g., $Ru(bpy)_3^{2+}$/TPrA system, where $Ru(bpy)_3^{2+}$ = tris(2,2′-bipyridyl) ruthenium (II) and TPrA = tri-*n*-propylamine) and newly developed (e.g., semiconductive nanoparticles or quantum dots) ECL systems so that simultaneous detection and quantification of trace amounts of multiple biomolecules may become feasible. In this chapter some of the most heavily used electrochemical techniques in our investigations as well as fundamental principles of ECL illustrated with several typical ECL systems are briefly reviewed. Other techniques (e.g., UV-Visible and fluorescence spectroscopy) that are prevalently used will be provided in the prospective chapters.

Electroanalytical Chemistry

Electroanalytical chemistry deals with the application of electrochemical techniques in the field of analytical chemistry. It often classified as a subdivision of analytical chemistry that investigates electrode processes focusing on properties of electrochemical analyses of interest rather than the electrode and solvent.[1] Electroanalytical chemistry utilizes the relationship between chemical phenomena which involve charge transfer (e.g., redox reactions, ion separation, etc.) and the electrical properties that accompany these phenomena for qualitative and quantitative analyses of the sample of interest. This relationship can be further broken down into various areas based on the type of measurement produced that are known as electroanalytical methods or techniques. A typical electroanalytical experiment can be conducted within an

electrochemical cell that contains a solution of the analyte in the presence of added electrolyte and a set of electrodes, namely the working, the reference, and the counter electrode.[2-4]

Electroanalytical Techniques

Cyclic Voltammetry

Cyclic voltammetry (CV) is a widely used and perhaps the most effective and versatile electroanalytical technique available for the mechanistic study of redox system that enables the electrode potential to be scanned at various scan rates in search of redox activity.[5-10] This simple technique provides useful qualitative data about redox reactions that can be easily obtained and interpreted. CV is often the first experiment performed in electroanlysis. CV consists of cycling the potential of an electrode, which is immersed in an unstirred solution, and measuring the resulting current. The potential of the working electrode is controlled versus a reference electrode such as a silver/silver chloride electrode ($Ag/AgCl/Cl^-$) or a saturated calomel electrode (SEC). Figure 1.1 shows a typical potential waveform for CV. The potential (E in volts (V)) is varied linearly from an initial potential $E_{initial}$ to a final potential E_{final} at a constant scan rate v ($= dE/dt$, where t is the time used); after the final potential is reached, the scan direction is then reversed and the same potential range is swept again in the opposite direction. A cyclic voltammogram is obtained by measuring the current at the working electrode during the potential scan. The current can be considered the response signal to the potential excitation signal. The voltammogram is a display of current (vertical axis) versus potential (horizontal axis). Because the potential varies linearly with time, the horizontal axis can also be thought of as a time axis.

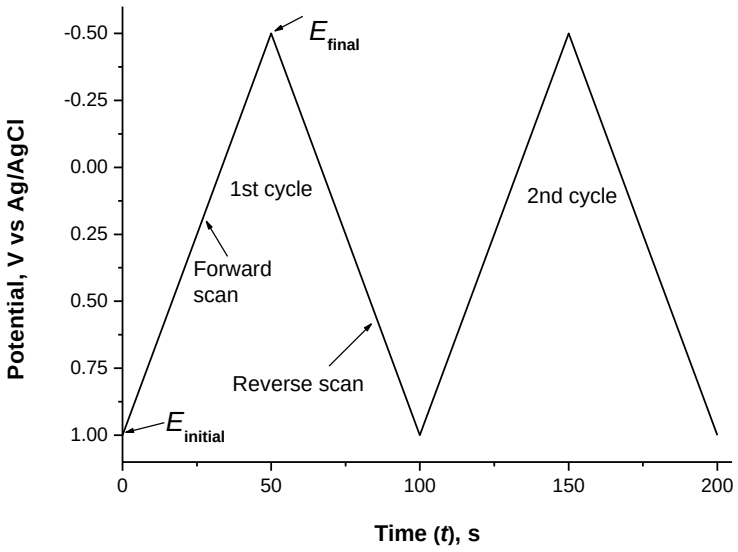

Figure 1.1. Cyclic voltammetric excitation signal used to obtain the voltammogram.

Figure 1.2 shows a typical cyclic voltammogram obtained from a solution of 6.0 mM $K_3[Fe(CN)_6]$ (electroactive species) and 1.0 M KNO_3 (supporting electrolyte) in an aqueous medium at a platinum working electrode. The potential excitation signal used to obtain this voltammogram is similar to that shown in Figure 1.1, but with a positive switching potential of 0.80 V vs. SCE and a negative switching potential of -0.15 V vs. SCE. The initial potential E_i of 0.80 V applied at point A is chosen to avoid any electrolysis of $Fe(CN)_6^{3-}$ when potential is applied to the electrode. As the potential is continually scanned in the negative direction indicated by the arrow, no current is observed prior to the potential of 0.40 V, indicating that no redox reaction occurs in this potential range. When the potential is sufficiently negative to reduce $Fe(CN)_6^{3-}$, reduction current is indicated at point B due to the electrode process

$$Fe(CN)_6^{3-} + e \rightarrow Fe(CN)_6^{4-} \qquad (1.1)$$

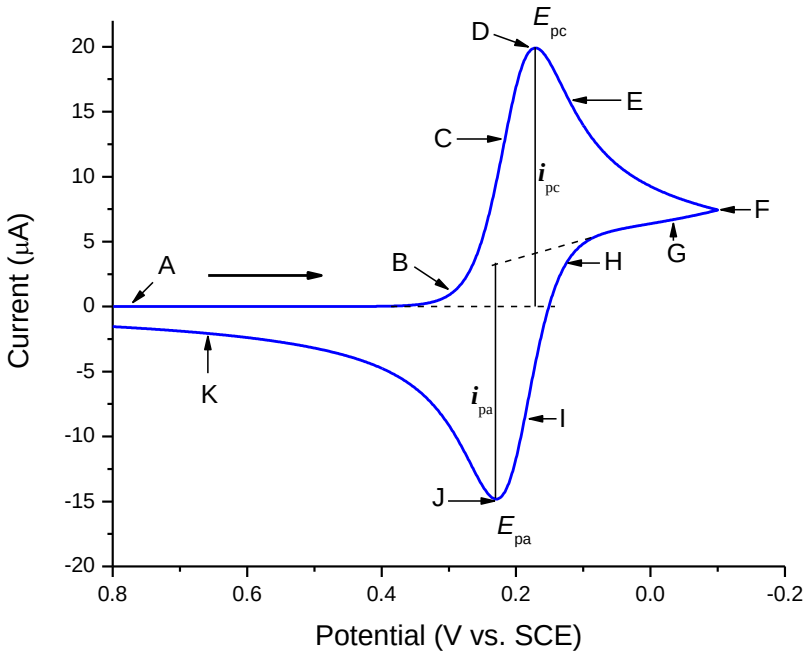

Figure 1.2. Cyclic voltammogram obtained from a solution containing 6.0 mM $K_3Fe(CN)_6$ and 1.0 M KNO_3 at a 2.54 mm-diameter Pt electrode with a scan rate of 50 mV/s.[11]

The cathodic current increases rapidly (B → D) until the concentration of $Fe(CN)_6^{3-}$ at the electrode surface is substantially diminished to zero, resulting in a maximum peak current (D). The current then decays (D → G) as the solution surrounding the electrode is depleted of $Fe(CN)_6^{3-}$ due to its electrolytic conversion to $Fe(CN)_6^{4-}$. The scan direction is switched to positive at -0.15 V (F) for the reverse scan. Even though scanning toward positive potential, the cathodic current continues because the potentials are even now negative enough to reduce $Fe(CN)_6^{3-}$. However, once the electrode surface has become an

adequately positive, the reduction of $Fe(CN)_6^{3-}$ ceases and the oxidation of $Fe(CN)_6^{4-}$ begins at the electrode surface.

$$Fe(CN)_6^{4-} - e \rightarrow Fe(CN)_6^{3-} \qquad (1.2)$$

This causes anodic current ($I \rightarrow K$). The anodic current rapidly increases until the surface concentration $Fe(CN)_6^{4-}$ is diminished, which is indicated by the peak current at J. The current then decays ($J \rightarrow K$) as the solution surrounding the electrode is depleted of $Fe(CN)_6^{4-}$. The first cycle is completed when the potential reaches +0.80 V.

A more detailed understanding can be gained by considering the Nernst equation and the changes in concentration that occur in solution adjacent to the electrode during electrolysis. The potential excitation signal exerts control of the ratio of $Fe(CN)_6^{3-}$ /$Fe(CN)_6^{4-}$ at the electrode surface as described by the Nernst equation for a reversible system.

$$E = E^{0'}_{Fe(CN)_6^{4-}/Fe(CN)_6^{3-}} + \frac{0.059}{1}\log\frac{[Fe(CN)_6^{3-}]}{[Fe(CN)_6^{4-}]} \quad \text{(in Volts at 25 °C)} \qquad (1.3)$$

where $E^{0\prime}$ is the formal reduction potential. The initial value of E_i is much more positive than $E^{0\prime}$ and sustains the ratio in which $Fe(CN)_6^{3-}$ would significantly be in the majority. However, while scanning toward the negative potential, conversion of $Fe(CN)_6^{3-}$ to $Fe(CN)_6^{4-}$ by reduction is mandatory for satisfaction of the Nernst equation. The logarithmic relationship between E and concentration ratio $[Fe(CN)_6^{3-}]/[Fe(CN)_6^{4-}]$ is reflected by a rapid rate of change in the region where $E = E^{0\prime}$ in which $[Fe(CN)_6^{3-}]/[Fe(CN)_6^{4-}]$ is equal to 1.

The important parameters of a cyclic voltammogram are magnitudes of the peak currents, i_{pa} and i_{pc}, and the potential at which the peaks occur, E_{pa} and E_{pc}. For a reversible system, the following equations are operative.

The formal potential ($E^{0\prime}$) is centered between the E_{pa} and $E_{pc.}$

$$E^{0'} = \frac{E_{pa} + E_{pc}}{2} \qquad (1.4)$$

The separation between the peak potential is provided by equation 1.5

$$\Delta E_p = E_{pa} - E_{pc} = \frac{0.057}{n} \qquad \text{(in V at 25 }^{\circ}\text{C)} \qquad (1.5)$$

where n is the number of electron transfer involved. For the reduction of $Fe(CN)_6^{3-}$ to $Fe(CN)_6^{4-}$, $n = 1$, thus, $\Delta E_p \approx 57$ mV is expected to be obtained.

The Randles-Sevick equation gives the reduction peak current for a reversible system.

$$i_p = (2.69 \times 10^5)\, n^{3/2} A D^{1/2} C v^{1/2} \qquad (1.6)$$

where n is the total number of electrons, A is the electrode surface area (cm^2), C is the concentration of the electractive species (mol/cm^3), D is the diffusion coefficient (cm^2/s), and v is the scan rate (V/s). Therefore, for a reversible process, $|i_{pc}|$ is proportional to the concentration, and the square root of the scan rate.

Chronoamperometry

Chronoamperometry (CA) is an electrochemical technique in which the potential of the working electrode is excited by a square-wave voltage signal, and the diffusion controlled current as the function of time is monitored during these processes. CA

experiments can be conducted either with single potential step, double potential step (Figure 1.3), or even multiple potential steps.

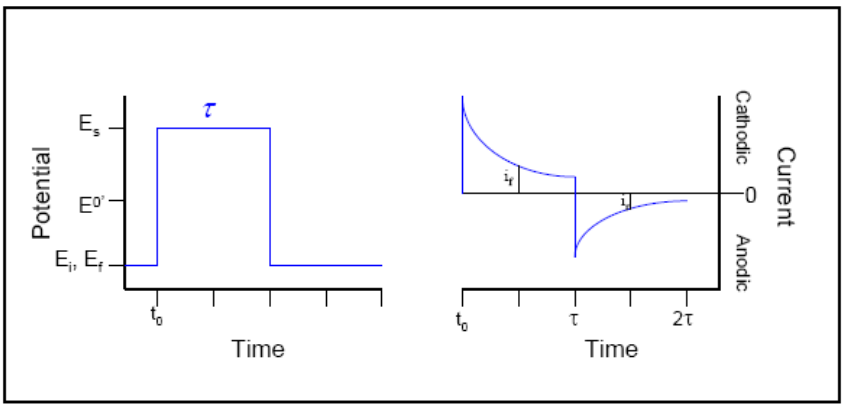

Figure 1.3. Double potential step chronoamperometry. (Left) the potential applied on the electrode, (right) the current response from the potential step.

In CA, the Cottrell equation (eq. (1.7)) is the fundamental law and the most useful equation. The equation describes the diffusion controlled current at any time (t) following a large forward potential step in a reversible redox reaction as a function of $t^{-1/2}$.

$$i_t = \frac{nFAC_o D_o^{1/2}}{\pi^{1/2} t^{1/2}} \qquad (1.7)$$

where n = stoichiometric number of electrons involved in the reaction; F = Faraday's constant (96,485 C/equivalent), A = electrode area (cm^2), C_o = concentration of electroactive species (mol/cm^3), and D_o = diffusion coefficient of the electroactive species (cm^2/s).

The charging current (i_c) which occurs during the charging process in the electrical double layer, contributes to the total observed current following a potential step. However, this charging current decays as a function of $1/t$ and is only significant during

the initial period following the step. Figure 1.3 shows a general principle of double potential step chronoamperometry, in which the potential step program is shown at left and the corresponding current at the electrode is displayed at right. The first potential step (or the forward potential step) starts at t_0 with a potential value of E_s and a duration of τ after the electrode is first held at an initial potential E_i. For the second potential step (or reverse potential step), the electrode potential is stepped from E_s down to a final potential E_f for a certain period of time. Generally, in a double potential step experiment, the final potential E_f is the same as E_i, and the two steps have the same time period.

As expected from the Cottrell equation, the observed current for the forward step decays as $t^{-1/2}$. A reversible system can be identified by comparing the reverse and forward current values measured at the same time interval following each respective potential step. The presence of chemical reaction(s) following electron transfer will generally result in ratios that deviate from this theoretical value.

CA could be used for the accurate measurement of an electrode area (A) by use of a well-defined redox couple (known n, C_o, and D_o). With a known electrode area, measurement of either n or D_o for an electroactive species is easily accomplished. As will be described in Chapter 2, CA can be also used to generate reduced and oxidized species from an ECL emitter within a short period of time so that the stability of the ECL emission over time can be monitored.

Electrogenerated Chemiluminescence

Electrogenerated chemiluminescence (also called electrochemiluminescence and abbreviated ECL) involves the formation of an excited state as a result of an energetic electron transfer between eletrochemically generated species, often radical ions, at the

surface of an electrode.[12-16] A classical ECL system would include two species A and D (A and D could be the same species) in the solution with supporting electrolyte, for example, phosphate buffer solution (PBS) in aqueous solution or tetra-*n*-butylammonium perchlorate (TBAP) in organic solution, in an electrochemical cell with a platinum working electrode. The first detailed ECL studies were published by Hercules and Bard et al. in the middle of 1960[17-19] After about forty-five years study, ECL has become a very powerful analytical technique and been widely used in the areas of, e.g., immunoassay, food and water testing, and biowarfare agent detection.[20,21] ECL has also been successfully employed as a detector of flow injection analysis (FIA), HPLC, capillary electrophoresis (CE), and micro total analysis (μTAS).[22] A considerable number of reviews on various topics of ECL are available in the literature,[22-51] in addition to a recently published ECL monograph.[20]

Apart from ECL, light could be generated through a number of other luminescent processes, which include photoluminescence (PL) and chemiluminescence (CL) (Table 1). ECL is a form of chemiluminescence, in which both ECL and CL involve the production of light by species that can undergo highly energetic electron-transfer reactions; however, luminescence in CL is initiated by the mixing of necessary reagents and often controlled by the careful manipulation of fluid flow. In contrast, luminescence in ECL is initiated and controlled by changing an electrode potential. Photoluminescence is a process in which a chemical compound absorbs a photon (electromagnetic radiation), thus the electron in the ground state jumps to a higher electronic energy state (an excited state), and then returns to the ground state accompanying a photon emission. The life time of excited state specie is extremely short, typically on the order of 10 nanoseconds.

Therefore, PL uses light to produce light, whereas ECL and CL result from electrochemical reactions at the electrode and in the solution, respectively.

Table 1

Photoluminescence, chemiluminescence, and electrogenerated chemiluminescence and their origins.

Type of luminescence	Way to form excited state	Refs
Photoluminescence	Electromagnetic radiation	52-54
Chemiluminescence	Chemical reactions	54-57
Electrogenerated chemiluminescence	Electrochemical reactions involving energetic electron-transfer processes	20,21,58

Fundamentals of Electrogenerated Chemiluminescence

Ion Annihilation ECL. In ion annihilation ECL, reactant R can be oxidized (eq. (1.8)) as well as reduced (eq. (1.9)) to form sufficiently stable radical cation ($R^{\bullet+}$) and anion ($R^{\bullet-}$) species. The produced radical ion is then annihilated by the oppositely charged radical ion, resulting in the formation of the excited state species (R*, eq. (1.10)) that emits light (*hv*, eq. (1.11)).

$$R - e \rightarrow R^{\bullet+} \quad (1.8)$$

$$R + e \rightarrow R^{\bullet-} \quad (1.9)$$

$$R^{\bullet+} + R^{\bullet-} \rightarrow R + R^* \quad (1.10)$$

$$R^* \rightarrow R + h\nu \quad (1.11)$$

Scheme 1.1 Ion Annihilation ECL

Based on the energy available in an ion annihilation, eq. (1.10), the produced R* could be either the lowest excited singlet state species (^{1}R*) or the triplet state species (^{3}R*). The energy available in eq. (1.10) can be calculated from the redox potentials for eq. (1.8) and eq. (1.9) as defined in eq. (1.12),[59]

$$-\Delta H_{ann} = E_p\,(R/R^{\bullet+}) - E_p\,(R/R^{\bullet-}) - 0.1\ eV \qquad (1.12)$$

where $-\Delta H_{ann}$ (in eV) is the enthalpy for ion annihilation, E_p is the peak potential for electrochemical oxidation or reduction, and 0.1 eV is the entropy approximation term ($T\Delta S$) at 25 °C. If the enthalpy ($-\Delta H_{ann}$) is larger than the energy (E_s) required to produce the lowest excited singlet state from the ground state, ^{1}R* maybe generated from eq. (1.10), and this system is called *the energy-sufficient system* or *the S-route*. A typical example of the energy-sufficient system is the $DPA^{\bullet+}$/ $DPA^{\bullet-}$ **(**DPA = 9,10-diphenylanthracene) system.[60,61]

S-route

$$R^{\bullet+} + R^{\bullet-} \rightarrow R + {}^1R^* \qquad (1.10a)$$

In contrast, if $-\Delta H_{ann}$ is smaller than E_s but larger than the triplet state energy (E_t), it is possibly to form ^{3}R*, and then ^{1}R* can be formed by the triplet-triplet annihilation (TTA) as shown in eq. (1.13). This is called *the energy-deficient system* or *the T-route*. Typical examples of the energy deficient system are $TMPD^{\bullet+}/DPA^{\bullet-}$ and $TMPD^{\bullet+}/AN^{\bullet-}$ (TMDP = N,N,N′,N′-tetramethyl-*p*-phenylenediamine and AN = anthracene).[61,62] The efficiency of direct emission from ^{3}R* is usually low in a solution phase because of the long radiative lifetime of ^{3}R* and its quenching by radical ions or other species, such as molecular oxygen.

T-route

$$R^{\bullet+} + R^{\bullet-} \rightarrow R + {}^3R^* \quad (1.10b)$$

$${}^3R^* + {}^3R^* \rightarrow R + {}^1R^* \quad (1.13)$$

If $-\Delta H_{ann}$ is at the edge of E_s, the T-route can contribute to the formation $^1R^*$ in addition to the S-route and it is called *the ST-route*. Although the T-route is inefficient in the presence of considerable S-route,[63-65] it is still possible for the ST-route to exist. A typical example is the rubrene anion-cation annihilation.

Coreactant ECL.[66] A coreactant is a species that forms a strongly reducing or oxidizing intermediate due to electrochemical oxidation or reduction, which can react with an oxidized or reduced ECL luminophore to generate excited states. The coreactant is useful especially when one of $R^{\bullet+}$ or $R^{\bullet-}$ is not stable enough for ECL reaction, or when the ECL solvent has a narrow potential window so that $R^{\bullet+}$ or $R^{\bullet-}$ cannot be formed. In an aqueous solvent, the coreactant is crucial because water has a narrow potential window (e.g., ~ -0.5 V to ~ +1.5 V vs SCE at Pt) and many radical ions of organic emitters are unstable in an aqueous solvent.

Advantages of coreactant ECL over ion annihilation ECL.

1. A coreactant can make ECL work even for some complexes that have only a electrochemical reduction or oxidation;
2. It is still possible to generate ECL by use of a coreactant even with solvents for ECL that have a narrow potential window;
3. A coreactant may produce more intense ECL when the annihilation reaction between oxidized and reduced species is not efficient.

Criteria for a good coreactant[66]. A number of factors could affect the ECL performance of a coreactant, which include:

1. Solubility. The coreactant should be reasonably soluble in the reaction media, because the ECL intensity is generally proportional to the concentration of the coreactants;

2. Stability. The intermediate species generated electrochemically and chemically should be sufficiently stable to allow appreciable reaction with the ECL precursor;

3. Electrochemical properties. The coreactant should be easily oxidized or reduced with the luminophore species at or near the electrode and undergo a rapid following chemical reaction to form an intermediate, which has a sufficiently reducing or oxidizing energy to react with the oxidized or reduced luminophore to form the excited state;

4. Kinetics. The reaction rate between the intermediate and the oxidized or reduced luminophore species should be fast;

5. Quenching effect. The coreactant and its redox products should not quench the emitter's luminescence;

6. ECL background. The coreactant itself should not give any ECL signal over the potential range scanned.

$Ru(bpy)_3^{2+}$/Oxalate ion ($C_2O_4^{2-}$) system. This was the first account of correactant ECL system reported in the literature by Bard's group in 1977,[67] and is a classical example of "oxidative-reduction" ECL. Scheme 1.2 presents the ECL mechanism of this system.[68]

$$Ru(bpy)_3^{2+} - e \rightarrow Ru(bpy)_3^{3+} \quad (1.14)$$

$$Ru(bpy)_3^{3+} + C_2O_4^{2-} \rightarrow Ru(bpy)_3^{2+} + C_2O_4^{\bullet-} \quad (1.15)$$

$$C_2O_4^{\bullet-} \rightarrow CO_2^{\bullet-} + CO_2 \quad (1.16)$$

$$Ru(bpy)_3^{3+} + CO_2^{\bullet-} \rightarrow Ru(bpy)_3^{2+*} + CO_2 \quad (1.17)$$

$$Ru(bpy)_3^{2+} + CO_2^{\bullet-} \rightarrow Ru(bpy)_3^{+} + CO_2 \quad (1.18)$$

$$Ru(bpy)_3^{3+} + Ru(bpy)_3^{+} \rightarrow Ru(bpy)_3^{2+*} + Ru(bpy)_3^{2+} \quad (1.19)$$

$$Ru(bpy)_3^{2+*} \rightarrow Ru(bpy)_3^{2+} + h\nu \quad (1.20)$$

Scheme 1.2 Proposed ECL mechanism of $Ru(bpy)_3^{2+}/C_2O_4^{2-}$ system.[69]

Firstly, the $Ru(bpy)_3^{2+}$ is oxidized at the electrode to the $Ru(bpy)_3^{3+}$. This species oxidized the oxalate ($C_2O_4^{2-}$) in the diffusion layer to form an oxalate radical anion ($C_2O_4^{\bullet-}$) which breaks down to form a highly reducing radical anion ($CO_2^{\bullet-}$, E^0 = -1.9 V vs. NHE [70]) and carbon dioxide. The $Ru(bpy)_3^{3+}$ reacts with $CO_2^{\bullet-}$ to the $Ru(bpy)_3^{2+*}$ excite state. And $CO_2^{\bullet-}$ reduces $Ru(bpy)_3^{2+}$ to form $Ru(bpy)_3^{+}$ that reacts with $Ru(bpy)_3^{3+}$ to generate the excited state $Ru(bpy)_3^{2+*}$, which emits light with λ_{max} ~620 nm.

$Ru(bpy)_3^{2+}$/peroxydisulphate ($S_2O_8^{2-}$) system. This was the first example of "reductive-oxidation" coreactant ECL system reported in the literature.[71,72] The MeCN-H_2O mixed solutions were used because $Ru(bpy)_3^{+}$ is unstable in aqueous solutions and $(NH_4)_2S_2O_8$ has a low solubility in MeCN solutions.[71] Scheme 1.3 summaries the possible pathways for the production of $Ru(bpy)_3^{2+}$* when $S_2O_8^{2-}$ is used as the coreactant, in which the strongly oxidizing intermediate $SO_4^{\bullet-}$, generated during reduction of $S_2O_8^{2-}$, has a redox potential of $E^0 \geq 3.15$ V vs. SCE.[73] $S_2O_8^{2-}$ anion was

reduced to $S_2O_8^{\bullet 3-}$ radical anion at the surface of the electrode; and $Ru(bpy)_3^{2+}$ was also reduced to $Ru(bpy)_3^{+}$ which reduce $S_2O_8^{2-}$ to form $S_2O_8^{\bullet 3-}$ radical anion. $S_2O_8^{\bullet 3-}$ broke down to form highly strong $SO_4^{\bullet}$ radical anion which reacted with respectively $Ru(bpy)_3^{+}$ and $Ru(bpy)_3^{2+}$ to form $Ru(bpy)_3^{2+}$*cation radical which emitted the light and $Ru(bpy)_3^{3+}$. $Ru(bpy)_3^{3+}$ could also react with $Ru(bpy)_3^{+}$ to $Ru(bpy)_3^{2+}$*.

$$S_2O_8^{2-} + e \rightarrow S_2O_8^{\bullet 3-} \quad (1.21)$$

$$Ru(bpy)_3^{2+} + e \rightarrow Ru(bpy)_3^{+} \quad (1.22)$$

$$Ru(bpy)_3^{+} + S_2O_8^{2-} \rightarrow Ru(bpy)_3^{2+} + S_2O_8^{\bullet 3-} \quad (1.23)$$

$$S_2O_8^{\bullet 3-} \rightarrow SO_4^{2-} + SO_4^{\bullet -} \quad (1.24)$$

$$Ru(bpy)_3^{+} + SO_4^{\bullet -} \rightarrow Ru(bpy)_3^{2+*} + SO_4^{2-} \quad (1.25)$$

$$Ru(bpy)_3^{2+} + SO_4^{\bullet -} \rightarrow Ru(bpy)_3^{3+} + SO_4^{2-} \quad (1.26)$$

$$Ru(bpy)_3^{3+} + Ru(bpy)_3^{+} \rightarrow Ru(bpy)_3^{2+*} + Ru(bpy)_3^{2+} \quad (1.27)$$

Scheme 1.3 ECL mechanism of $Ru(bpy)_3^{2+}/S_2O_8^{2-}$system.[69]

$Ru(bpy)_3^{2+}$/Tri-n-propylamine (TPrA) system. Although a number of coreactants, such as oxalate,[67] pursulfate,[71] and hydrogen peroxide,[73] have been studied, the majority of ECL applications reported involve $Ru(bpy)_3^{2+}$ or its derivatives as an emitter (or label) and TPrA as a coreactant because the $Ru(bpy)_3^{2+}$/TPrA system exhibits the highest ECL efficiency known so far. The ECL mechanism of $Ru(bpy)_3^{2+}$/TPrA system is intricate and has been investigated by many workers.[12-16,74] When a low concentration of $Ru(bpy)_3^{2+}$ (e.g., in nM-μM levels) is used, the ECL emission of this system shows two distinct waves as a function of applied potential at glassy carbon (GC) or gold (Au) electrode

(Figure 1.4).[74] Scheme 1.4 describes the mechanism of the first ECL wave, where cation radical species $TPrA^{\bullet+}$ formed during TPrA oxidation which is a sufficiently stable intermediate with a half-time of ~0.2 ms that it can oxidize $Ru(bpy)_3^{+}$ (formed from the reduction of $Ru(bpy)_3^{2+}$ by $TPrA^{\bullet}$ free radical) to give $Ru(bpy)_3^{2+}*$.[74,75]

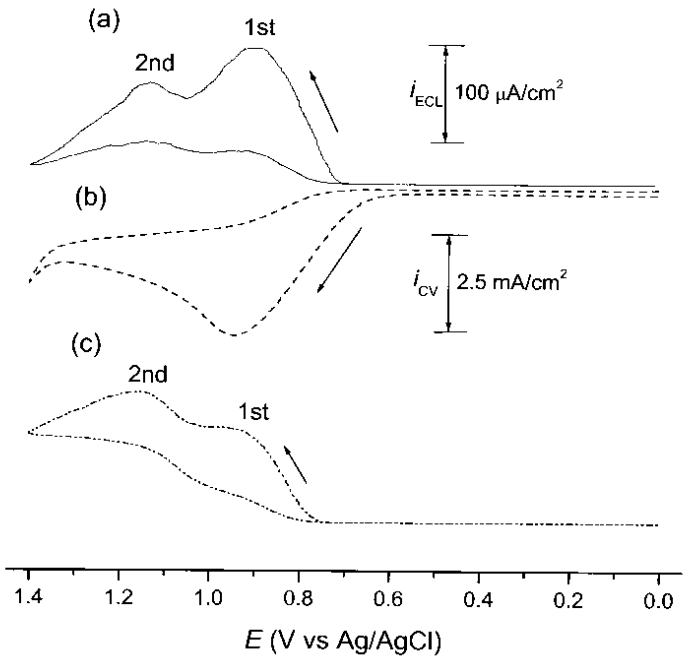

Figure 1.4 (a) ECL and (b) cyclic voltammogram of 1.0 nM $Ru(bpy)_3^{2+}$ in the presence of 0.10 M TPrA with 0.10 M Tris/0.10 M $LiClO_4$ buffer (pH = 8) at a 3 mm diameter glassy carbon electrode at a scan rate of 50 mV/s. (c) As (a) but with 1.0 μM $Ru(bpy)_3^{2+}$. The ECL intensity scale is given for (c) and should be multiplied by 100 for (a).[74]

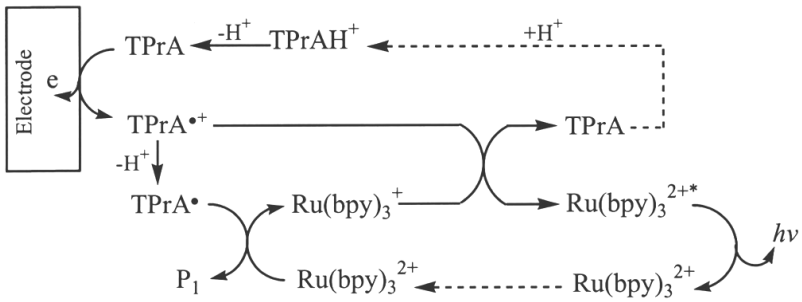

[where $TPrA^{\bullet+} = (CH_3CH_2CH_2)_3N^{\bullet+}$, $TPrAH^+ = Pr_3NH^+$, $TPrA^{\bullet} = Pr_2NC^{\bullet}HCH_2CH_3$, $P_1 = Pr_2N^+C{=}HCH_2CH_3$]

Scheme 1.4 Mechanism of the first ECL wave for the $Ru(bpy)_3^{2+}$/TPrA system.[74]

The mechanism of the second ECL wave follows the classic "oxidative-reduction" coreactant mechanism, where oxidation of TPrA generates a strongly reducing species $TPrA^{\bullet}$ free radical. This oxidation can occur via a "catalytic route" where electrogenerated $Ru(bpy)_3^{3+}$ reacts with TPrA as well as by direct reaction of TPrA at the electrode described by both Scheme 1.5 and Scheme 1.6:

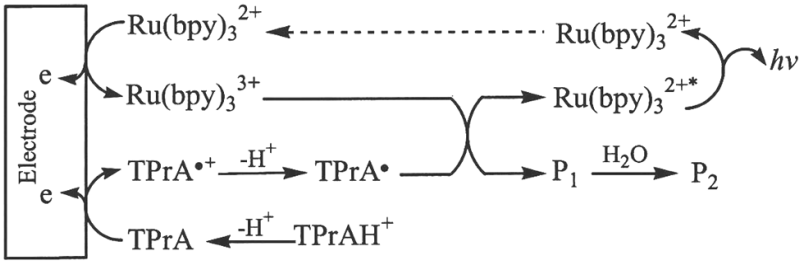

[where $P_2 = Pr_2NH + CH_3CH_2CHO$]

Scheme 1.5 Mechanism of the second ECL wave for the $Ru(bpy)_3^{2+}$/TPrA system.[74]

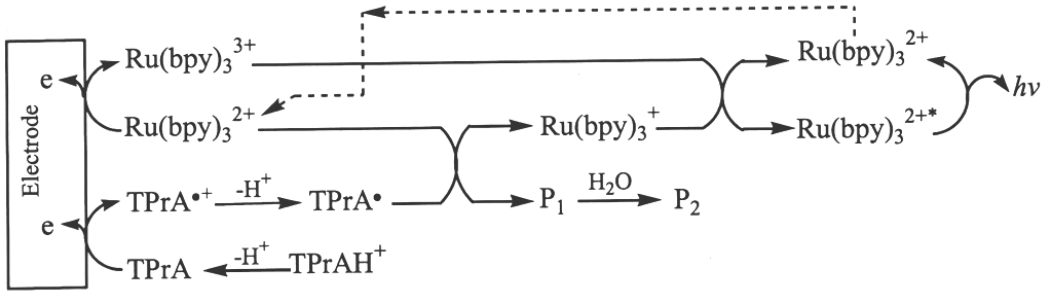

Scheme 1.6 Mechanism of the second ECL wave for the $Ru(bpy)_3^{2+}$/TPrA system.[74]

Electrochemical Quartz Crystal Microbalance (EQCM)

EQCM is a technique that combines electrochemistry and the quartz crystal microbalance (QCM). QCM is a very sensitive device, allowing measurement of mass changes in the order of nanograms, which correspond to a small fraction of a monolayer of an absorbed or dissolved species. It comprises a thin quartz crystal sandwiched between two metal electrodes that establish an alternating electric field across the crystal.

This type of phenomenon is better known as the piezoelectric effect which was first discovered in 1880 by Jacques and Pierre Curie when a mechanical stress was applied to the surfaces of various crystals including quartz.[75] For the QCM, the piezoelectric effect causes a vibrational motion of the crystal at its resonant frequency.

In many cases, such as in solid state voltammetry and in processes involving species adsorption or desorption, mass changes occur at the electrode surface as oxidation and reduction occur. The QCM utilizes the piezoelectric[76-79] qualities of quartz crystals to measure changes in the attached surface mass. Figure 1.5 shows a schematic representation of EQCM instrumentation. In the electrochemical application, the quartz crystal is often coated with a gold disc on both sides. One side is exposed to the solution in the electrochemical cell, while the other is exposed to air. Voltammetry is carried out using the gold disc exposed to solution as the working electrode. This EQCM setup allows the simultaneous measurement of mass (frequency) changes along with the electrochemical current at the electrode. The first in situ application of the QCM to electrochemistry was reported by Nomura et al. for Cu(II)[80] and Ag(I)[81] electrodeposition.

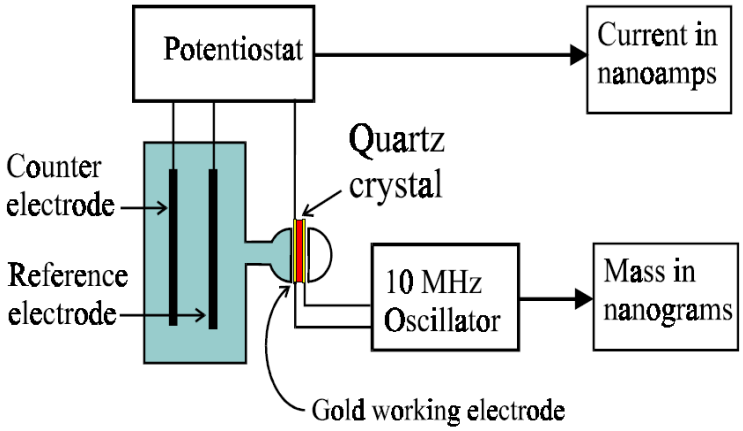

Figure 1.5. Schematic diagram of electrochemical quartz crystal microbalance instrumentation.[82]

The inverse piezoelectric effect is the key to the operation of the QCM. The application of an electric field to the quartz crystal causes a shear deformation (strain) as shown in Figure 1.6a. This deformation arises from the realigning of dipoles in the crystal structure with the applied electric field. This deformation is typically 10-100 nm, for AT-cut crystals operating in the frequency range of 1-10 MHz.[83] Figure 1.6b, illustrates a side 2D view of the shear deformation.

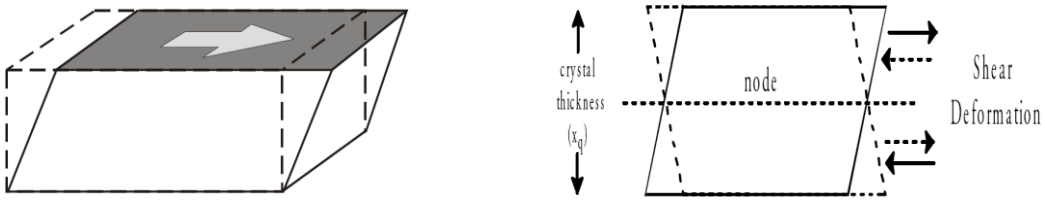

(a) (b)

Figure 1.6. (a) Illustration of shear deformation. (b) Side view of crystal oscillating in an alternating electric field.[82]

Sauerbrey was the first to recognize the potential usefulness of the QCM technology and demonstrate the extremely sensitive nature of these piezoelectric devices towards mass changes at the surface of QCM electrodes.[83] The results of his work are embodied in the Sauerbrey equation, which relates the mass change per unit area at the QCM electrode surface to the observed change in oscillation frequency of the crystal:

$$\Delta f = -C_f \bullet \Delta m \qquad (1.28)$$

Δf = the observed frequency change in Hz,

Δm = the change in mass per unit area in g/cm^2,

C_f = the sensitivity factor for the crystal (56.6 Hz μg^{-1} cm^2 for a 5 MHz AT-cut quartz crystal at room temperature).

The Sauerbrey equation relies on a linear sensitivity factor, C_f, which is a fundamental property of the QCM crystal. Thus, *in theory*, the QCM mass sensor does not require calibration. However, it must be kept in mind, that the Sauerbrey equation is only strictly applicable to uniform, rigid, thin-film deposits. For many years, QCMs were regarded as just gas-phase mass detectors. Recently their application has been extended since scientists realized that they can be operated in contact with liquids and viscoelastic deposits. In this case, both resonance frequency and series resonance resistance of the quartz oscillator are important to completely characterize the material in contact with the crystal electrode.

References

1. Plambeck, J. A. *Electroanalytical Chemistry: Basic Principles and Applications* (John Wiley and Sons, New York, 1982).

2. Koryta, J. & Dvorak, J. *Principles of Electrochemistry* (John Wiley and Sons, New York, 1987).

3. Bard, A. J. & Faulkner, L. R. *Electrochemical Methods: Fundamentals and Applications* (John Wiley & Sons, Inc., New York, 2001).

4. Sawyer, D. T., Sobkowiak, A., Roberts, J. J. L. & Editors. *Electrochemistry for Chemists: Second Edition* (John Wiley and Sons, New York, 1995).

5. Arrigan, D. W. Voltammetric determination of trace metals and organics after accumulation at modified electrodes. *Analyst* **119**, 1953-66 (1994).

6. Dong, S. & Wang, Y. The application of chemically modified electrodes in analytical chemistry. *Electroanalysis* **1**, 99-106 (1989).

7. Kalcher, K. Chemically modified carbon paste electrodes in voltammetric analysis. *Electroanalysis* **2**, 419-33 (1990).

8. Kalcher, K., Kauffmann, J. M., Wang, J., Svancara, I., Vytras, K., Neuhold, C. & Yang, Z. Sensors based on carbon paste in electrochemical analysis: a review with particular emphasis on the period 1990-1993. *Electroanalysis* **7**, 5-22 (1995).

9. Walcarius, A. Zeolite-modified electrodes. Analytical applications and prospects. *Electroanalysis* **8**, 971-986 (1996).

10. Walcarius, A., Despas, C., Trens, P., Hudson, M. J. & Bessiere, J. Voltammetric in situ investigation of a MCM-41-modified carbon paste electrode - a new sensor. *J. Electroanal. Chem.* **453**, 249-252 (1998).

11. Heineman, W. R. & Kissinger, P. T. Cyclic voltammetry: the electrochemical equivalent of spectroscopy. *Curr. Sep.* **9**, 15-18 (1989).

12. He, L., Cox, K. A. & Danielson, N. D. Chemiluminescence detection of amino acids, peptides, and proteins using tris(2,2'-bipyridine)ruthenium(III). *Anal. Lett.* **23**, 195-210 (1990).

13. Leland, J. K. & Powell, M. J. Electrogenerated chemiluminescence: An oxidative-reduction type ECL reaction sequence using tripropyl amine. *J. Electrochem. Soc.* **137**, 3127-31 (1990).

14. Noffsinger, J. B. & Danielson, N. D. Generation of chemiluminescence upon reaction of aliphatic amines with tris(2,2'-bipyridine)ruthenium(III). *Anal. Chem.* **59**, 865-8 (1987).

15. Zu, Y. & Bard, A. J. Electrogenerated Chemiluminescence. 66. The Role of Direct Coreactant Oxidation in the Ruthenium Tris(2,2')bipyridyl/Tripropylamine System and the Effect of Halide Ions on the Emission Intensity. *Anal. Chem.* **72**, 3223-3232 (2000).

16. Kanoufi, F., Zu, Y. & Bard, A. J. Homogeneous Oxidation of Trialkylamines by Metal Complexes and Its Impact on Electrogenerated Chemiluminescence in the Trialkylamine/$Ru(bpy)_3^{2+}$ System. *J. Phys. Chem. B* **105**, 210-216 (2001).

17. Santhanam, K. S. V. & Bard, A. J. Chemiluminescence of electrogenerated 9,10-diphenylanthracene anion radical. *J. Am. Chem. Soc.* **87**, 139-140 (1965).

18. Hercules, D. M. Chemiluminescence resulting from electrochemically generated species. *Science* **145**, 808-9 (1964).

19. Visco, R. E. & Chandross, E. A. Electroluminescence in solutions of aromatic hydrocarbons. *J. Am. Chem. Soc.* **86**, 5350-1 (1964).

20. Bard, A. J. (ed.) *Electrogenerated Chemiluminescence* (Marcel Dekker, Inc., New York, 2004).

21. Miao, W. Electrogenerated Chemiluminescence and Its Biorelated Applications. *Chem. Rev.* **108**, 2506-2553 (2008).

22. Yin, X.-B., Dong, S. & Wang, E. Analytical applications of the electrochemiluminescence of tris(2,2'-bipyridyl) ruthenium and its derivatives. *TrAC, Trends in Anal. Chem.* **23**, 432-441 (2004).

23. Andersson, A.-M. & Schmehl, R. H. Sensors based on electrogenerated chemiluminescence. *Mol. Supramol. Photochem.* **7**, 153-187 (2001).

24. Andersson, A.-M. & Schmehl, R. H. Radiative charge recombination and electrochemiluminescence, in *Electron Transfer in Chemistry* (ed. Balzani, V.), 312-341 (Wiley-VCH Verlag GmbH, Weinheim, Germany, 2001).

25. Anon. Electrochemiluminescence - improving the performance of immunoassays. *Indian J. Clin. Biochem.* **13**, 129-132 (1998).

26. Armstrong, N. R., Wightman, R. M. & Gross, E. M. Light-emitting electrochemical processes. *Annu. Rev. Phys. Chem.* **52**, 391-422 (2001).

27. Balzani, V. & Juris, A. Photochemistry and photophysics of Ru(II)-polypyridine complexes in the Bologna group. From early studies to recent developments. *Coord. Chem. Rev.* **211**, 97-115 (2001).

28. Bard, A. J. & Fan, F.-R. F. Electrochemical Detection of Single Molecules. *Acc. Chem. Res.* **29**, 572-578 (1996).

29. Beier, R. C. & Stanker, L. H. Application of immunoassay for detection of antibiotics in foods and feed: a review. *Recent Res. Develop. Agri. Food Chem.* **4**, 59-93 (2000).

30. Bolletta, F. & Bonafede, S. Chemiluminescence and electrochemiluminescence of coordination compounds. *Pure Appl. Chem.* **58**, 1229-32 (1986).

31. Fahnrich, K. A., Pravda, M. & Guilbault, G. G. Recent applications of electrogenerated chemiluminescence in chemical analysis. *Talanta* **54**, 531-559 (2001).

32. Gerardi, R. D., Barnett, N. W. & Lewis, A. W. Analytical Apllications of tris(2,2'--bipyridyl)ruthenium (III) as a Chemiluminescenct Reagent. *Anal. Chim. Acta* **378**, 1-41 (1999).

33. Gonzalez Velasco, J. Electroluminescence. *Electroanalysis* **3**, 261-71 (1991).

34. Gonzalez Velasco, J. Electrogenerated chemiluminescence. *Bull. Electrochem.* **10**, 29-38 (1994).

35. Greenway, G. M. Analytical applications of electrogenerated chemiluminescence. *TrAC, Trends in Anal. Chem.* **9**, 200-3 (1990).

36. Kapturkiewicz, A. Marcus theory in the qualitative and quantitative description of electrochemiluminescence phenomena. *Adv. Electrochem. Sci. Eng.* **5**, 1-60 (1997).

37. Kissinger, P. T. Electrochemical detection in bioanalysis. *J. Pharm. Biomed. Anal.* **14**, 871-880 (1996).

38. Knight, A. W. A review of recent trends in analytical applications of electrogenerated chemiluminescence. *TrAC, Trends in Anal. Chem.* **18**, 47-62 (1999).

39. Knight, A. W. & Greenway, G. M. occurrence, mechanisms and analytical applications of electrogenerated chemiluminescence. A review. *Analyst* **119**, 879-90 (1994).

40. Knight, A. W. & Greenway, G. M. Relationship between structural attributes and observed electrogenerated chemiluminescence (ECL) activity of tertiary amines as potential analytes for the tris(2,2-bipyridine)ruthenium(II) ECL reaction - a review. *Analyst* **121**, 101R-106R (1996).

41. Kukoba, A. V., Bykh, A. I. & Svir, I. B. Analytical applications of electrochemiluminescence: an overview. *Fresenius J. Anal. Chem.* **368**, 439-442 (2000).

42. Kulmala, S. & Suomi, J. Current status of modern analytical luminescence methods. *Anal. Chim. Acta* **500**, 21-69 (2003).

43. Lee, W. Y. Tris-(2,2'-bipyridyl)ruthenium(II) electrogenerated chemiluminescence in analytical science. *Mikrochim. Acta* **127**, 19-39 (1997).

44. Mitschke, U. & Bauerle, P. The electroluminescence of organic materials. *J. Mater. Chem.* **10**, 1471-1507 (2000).

45. Nabi, A., Yaqoob, M. & Anwar, M. Chemiluminescence and bioluminescence monitoring. A flow-injection approach. *Lab. Rob. Autom.* **11**, 91-96 (1999).

46. Nieman, T. A. Detection based on solution-phase chemiluminescence systems, in *Chemiluminescence and Photochemical Reaction Detection in Chromatography* (ed. Birks, J. W.), 99-123, Chapter 9 (VCH, New York, NY, 1989).

47. Richter, M. M. Electrochemiluminescence, in *Optical Biosensors: Present and Future* (eds. Ligler, F. S. & Taitt, C. A. R.), 173-205 (Elsevier, New York, 2002).

48. Richter, M. M. Electrochemiluminescence (ECL). *Chem. Rev.* **104**, 3003-3036 (2004).

49. Tortorello, M. L. & Stewart, D. An overview of methods for identification of E. coli O157:H7, in *New Techniques in the Analysis of Foods* (eds. Tunick, M. H., Fratamico, P. M. & Palumbo, S. A.), 91-102 (American Chemical Society, 1998).

50. Zaleski, J. M., Turro, C., Mussell, R. D. & Nocera, D. G. Electron transfer reactions of geminate pairs at high exergonicities. *Coord. Chem. Rev.* **132**, 249-58 (1994).

51. Zhou, M., Heinze, J., Borgwarth, K. & Grover, C. P. Direct voltammetric evidence for a reducing agent generated from the electrochemical oxidation of tripropylamine for electrochemiluminescence of ruthenium tris(bipyridine) complexes? *ChemPhysChem* **4**, 1241-1243 (2003).

52. Agbaria, R. A., Oldham, P. B., McCarroll, M., McGown, L. B. & Warner, I. M. Molecular Fluorescence, Phosphorescence, and Chemiluminescence Spectrometry. *Anal. Chem.* **74**, 3952-3962 (2002).

53. Oldham, P. B., McCarroll, M. E., McGown, L. B. & Warner, I. M. Molecular fluorescence, phosphorescence, and chemiluminescence spectrometry. *Anal. Chem.* **72**, 197R-209R (2000).

54. Powe, A. M., Fletcher, K. A., St. Luce, N. N., Lowry, M., Neal, S., McCarroll, M. E., Oldham, P. B., McGown, L. B. & Warner, I. M. Molecular Fluorescence, Phosphorescence, and Chemiluminescence Spectrometry. *Anal. Chem.* **76**, 4614-4634 (2004).

55. Gubitz, G., Schmid, M. G., Silviaeh, H. & Aboul-Enein, H. Y. Chemiluminescence flow-injection immunoassays. *Crit. Rev. Anal. Chem.* **31**, 167-174 (2001).

56. Roda, A., Guardigli, M., Michelini, E., Mirasoli, M. & Pasini, P. Analytical bioluminescence and chemiluminescence. *Anal. Chem.* **75**, 462A-470A (2003).

57. Kuyper, C. & Milofsky, R. Recent developments in chemiluminescence and photochemical reaction detection for capillary electrophoresis. *TrAC, Trends in Anal. Chem.* **20**, 232-240 (2001).

58. Richter, M. M. Electrochemiluminescence (ECL). *Chem. Rev.* **104**, 3003-3036 (2004).

59. Miao, W. Electrogenerated Chemiluminescence, in *Handbook of Electrochemistry, Chapter 13 Electrogenerated Chemiluminescence* (ed. Zoski, C. G.), (Elsevier, HR Amsterdam, 2006).

60. Bezman, R. & Faulkner, L. R. Mechanisms of chemiluminescent electron-transfer reactions. III. Theoretical and practical considerations for measurements of the efficiencies of chemiluminescent electron-transfer reactions. *J. Am. Chem. Soc.* **94**, 3699-707 (1972).

61. Faulkner, L. R., Tachikawa, H. & Bard, A. J. Electrogenerated chemiluminescence. VII. Influence of an external magnetic field on luminescence intensity. *J. Am. Chem. Soc.* **94**, 691-9 (1972).

62. Faulkner, L. R. & Bard, A. J. Electrogenerated chemiluminescence. IV. Magnetic field effects on the electrogenerated chemiluminescence of some anthracenes. *J. Am. Chem. Soc.* **91**, 209-10 (1969).

63. Bezman, R. & Faulkner, L. R. Mechanisms of chemiluminescent electron-transfer reactions. IV. Absolute measurements of 9,10-diphenylanthracene luminescence in N,N-dimethylformamide. *J. Am. Chem. Soc.* **94**, 6317-23 (1972).

64. Bezman, R. & Faulkner, L. R. Mechanisms of chemiluminescent electron-transfer reactions. V. Absolute measurements of rubrene luminescence in benzonitrile and N,N-dimethylformamide. *J. Am. Chem. Soc.* **94**, 6324-30 (1972).

65. Bezman, R. & Faulkner, L. R. Mechanisms of chemiluminescent electron-transfer reactions. VI. Absolute measurements of luminescence from the fluoranthene-10-methylphenothiazine system in N,N-dimethylformamide. *J. Am. Chem. Soc.* **94**, 6331-7 (1972).

66. Miao, W. & Choi, J.-P. Coreactants, in *Electrogenerated Chemiluminescence* (ed. Bard, A. J.), 213-272, Chapter 5 (Marcel Dekker, Inc., New York, 2004).

67. Chang, M.-M., Saji, T. & Bard, A. J. Electrogenerated chemiluminescence. 30. Electrochemical oxidation of oxalate ion in the presence of luminescers in acetonitrile solutions. *J. Am. Chem. Soc.* **99**, 5399-403 (1977).

68. Rubinstein, I. & Bard, A. J. Electrogenerated chemiluminescence. 37. Aqueous ecl systems based on tris(2,2'-bipyridine)ruthenium(2+) and oxalate or organic acids. *J. Am. Chem. Soc.* **103**, 512-16 (1981).

69. Miao, W. & Choi, J.-P. Coreactants, in *Electrogenerated Chemiluminescence* (ed. Bard, A. J.), Chapter 5--Coreactants (Marcel Dekker, Inc., New York, 2004).

70. Butler, J. & Henglein, A. Elementary reactions of the reduction of thallium(1+) in aqueous solution. *Radiat. Phy. Chem.* **15**, 603-12 (1980).

71. White, H. S. & Bard, A. J. Electrogenerated chemiluminescence. 41. Electrogenerated chemiluminescence and chemiluminescence of the tris(2,2'-bipyridine)ruthenium(2+)-peroxydisulfate(2-) system in acetonitrile-water solutions. *J. Am. Chem. Soc.***104**, 6891-5 (1982).

72. Bolletta, F., Ciano, M., Balzani, V. & Serpone, N. Polypyridine transition metal complexes as light emission sensitizers in the electrochemical reduction of the persulfate ion. *Inorg, Chim. Acta* **62**, 207-13 (1982).

73. Memming, R. Mechanism of the electrochemical reduction of persulfates and hydrogen peroxide. *J. Electrochem. Soc.* **116**, 785-90 (1969).

74. Miao, W., Choi, J.-P. & Bard, A. J. Electrogenerated Chemiluminescence 69: The Tris(2,2'-bipyridine)ruthenium(II), ($Ru(bpy)_3^{2+}$)/Tri-n-propylamine (TPrA) System Revisited-A New Route Involving $TPrA^{\cdot+}$ Cation Radicals. *J. Am. Chem. Soc.* **124**, 14478-14485 (2002).

75. Buttry, D. A. & Ward, M. D. Measurement of interfacial processes at electrode surfaces with the electrochemical quartz crystal microbalance. *Chem. Rev.* **92**, 1355-79 (1992).

76. Callister, W. D. *Materials Science and Engineering: An Introduction. Second Edition* (John Wiley and Sons, Brisbane, 1985).

77. Bottcher, C. J. F. *Theory of Electric Polarisation* (John Wiley and Sons, Brisbane, 1952).

78. Ruoff, A. L. *Materials Science* (Prentice-Hall, New Jersey, 1973).

79. Bunget, I. & Popescu, M. *Materials Science Monographs, Vol. 19: Physics of Solid Dielectrics* (1984).

80. Nomura, T., Nagamune, T., Izutsu, K. & West, T. S. New electrolytic method of metal-ion analysis with a piezoelectric quartz crystal and its application to the determination of minute amounts of copper(II). *Bunseki Kagaku* **30**, 494-9 (1981).

81. Nomura, T. & Iijima, M. Electrolytic determination of nanomolar concentrations of silver in solution with a piezoelectric quartz crystal. *Anal. Chim. Acta* **131**, 97-102 (1981).

82. Snook, G.*Investigation of Solid-State Reactions by Electrochemical and Quartz Crystal Microbalance Measurements*. Monash University (Melbounre, 2000) PhD thesis.

83. Sauerbrey, G. The use of quartz oscillators for weighing thin layers and for microweighing. *Zeitschrift fuer Physik* **155**, 206-22 (1959).

CHAPTER II

EQCM STUDY OF THE ECL QUENCHING OF THE TRIS (2,2′-BIPYRIDYL)RUTHENIUM (II)/TRIS-*n*-PROPYLAMINE SYSTEM AT AN Au ELECTRODE IN THE PRESENCE OF CHLORIDE IONS*

Introduction

Since the first report of the electrogenerated chemiluminescence (ECL) of the ruthenium(II) tris(2,2′-bipyridine) ($Ru(bpy)_3^{2+}$)/tri-*n*-propylamine (TPrA) system in 1990,[1] a large number of fundamental studies and bio-related applications involving the $Ru(bpy)_3^{2+}$ (or its derivatives) as ECL emitting species or labels and TPrA as a coreactant have been published.[2-4] This system has been demonstrated to be the most efficient ECL system known so far, and forms the basis of commercial systems for flow-cell bead-based and multi-spot plate-based immunoassay and DNA analysis.[5] Many efforts have been made in investigating the ECL mechanism of the $Ru(bpy)_3^{2+}$ (or its derivatives)/TPrA (or its analogues) system,[6] so that new ECL labels and coreactants could be designed and the sensitivity and the reproducibility could be improved. Thus, it has been reported that when relatively low concentrations of $Ru(bpy)_3^{2+}$ (in μM levels) are used, two ECL waves appeared (i.e., at ~0.90 and ~1.10 V vs Ag/AgCl, respectively) at a glassy carbon (GC) and a gold (Au) electrode upon the anodic potential scanning in the presence of phosphate buffered TPrA solution.[7-10] The modification of the working electrode by increasing its surface hydrophobicity, hence promoting the direct oxidation of TPrA, has led to significant enhancement in ECL intensity.[11-13] Although GC, Au and Pt electrodes have been extensively used in solution-phase ECL studies, for surface-confined

* Part of the results presented in this chapter have been published: Wang, S., Neshkova, M. T. & Miao, W. *Electrochim. Acta* **53**, 7661-7667 (2008).

immunoassays and DNA probes, Au working electrodes have been predominately used for the immobilization of biomolecules via a thiol self-assembled monolayer and the ECL detection is often carried out in a buffered TPrA solution containing chloride ions (e.g., 0.10 M Tris–HCl–0.10 M $LiClO_4$ and 0.10 M phosphate buffered saline (PBS) that contains 0.15 M NaCl).[14] Unexpectedly, in such cases, only the first ECL wave at ~0.90 V vs Ag/AgCl was observed and the second wave was completely inhibited.[14] Further understanding of the ECL inhibition mechanism involving Cl^- and gold seems fundamental, thus providing with technical know-how on ultrasensitive ECL-based biosensors construction.

The present chapter presents studies of the chloride ions inhibitive effect on the ECL behavior of the $Ru(bpy)_3^{2+}$/TPrA system at a Au electrode. Furthermore, the mechanism of the observed ECL quenching is revealed on the ground of a series of experiments carried out using the electrochemical quartz-crystal microbalance (EQCM) approach.

Experimental Section

Chemicals and Materials

Tris(2,2′-bipyridyl)ruthenium(II) dichloride hexahydrate ($Ru(bpy)_3Cl_2 \cdot 6H_2O$; 99.95%), TPrA (99+%), sulfuric acid (H_2SO_4, 98%), and nitric acid (HNO_3, 70%) from Aldrich (Milwaukee, WI), perchloric acid ($HClO_4$, 70%), hydrochloric acid (HCl, 37.5%), hydrogen peroxide (H_2O_2, 30%), and sodium chloride (NaCl, certified A.C.S.) from Fisher (Fairlawn, NJ), phosphoric acid (H_3PO_4, 85.5%), sodium phosphate dibasic heptahydrate ($Na_2HPO_4 \cdot 7H_2O$, 98.0%), potassium phosphate monobasic (KH_2PO_4, 99.6%), and sodium hydroxide (NaOH, 98.7%) from J.T. Baker (Phillipsburg, NJ), silver

nitrate ($AgNO_3$, 99.5%) from Fluka (Milwaukee, WI), and hydrogen tetrachloroaurate ($HAuCl_4$, 99.999%) from GFS (Powell, OH.) were used without further purification. All solutions were prepared with deionized-distilled water produced from a Barnstead MP-6A Mega-Pure® System (Barnstead International, Dubuque, IA).

Preparation of TPrA Coreactant Solutions

0.10 M TPrA–0.10M phosphate buffer solutions (pH 7.5) were prepared by dissolving an appropriate amount of TPrA in 0.10 M phosphate buffer solutions and re-adjusting the pH of the TPrA–phosphate mixture with a concentrated H_3PO_4, $HClO_4$, or HCl solution while the mixture was stirred magnetically. At the final pH value of 7.5, all TPrA droplets should totally disappear (be completely dissolved).

Electrochemical, ECL, and EQCM Measurements

Cyclic voltammetry (CV) was performed with a model 660A electrochemical workstation (CH Instruments, Austin, TX). A conventional three-electrode cell was used, with a Pt wire as the counter electrode and an $Ag/AgCl/Cl^-$ (3.0 M KCl) (or a Pt wire) as the reference electrode (or quasi-reference electrode, QRE) electrode. The Pt QRE potential was calibrated using ferrocenemethanol as an internal reference and had a potential value of 0.143 V vs Ag/AgCl. Three different types of working electrodes, namely GC (3-mm diameter), Au (2-mm diameter), and Pt (2-mm diameter), were used for electrochemical (CV and ECL) measurements. These electrodes were polished with 0.3-0.05 μm alumina slurry, thoroughly rinsed with Mega-Pure water, and dried with the Kimwipes facial tissue before each experiment. The leaked chloride ions from the frit of an Ag/AgCl (3.0 M KCl) reference electrode were determined with CV in a 1.0 mL solution containing 5.0 mM $AgNO_3$–0.10 M $LiNO_3$.White AgCl precipitations were

accompanied by gradual decreases in Ag^+ reduction peak currents at a Au electrode. The CV was scanned between 1.0 and 0 V vs Ag/AgCl at a scan rate of 50 mV/s about every 5 minutes with a freshly polished Au working electrode. The remained Ag^+ concentration was evaluated on the basis of a standard $AgNO_3$ (0.10 M $LiNO_3$) calibration curve, and the original chloride concentrations were calculated accordingly. Assumptions of this technique included the solution viscosity changes resulted from the formation of AgCl precipitates and the inclusion of free Ag^+ into the precipitates were negligible.

The ECL along with the CV or chronoamperometric signals were measured simultaneously with the 660A electrochemical workstation (see above) combined with a photomultiplier tube (PMT, Hamamatsu R928, Japan) installed under the electrochemical cell. A voltage of −700V was supplied to the PMT with a high voltage power supply (Model 472A Brandenburg PMT power supply, England). The light signal (as photocurrent) was detected with a high sensitive Keithley 6514 electrometer (Keithley, Cleveland, OH) and converted to a voltage (in ±2V) that was collected to the electrochemical workstation computer. In order to eliminate the possible contamination effect of $Ru(bpy)_3^{2+}$ on blank ECL, virgin electrochemical cells were always used, and whenever necessary, the working and counter electrodes were cleaned with either chromic acid or freshly prepared piranha solution (98% H_2SO_4/30% H_2O_2, 70/30 in v/v) and a new Vycor tip of the Ag/AgCl reference electrode was employed (*CAUTION*: Chromic acid and Piranha solution can react violently with organic materials, and should be handled with extreme caution.). EQCM experiments were performed on a QCM200 Quartz-Crystal Microbalance Digital Controller with a QCM25 5MHz Crystal Oscillator (Stanford Research Systems, Sunnyvale, CA) combined with the 660A electrochemical

workstation. A 5 MHz polished gold/Cr-coated AT-cut quartz crystals was used as the working electrode, and the reference and the counter electrodes were the same as those used in ECL studies. The quartz crystal and gold electrodes had diameters of 2.54 and 1.32 cm, respectively. The relative frequency changes were outputted through the "frequency analog out" to the "signals" interface of the potentiostat and displayed as voltages. Data obtained from deposition of silver by potential-step experiments (0.70 V stepped to 0.0 V Ag/AgCl with a step width of 15 s) from a 5.0 mM $AgNO_3$ solution in 0.50 M HNO_3 were used to calibrate the EQCM. On the basis of the Sauerbrey equation,[15-18] a sensitivity factor of 51.7 Hz $cm^2/\mu g$ was obtained. This value is very close to a previously reported sensitivity factor, 51.3 Hz $cm^2/\mu g$ from 1 mM $AgNO_3$–0.1 M $HClO_4$ and 52.3 Hz $cm^2/\mu g$ from 5 mM PbO_2–0.1 M $HClO_4$, for a 5 MHz AT-cut quartz crystal.[19]

All measurements were conducted at a temperature of $24 \pm 1\ ^{\circ}C$, unless otherwise stated.

Results and Discussion

ECL Inhibitive Behavior at a Au Electrode in the Presence of Chloride Ions

In order to prepare a TPrA coreactant solution, concentrated acids, such as H_3PO_4, HCl and $HClO_4$ are most often used to neutralize the TPrA after its mixing with the initial buffer solution (e.g., phosphate buffer[8] and Tris–HCl–$LiClO_4$ buffer[7,14] solutions). Besides, for the detection and quantification of biomolecules, PBS buffer solutions (with 0.15 M NaCl) are frequently used. Therefore, ECL behavior of the $Ru(bpy)_3^{2+}$/TPrA system in different electrolytes at different electrodes was examined first. As shown in Figure 2.1, in phosphate buffer solutions containing no chloride ions, two ECL waves

with similar light emission intensities are observed at GC (Figure 2.1a) and Au (Figure 2.1b) electrodes, while only one ECL wave is produced at a Pt electrode (Figure 2.1c). The first ECL waves in Figure 2.1a and b are originated from the initial TPrA oxidation and the second ones are associated with the oxidation of $Ru(bpy)_3^{2+}$ at the electrode surfaces.[7] Because the direct oxidation of TPrA and $Ru(bpy)_3^{2+}$ is inhibited at a Pt electrode due to the formation of platinum oxide on the electrode surface,[8] no first ECL wave is observed at the Pt electrode, and "the second ECL wave" intensity is about 100 times lower than those obtained using GC or Au electrodes (Figure 2.1c) under the current experimental conditions (i.e.,[$Ru(bpy)_3^{2+}$] = 1.0 μM). Similar ECL behavior was found in ClO_4^-- containing phosphate buffer solutions at respective electrodes. In contrast, remarkable effect of chloride ions on ECL at a Au electrode was discovered. When HCl was used to replace H_3PO_4 or $HClO_4$ as the TPrA neutralization agent, the first ECL wave was reduced by~50%, and the second ECL wave completely disappeared at a Au electrode in1.0 μM $Ru(bpy)_3^{2+}$–0.10 M TPrA–0.10 M phosphate buffer (pH 7.5) (Figure 2.2).

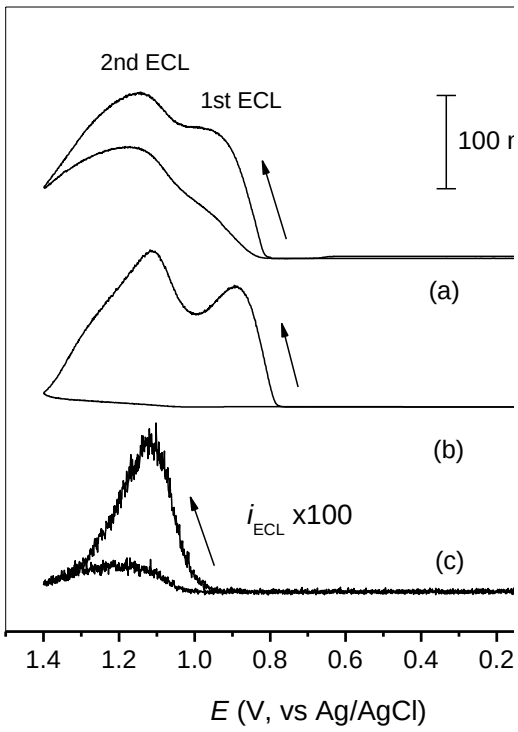

Figure 2.1. ECL profiles obtained from a 1.0 μM $Ru(bpy)_3^{2+}$–0.10 M TPrA–0.10 M phosphate buffer (pH 7.5) solution at (a) a GC, (b) a Au, and (c) a Pt electrode with a scan rate of 10 mV/s.

However, no such differences in the ECL responses at GC and Pt electrodes were observed irrespective of the composition of the electrolyte used. These data suggest that the observed ECL inhibitive behavior in the presence of Cl^- is inherent to the Au electrode only. Figure 2.3 outlines the dependence of ECL intensities on added chloride ion (as NaCl) concentrations in 1.0 μM $Ru(bpy)_3^{2+}$–0.10 M TPrA–0.10 M phosphate buffer (pH 7.5) at a Au electrode. Both the first and the second ECL waves increase initially with the concentration of Cl^- and reach the maximum ECL intensity values at added [Cl^-] of 0.3 and 0.7 mM, respectively (Figure 2.3, inset); about 3 times in ECL enhancement are attained for both ECL waves. The ECL intensities then decrease, and at

[Cl^-] ≈ 5 mM, their intensities approach the values equivalent to those obtained in the absence of added Cl^-. Finally, the second ECL wave is inhibited by ~97% at [Cl^-] = 80 mM and by 100% at [Cl^-] = 90 mM. The first ECL wave, however, is not completely inhibited even in the presence of 0.10 M Cl^-.

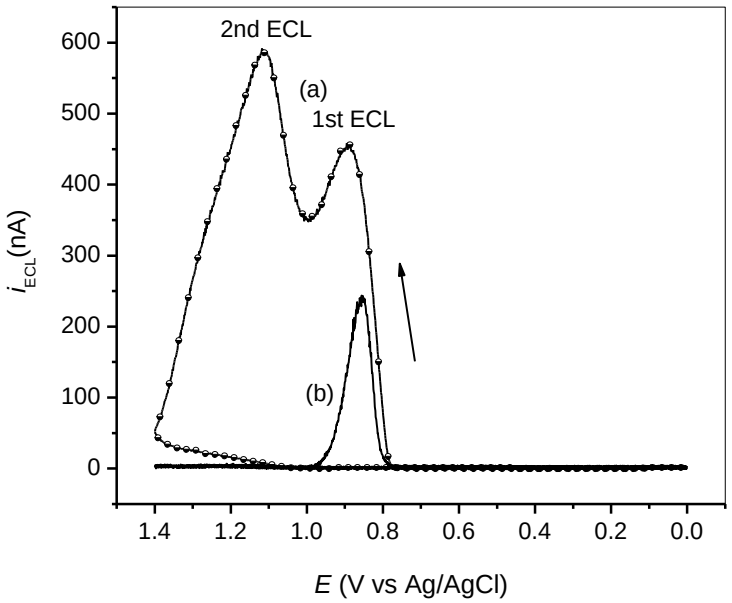

Figure 2.2. ECL responses obtained from 1.0 μM $Ru(bpy)_3^{2+}$–0.10 M TPrA–0.10 M phosphate buffer (pH 7.5) at a 2-mm diameter Au electrode with a scan rate of 10 mV/s when TPrA was neutralized with (a) H_3PO_4 and (b) HCl.

Although in the present situation Cl^- contribution from 1.0 μM $Ru(bpy)_3Cl_2$ to the ECL intensity change is negligible, it could be significant when sub-mM concentrations of $[Ru(bpy)_3]Cl_2$ are used in ECL studies at a Au electrode. The ECL enhancement at low Cl^- concentration has been previously attributed to the inhibition of surface oxides on Au electrode and the activation of anodic dissolution of Au in chloride-containing solution, leading to an increase in direct TPrA oxidation efficiency and thus to ECL enhancement [8].

ECL profiles of the $Ru(bpy)_3^{2+}$/TPrA system were often found to change with the CV potential cycles at a Au electrode when a chloride-containing reference electrode was used. For example, at a relatively slow scan rate of 10 mV/s, in a 1.0 μM $Ru(bpy)_3^{2+}$–0.10 M TPrA–0.10 M phosphate buffer (pH 7.5) solution, the ECL intensities increased in the first several cycles and then decreased gradually at a Au electrode with an Ag/AgCl (3.0 M KCl) as the reference electrode. This "poor reproducibility" can be attributed to the influence of small amounts of chloride ions leaked from the reference electrode. As discussed earlier, ECL starts to inhibit at ~5 mM of Cl^- (Figure 2.3), which is equivalent to ~1.7 μL of 3.0 M KCl (leaked from the reference electrode) dissolved in a 1.0 mL of electrolyte solution. The effect of chloride-containing reference electrode on ECL behavior was confirmed by chronoamperometric experiments. As shown in Figure 2.4a, when a Au electrode potential is pulsed between 0 and 0.95 V vs Ag/AgCl, no redox reaction is expected to occur during the first potential-step held at 0 V, and the TPrA will be oxidized during the second potential-step held at 0.95 V, leading to the generation of the first ECL wave.[7] The ECL intensity goes up steeply during the first 500 s, and then gradually goes down in the next 1500 s before it approaches a close stable-state. When the second potential-step potential is held at 1.20 V vs Ag/AgCl (Figure 2.4b), both the first and the second ECL waves are generated. As a result, the initial ECL signal is much stronger than that shown in Figure 2.4a. The ECL signal is enhanced with the potential pulsing during the first 300 s, and then rapidly decreases to ECL levels much weaker than its initial value. The above two sets of experiments are consistent

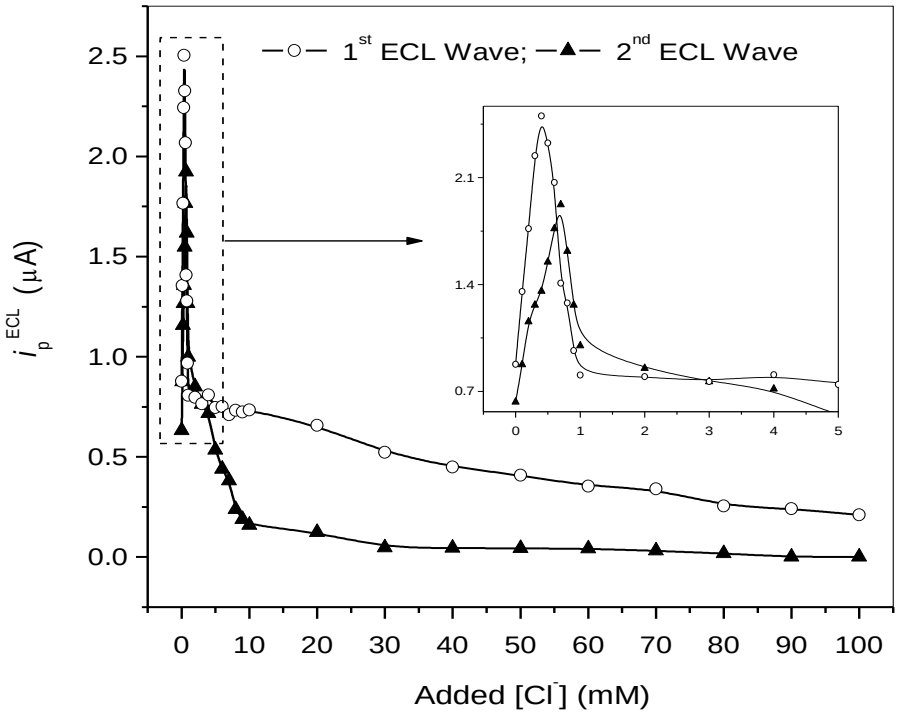

Figure 2.3. Dependence of ECL intensity on added chloride ion (as NaCl) concentration. The electrolyte solution contained 1.0 μM $Ru(bpy)_3^{2+}$–0.10 M TPrA–0.10 M phosphate buffer (pH 7.5) in which TPrA was neutralized with H_3PO_4. The experiments were carried out immediately after all electrodes were placed in contact with the electrolyte solution. The ECL peak intensity was measured from the first cycle of CV excitation between 0 and 1.40 V vs Ag/AgCl at a scan rate of 10 mV/s using a 2-mm diameter Au electrode as the working electrode and an Ag/AgCl (3.0 M KCl) as the reference electrode.

with the continually slow chloride leaking from the reference electrode into the ECL reaction medium as revealed in Figure 2.4d, and the remaining ECL signals can be ascribed to the

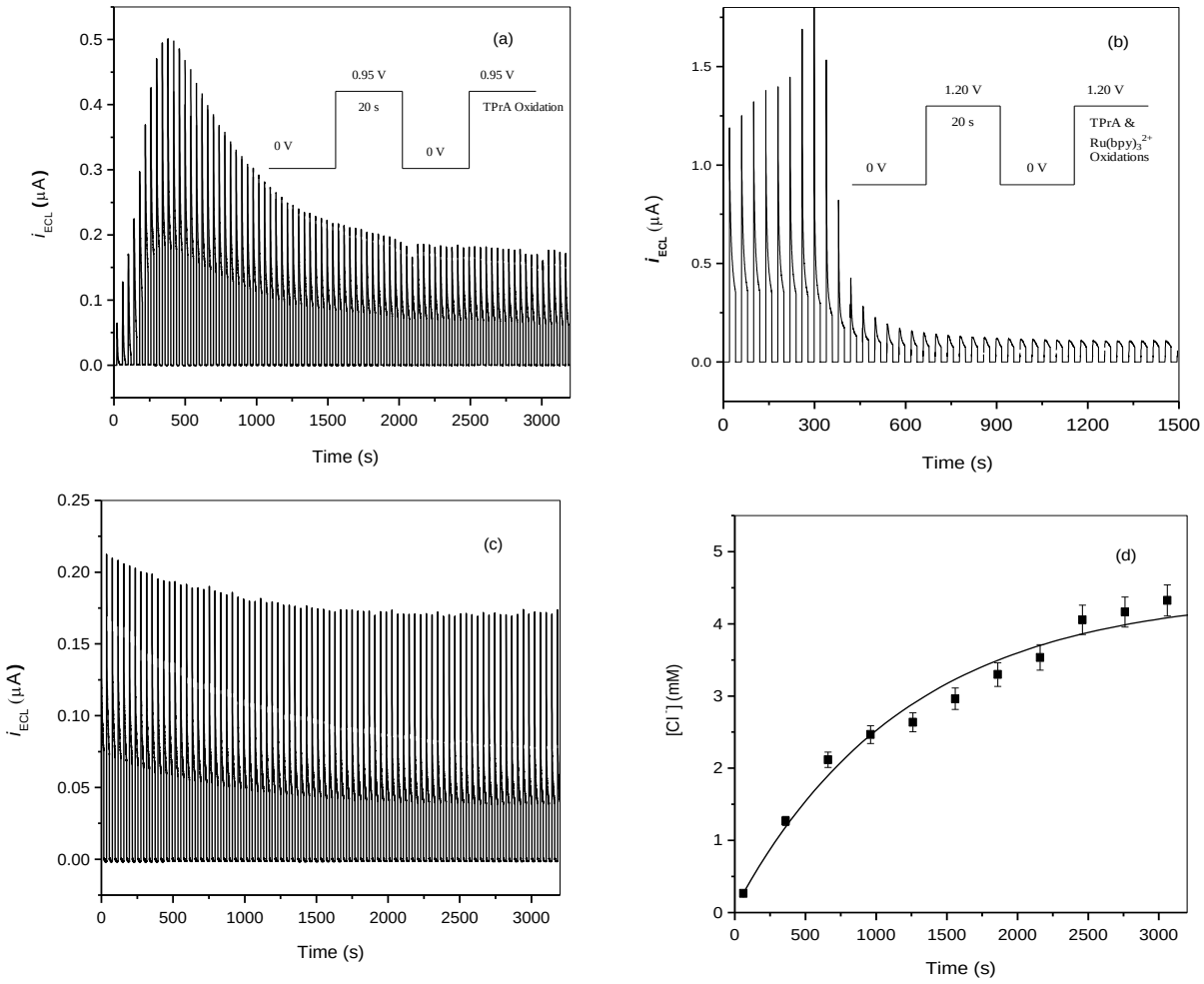

Figure 2.4. Dependence of ECL intensity on the reference electrode used. The 1.0 mL solution contained 1.0 μM $Ru(bpy)_3^{2+}$–0.10 M TPrA–0.10 M phosphate buffer (pH 7.5), and the potential-step experiments were conducted at a 2-mm diameter Au electrode with a pulse width of 20 s. (a) Ag/AgCl (3.0M KCl) reference electrode with a pulse potential between 0 and 0.95 V vs Ag/AgCl, (b) Ag/AgCl (3.0 M KCl) reference electrode with a pulse potential between 0 and 1.2 V vs Ag/AgCl, and (c) Pt QRE with a pulse potential between 0 and 1.2 V vs Pt QRE (~1.34 V vs Ag/AgCl). (d) Increases of chloride concentrations over time resulted from the leaking of chloride ions from the frit of an Ag/AgCl (3.0 M KCl) reference electrode (overall volume: 1.0 mL).

non-diminished first ECL wave as described earlier. When the Ag/AgCl electrode in Figure 2.4b is replaced with a Pt QRE, no ECL enhancement effect is observed, and the overall ECL profile is relatively stable (Figure 2.4c). The slow decay in ECL intensity over the first 1500s is probably due to the Au electrode fouling. On the basis of the above studies, care must be taken when a chloride-containing reference electrode (e.g., Ag/AgCl, saturated calomel electrode (SCE)) is used with a Au electrode for quantitative measurements of the $Ru(bpy)_3^{2+}$/TPrA ECL system. In order to eliminate such an effect, an Ag/AgCl or SCE reference electrode may be incorporated with a second salt-bridge filled with a non chloride electrolyte such as $NaNO_3$. Alternatively, a "no-leaking" Ag/AgCl reference electrode[20] or a QRE can be used.

ECL Inhibition Mechanism at a Au Electrode in the Presence of Chloride Ions

When HCl is used to neutralize the 0.10 M TPrA in a phosphate buffer (pH 7.5) solution, the final Cl^- concentration in the buffer, which can be estimated on the basis of the p*K*a value of TPrA (10.44)[21,22], is close to 0.1 M. Accordingly, 0.10 M NaCl solutions were employed for the studies of species generation during the electrolysis within a potential range of 0 to 1.2 V vs Ag/AgCl at a Au electrode. ECL mechanisms of the $Ru(bpy)_3^{2+}$/TPrA system [7,8] suggest that any species that promotes the direct oxidation of TPrA and $Ru(bpy)_3^{2+}$ could enhance the ECL, whereas any species that consumes the intermediate TPrA free radicals (TPrA•, $E^0 \approx -1.7$ V vs Ag/AgCl[23]) could reduce or inhibit the ECL. During the electrolysis of a 0.10 M NaCl solution at a Au electrode, three strong oxidizing agents, namely chlorine ($E^0(Cl_2(g)/Cl^-) = 1.17$ V vs Ag/AgCl)[24], $AuCl_2^-$ ($E^0(AuCl_2^-/Au) = 0.94$ V vs Ag/AgCl)[25], and $AuCl_4^-$ ($E^0(AuCl_4^-/Au) = 0.79$ V vs

Ag/AgCl)[25], could be produced. Identification or verification of these three species could elucidate the ECL inhibition mechanism of the system.

In order to examine if chlorine is formed during the anodic electrolysis of 0.10 M NaCl (in 1 mL), a double-potential step (pulsing) between 0 and 1.2 V vs Ag/AgCl with a pulse width of 5 s was imposed to a 2-mm diameter Au electrode for ~20 min. A gradual change in solution color from colorless to yellow-green was observed. Two tests were subsequently conducted. First, a few NaOH flakes were added into the newly produced solution; no color change was seen. Second, a wet filter paper strip soaked with KI-starch was placed over the slightly heated solution; no characteristic blue color was produced. Furthermore, severe damage of the Au electrode surface was found after the electrolysis. This suggests that no chlorine was generated during the electrolysis, and the change in solution color was due to the anodic Au dissolution.

The formation of gold complexes was investigated by an EQCM method using a Au-coated quartz-crystal as the working electrode, with an assumption that the Au dissolution was uniform over the electrode within the experimental time scales. According to the Sauerbrey equation:[15-18]

$$\Delta f = -C_f \times m \qquad (2.1)$$

where Δf is the experimentally measured frequency shift caused by change of a mass per unit area, m, to the crystal surface, and C_f is the sensitivity factor which has a calibrated value of 51.7 Hz cm^2/μg under present experimental conditions. Thus, the overall mass change, Δm, at the electrode can be calculated as:

$$\Delta m = m \times A = -\Delta f \times A/C_f \qquad (2.2)$$

in which A is the active electrode area (1.37 cm^2).[26] On the other hand, for an electrochemical reaction, Faraday's law (on the assumption of 100% current efficiency) states that the charge consumed (Q) is related to the mass change by the expression:

$$Q = \int_0^t i \bullet t = \frac{\Delta m}{(M/n)} F \tag{2.3}$$

where i is the electrochemical current, t is the time, M is the atomic (or molecular) weight of the chemical species, F is the Faraday constant (96,485 C/mol), and n is the number of electrons involved in the electrochemical reaction.

For anodic dissolution of Au in a chloride-containing solution,[19,25,27-31] a decrease in mass (or increases in frequency) is expected, if any of the following reactions occur:

$$Au\ (s) + 2Cl^-\ (aq) - e = AuCl_2^-\ (aq) \tag{2.4}$$

$$Au\ (s) + 4Cl^-\ (aq) - 3e = AuCl_4^-\ (aq) \tag{2.5}$$

Therefore, the overall number of the electron transfer for each mole of Au loss can be calculated as

$$n = \frac{M_{Au} \bullet Q}{\Delta m \bullet F} \tag{2.6}$$

in which the atomic weight of Au, M_{Au}, is 196.97 g/mole. The experimentally obtained n value can be used to verify which Au complex is formed. If n = 1, then Reaction (2.4) is operative; if n = 3, then $AuCl_4^-$ electrogeneration is to be expected; if $1 < n < 3$, a mixture of both $AuCl_2^-$ and $AuCl_4^-$ complexes is electrochemically generated.

Figure 2.5A shows a set of EQCM experimental data, in which the Au/QCM electrode potential is held at 0 V vs Ag/AgCl for 100 s before it is stepped up to 0.73 V vs Ag/AgCl for another 100 s. Since no redox reaction occurs at 0 V, no Faradaic current is observed at this potential. After the electrode potential is switched to 0.73 V vs Ag/AgCl, however, significant Faradaic current is generated (Figure 2.5A(a)). In order to

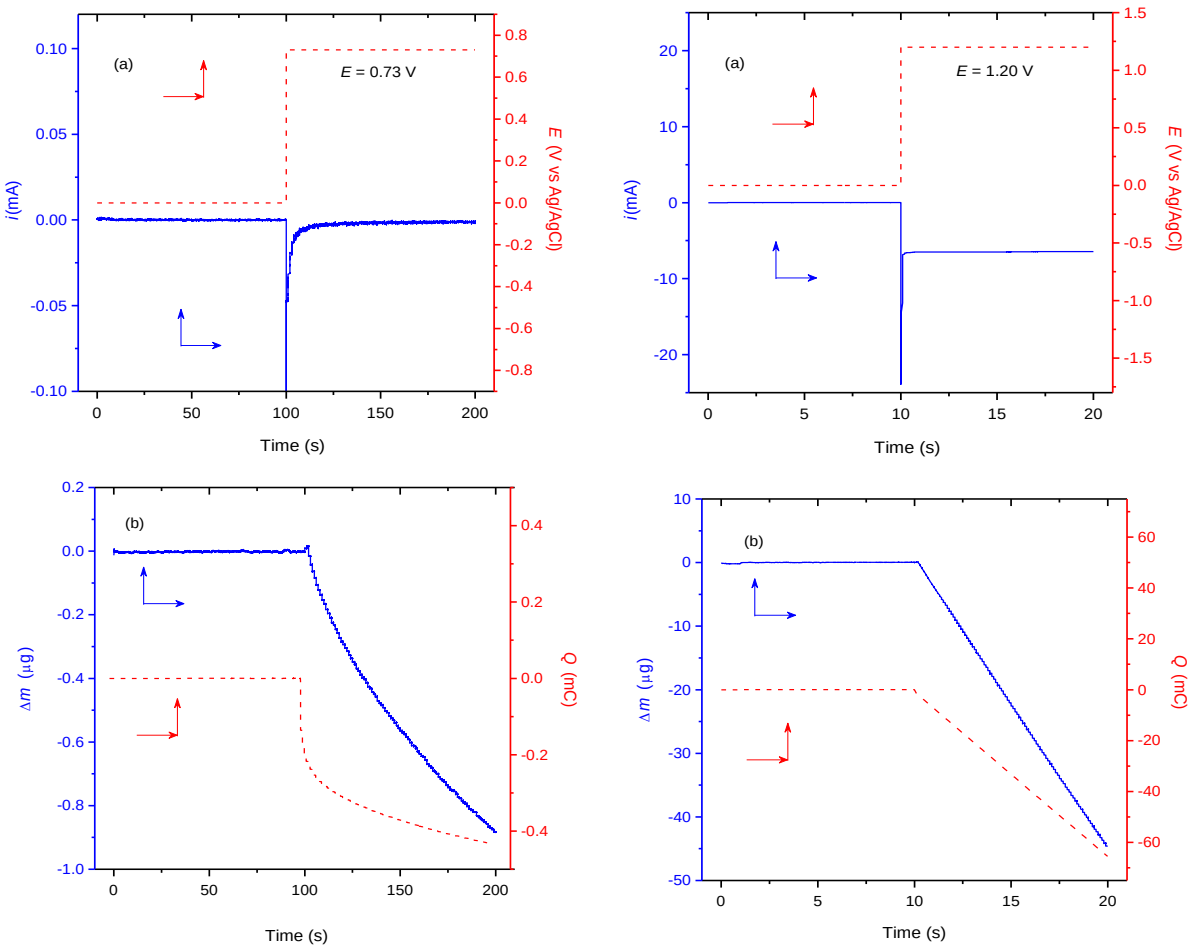

Figure 2.5. EQCM experiment data obtained from a Au-coated QCM electrode in a 0.10 M NaCl solution with a potential-step of (A) 0 to 0.73 V vs Ag/AgCl and (B) 0 to 1.20 V vs Ag/AgCl. (a) electrode potential (dashed line) and current (solid line) as a function of time, (b) corresponding change in mass decrease (solid line) and charge consumed (dashed line). Arrows refer to the X and Y axes of related plots.

minimize the non-Faradaic current contribution to the overall electrochemical processes, a relatively long standing time of 100 s is used for the potential-step experiment. The corresponding charge consumed (Q = 0.43 mC at 200 s) along with the decrease in mass (Δm = 0.88 μg at 200 s) is displayed in Figure 2.5A(b). The overall electron transfer

number involved at this potential as calculated via eq. (2.6) is 1.0, suggesting that only $AuCl_2^-$ complex is formed. The Au dissolution in 0.10 M NaCl starts at ~0.64 V vs Ag/AgCl as shown in Figure 2.6a. However, potential-step/EQCM-based measurements of the electron transfer numbers below 0.73 V proved difficult, since the minor changes in the current and frequency under the given conditions bring about inaccurate EQCM results. A similar approach as in Figure 2.5A was used to identify the Au complex formation at a step-potential of 1.20 V vs Ag/AgCl (Figure 2.5B). In this case, a much shorter pulse width of 10 s was used, and on the basis of Q = 65.6 mC and Δm = 44.6 μg at 20 s, n = 3.0 was calculated. That is, the $AuCl_4^-$ complex is exclusively produced at an electrode potential of 1.2 V vs Ag/AgCl. Note that contributions from the background EQCM experiments in the absence of chloride ions were not subtracted from the data shown in Figure 2.5, because no mass change was observed from the background and the charging current upon the potential step was negligible compared to the related Faradaic current.

When the electrode was held in the potential range of 0.73 V < E < 1.20 V vs Ag/AgCl, the overall electron transfer number of 1 < n < 3 was obtained (Figure 2.6). In other words, within this potential range both $AuCl_2^-$ and $AuCl_4^-$ complexes are electrochemically produced at the electrode surface. This finding is consistent with the cyclic voltammetric-EQCM data shown in Figure 2.7b, where two reduction waves are observed when the electrode potential is reversed at 1.2 V vs Ag/AgCl. Since this potential range coincides with the potentials of TPrA and $Ru(bpy)_3^{2+}$ oxidations as well as that for ECL emitting (see refs[7,8] and Figures 2.1b and 2.2), it seems reasonable to conclude that $AuCl_2^-$ and $AuCl_4^-$ complexes are responsible for the ECL inhibiting of the

$Ru(bpy)_3^{2+}$/TPrA system at a Au electrode.[7-12] Eqs. (2.7-2.16) summarize the three major pathways accompanying the course of ECL generation and inhibition. The formation of TPrA free radicals (pathway 1) initiates the generation of two ECL waves, in which the second wave accompanies the electro-oxidation of $Ru(bpy)_3^{2+}$ that has a peak potential of ~1.10 V vs Ag/AgCl (pathway 2) (see refs[7,8] and Figure 2.1b). The reactions between the electrogenerated $AuCl_2^-$/$AuCl_4^-$ complexes and TPrA free radicals (pathway 3) result in a significant decrease (for the potential range of the first ECL wave) or a complete depletion (beyond first ECL wave) of $TPrA^\bullet$ species near the electrode surface. Consequently, about 50% of the first ECL wave and 100% of the second ECL wave are inhibited (Figure 2.2). The inhibitive capacity depends on the relative concentrations of gold complexes with respect to [$TPrA^\bullet$] as well as the ratio of $AuCl_4^-$/$AuCl_2^-$ (e.g., in pathway 3, one $AuCl_4^-$ could consume three moles of $TPrA^\bullet$). Since large amounts of $TPrA^\bullet$ but relatively small amounts of gold complexes (mainly $AuCl_2^-$, Figure 2.6) are produced within the potential range of the first ECL wave, part of this ECL wave remains. The massive production of high inhibitive capacity $AuCl_4^-$ complexes within the potential range of the second ECL wave must account largely for the complete inhibition of the ECL. Although the gold dissolution in a variety of electrolyte solutions containing chloride ions has been previously studied using a number of techniques such as a rotating disk electrode,[32] in-situ surface-enhanced Raman spectroscopy[30] and the EQCM,[25] no report has been published on Au dissolution in a neutral 0.10 M NaCl solution.

(1) TPrA free radicals ($TPrA^\bullet$) formation

$$TPrA \xrightarrow{-e} TPrA^{\bullet+} \xrightarrow{-H^+} TPrA^\bullet \ (E_p \sim 0.90 \text{ V vs Ag/AgCl}) \qquad (2.7)$$

(2) Generation of the first and the second ECL waves

$$Ru(bpy)_3^{2+} \xrightarrow{TPrA^{\bullet}} Ru(bpy)_3^{+} \quad (2.8)$$

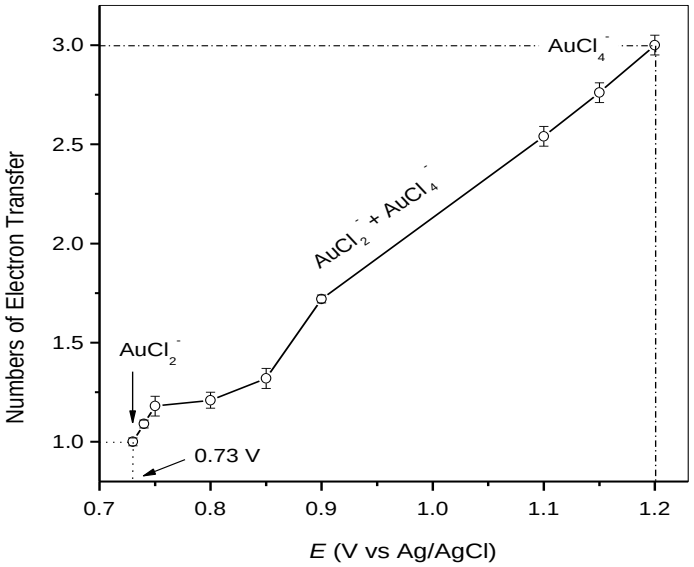

Figure 2.6 Overall electron transfer number involved in the anodic dissolution of Au as a function of electrode potential in 0.10 M NaCl. The data were based on EQCM experiments with Au-coated QCM electrodes.

$$Ru(bpy)_3^{+} \xrightarrow{TPrA^{\bullet+}} [Ru(bpy)_3^{2+}]^* \rightarrow Ru(bpy)_3^{2+} + h\nu \text{ (1st ECL wave)} \quad (2.9)$$

$$Ru(bpy)_3^{2+} \xrightarrow{-e} Ru(bpy)_3^{3+} \ (E_p \sim 1.10 \text{ V vs Ag/AgCl}) \quad (2.10)$$

$$Ru(bpy)_3^{3+} \xrightarrow{Ru(bpy)_3^{+}} [Ru(bpy)_3^{2+}]^* \rightarrow Ru(bpy)_3^{2+} + h\nu \text{ (2nd ECL wave)} \quad (2.11)$$

$$Ru(bpy)_3^{3+} \xrightarrow{TPrA^{\bullet}} [Ru(bpy)_3^{2+}]^* \rightarrow Ru(bpy)_3^{2+} + h\nu \text{ (2nd ECL wave)} \quad (2.12)$$

(3) ECL inhibition by the electrogenerated gold complexes

$$Au \xrightarrow[Cl^-]{-e} AuCl_2^- \ (\sim 0.64 \text{ V} < E < 1.2 \text{ V vs Ag/AgCl}) \quad (2.13)$$

$$Au \xrightarrow[Cl^-]{-3e} AuCl_4^- \ (E > 0.73 \text{ V vs Ag/AgCl}) \quad (2.14)$$

$$AuCl_2^- + TPrA^{\bullet} \rightarrow Au + 2Cl^- + \text{Products} \quad (2.15)$$

$$AuCl_4^- + 3TPrA^{\bullet} \rightarrow Au + 4Cl^- + \text{Products} \quad (2.16)$$

Scheme 2.1 ECL generation and inhibition of $Ru(bpy)_3^{2+}$/TPrA system at a gold electrode in the presence of relatively high concentrations of chloride ions.

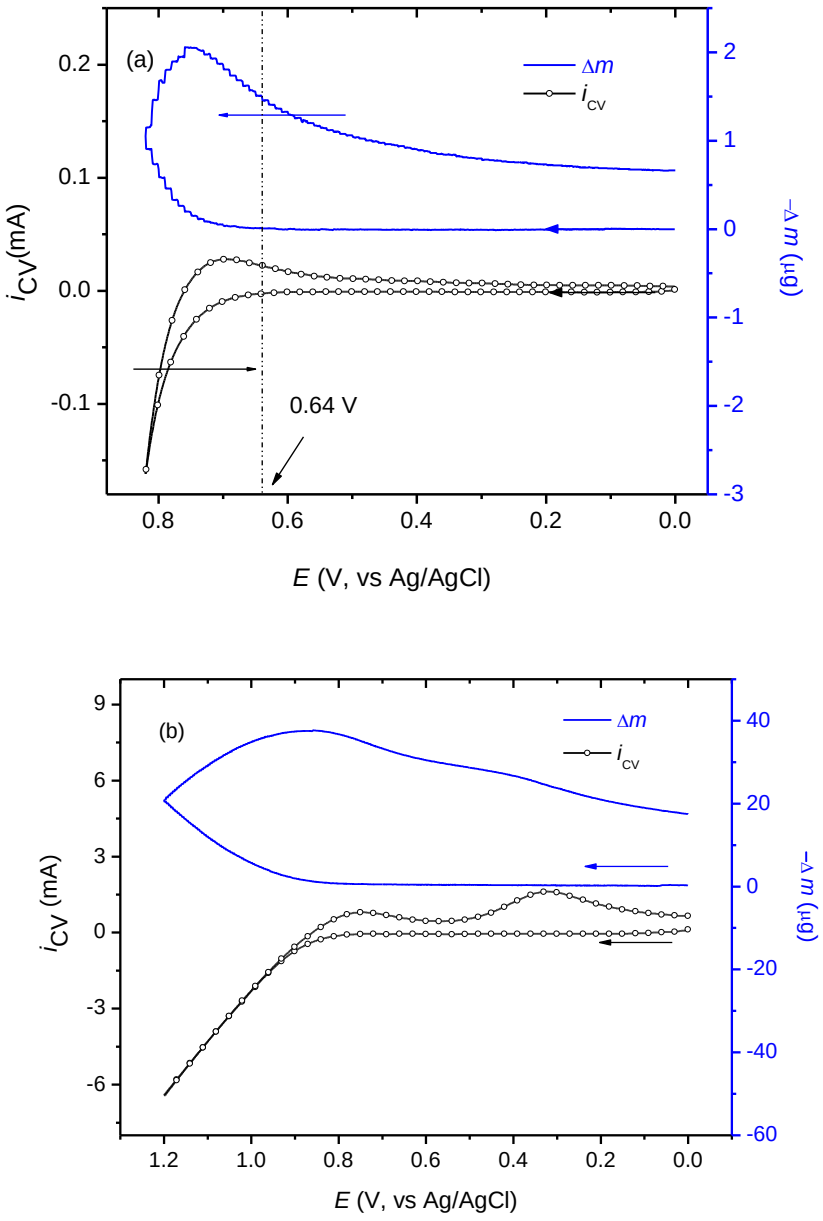

Figure 2.7. Cyclic voltammograms and EQCM mass changes obtained from a 0.10 M NaCl solution at a Au-coated/QCM electrode with a scan rate of 10 mV/s. (a) 0 to 0.82 V vs Ag/AgCl, (b) 0 to 1.2 V vs Ag/AgCl.

Based on the above ECL inhibition mechanism, one would expect the decrease in ECL intensity after the addition of a small amount of $HAuCl_4$ into the ECL electrolyte solution (e.g., 1.0 μM $Ru(bpy)_3^{2+}$-0.10 M TPrA-0.10 M phosphate buffer (pH 7.5)). Experimentally, however, no change was found. This is because the added $AuCl_4^-$ is a relatively strong oxidant and immediately reduced by TPrA in the bulk solution. In other words, no added $AuCl_4^-$ can survive before the ECL generation. Thus, only in-situ electrogenerated gold complexes at the electrode interface have to be considered as ECL inhibiters. The proposed inhibition mechanism provides a reasonable explanation why only one ECL wave (around 0.9 V vs Ag/AgCl) was observed during the ECL detection of surface-confined biomolecules on Au in chloride-containing electrolytes.[14] Most likely, the second ECL wave was inhibited by newly formed $AuCl_2^-$ and $AuCl_4^-$ complexes.

Conclusions

Chloride ions in the electrolyte solution can significantly affect the ECL responses at a Au electrode. When $[Cl^-] < 5$ mM, ECL enhancement was observed. At relatively high concentrations (from 5 mM to 100 mM), ECL intensities decreased with the increase of the chloride concentration. Complete inhibition of the second ECL wave was seen when $[Cl^-] \approx 90$ mM. This inhibitive behavior results from the depletion of TPrA free radicals by electrogenerated $AuCl_2^-$ and $AuCl_4^-$ complexes that are produced in the same potential range as that for TPrA and $Ru(bpy)_3^{2+}$ oxidation. Care must be taken when a chloride-containing reference electrode is used for the ECL study at a Au electrode, since the leaking of chloride ions into the electrolyte solution could change the ECL intensity considerably. Usage of double-junction chloride reference electrodes or other reference electrodes such as Hg/Hg_2SO_4 are strongly recommended.

References

1. Leland, J. K. & Powell, M. J. Electrogenerated chemiluminescence: An oxidative-reduction type ECL reaction sequence using tripropyl amine. *J Electrochem. Soc.* **137**, 3127-31 (1990).

2. Bard, A. J. (ed.) *Electrogenerated Chemiluminescence* (Marcel Dekker, Inc., New York, 2004).

3. Richter, M. M. Electrochemiluminescence (ECL). *Chem. Rev.* **104**, 3003-3036 (2004).

4. Miao, W. Electrogenerated Chemiluminescence and Its Biorelated Applications. *Chem. Rev.* **108**, 2506-2553 (2008).

5. Debad, J. D., Glezer, E. N., Leland, J. K., Sigal, G. B. & Wohlsadter, J. Clinical and biological Applications of ECL, in *Electrogenerated Chemiluminescence* (ed. Bard, A. J.), Chapter 8--Clinical and biological Applications of ECL (Marcel Dekker, Inc., New York, 2004).

6. Miao, W. & Choi, J.-P. Coreactants, in *Electrogenerated Chemiluminescence* (ed. Bard, A. J.), 213-272, Chapter 5 (Marcel Dekker, Inc., New York, 2004).

7. Miao, W., Choi, J.-P. & Bard, A. J. Electrogenerated Chemiluminescence 69: The Tris(2,2'-bipyridine)ruthenium(II), ($Ru(bpy)_3^{2+}$)/Tri-n-propylamine (TPrA) System Revisited-A New Route Involving TPrA.bul.+ Cation Radicals. *J. Am. Chem. Soc.* **124**, 14478-14485 (2002).

8. Zu, Y. & Bard, A. J. Electrogenerated Chemiluminescence. 66. The Role of Direct Coreactant Oxidation in the Ruthenium Tris(2,2')bipyridyl/Tripropylamine System and the Effect of Halide Ions on the Emission Intensity. *Anal. Chem.* **72**, 3223-3232 (2000).

9. Zheng, H. & Zu, Y. Emission of Tris(2,2'-bipyridine)ruthenium(II) by Coreactant Electrogenerated Chemiluminescence: From O_2-Insensitive to Highly O_2-Sensitive. *J. Phy. Chem. B* **109**, 12049-12053 (2005).

10. Zu, Y. & Li, F. Characterization of the low-oxidation-potential electrogenerated chemiluminescence of tris(2,2'-bipyridine)ruthenium(II) with tri-n-propylamine as coreactant. *Anal. Chim. Acta* **550**, 47-52 (2005).

11. Zu, Y. & Bard, A. J. Electrogenerated chemiluminescence. 67. Dependence of light emission of the tris(2,2')bipyridylruthenium(II)/tripropylamine system on electrode surface hydrophobicity. *Anal. Chem.* **73**, 3960-3964. (2001).

12. Li, F. & Zu, Y. Effect of Nonionic Fluorosurfactant on the Electrogenerated Chemiluminescence of the Tris(2,2'-bipyridine)ruthenium(II)/Tri-n-propylamine System: Lower Oxidation Potential and Higher Emission Intensity. *Anal. Chem.* **76**, 1768-1772 (2004).

13. Walworth, J., Brewer, K. J. & Richter, M. M. Enhanced electrochemiluminescence from $Os(phen)_2(dppene)^{2+}$ (phen = 1,10-phenanthroline and dppene = bis(diphenylphosphino)ethene) in the presence of Triton X-100 (polyethylene glycol tert-octylphenyl ether). *Anal. Chim. Acat* **503**, 241-245 (2004).

14. Miao, W. & Bard, A. J. Electrogenerated chemiluminescence. 72. Determination of immobilized DNA and C-reactive protein on Au(111) electrodes using tris(2,2'-bipyridyl)ruthenium(II) labels. *Anal. Chem.* **75**, 5825-5834 (2003).

15. Sauerbrey, G. The use of quartz oscillators for weighing thin layers and for microweighing. *Zeitschrift fuer Physik* **155**, 206-22 (1959).

16. Buttry, D. A. & Ward, M. D. Measurement of interfacial processes at electrode surfaces with the electrochemical quartz crystal microbalance. *Chem. Rev.* **92**, 1355-79 (1992).

17. Buttry, D. A. Applications of the quartz crystal microbalance to electrochemistry. *Electroanal. Chem.* **17**, 1-85 (1990).

18. Ward, M. D. Principles and applications of the electrochemical quartz crystal microbalance. *Phys. Electrochem.*, 293-338 (1995).

19. Uosaki, K., Ye, S., Oda, Y., Haba, T. & Hamada, K.-i. Adsorption of hexachloroplatinate complex on Au(111) electrode. An in situ scanning tunneling

microscopy and electrochemical quartz microbalance study. *Langmuir* **13**, 594-596 (1997).

20. Cypress Sytems, http://www.cypresssystems.com/

21. Pastore, P., Badocco, D. & Zanon, F. Influence of nature, concentration and pH of buffer acid-base system on rate determining step of the electrochemiluminescence of Ru(bpy)32+ with tertiary aliphatic amines. *Electrochim. Acta* **51**, 5394-5401 (2006).

22. Masui, M., Sayo, H. & Tsuda, Y. Anodic oxidation of amines. I. Cyclic voltammetry of aliphatic amines at a stationary glassy-carbon electrode. *J. Chem. Soc. B: Phys. Org.* 973-6 (1968).

23. Lai, R. Y. & Bard, A. J. Electrogenerated Chemiluminescence. 70. The Application of ECL to Determine Electrode Potentials of Tri-n-propylamine, Its Radical Cation, and Intermediate Free Radical in MeCN/Benzene Solutions. *J. Phys. Chem. A* **107**, 3335-3340 (2003).

24. Bard, A. J. & Faulkner, L. R. *Electrochemical Methods: Fundamentals and Applications* (John Wiley & Sons, Inc., New York, 2001).

25. Ye, S., Ishibashi, C., Shimazu, K. & Uosaki, K. An in situ electrochemical quartz crystal microbalance study of the dissolution process of a gold electrode in perchloric acid solution containing chloride ion. *J. Electrochem. Soc.* **145**, 1614-1623 (1998).

26. *QCM200 Quartz Crstal microbalance Digital Controller and QCM25 5 MHz Crystal Oscillator: Operation and Service Manual* (Stanford Research Systems, 2006).

27. Frankenthal, R. P. & Siconolfi, D. J. The anodic corrosion of gold in concentrated chloride solutions. *J. Electrochem. Soc.* **129**, 1192-6 (1982).

28. Frankenthal, R. P. & Thompson, D. E. The anodic behavior of gold in sulfuric acid solutions. Effect of chloride and electrode potential. *J. Electrochem. Soc.* **123**, 799-804 (1976).

29. Horikoshi, T., Yoshimura, S., Kubota, N. & Sato, E. The anodic dissolution behavior of gold in sulfuric acid solutions containing chloride ions. *Nippon Kagaku Kaishi*, 1118-23 (1983).

30. Loo, B. H. In situ identification of halide complexes on gold electrode by surface-enhanced Raman spectroscopy. *J. Phys. Chem.* **86**, 433-7 (1982).

31. Martin, S. J., Spates, J. J., Wessendorf, K. O., Schneider, T. W. & Huber, R. J. Resonator/Oscillator Response to Liquid Loading. *Anal. Chem.* **69**, 2050-2054 (1997).

32. Diaz, M. A., Kelsall, G. H. & Welham, N. J. Electrowinning coupled to gold leaching by electrogenerated chlorine. I. Au(III)-Au(I)/Au kinetics in aqueous Cl_2/Cl^- electrolytes. *J. Electroanal. Chem.* **361**, 25-38 (1993).

CHAPTER III

ELECTOCHEMICAL AND ELCTROGENERATED CHEMILUMINESCENT STUDIES OF A TRINUCLEAR COMPLEX–$[((phen)_2Ru(dpp))_2RhCl_2]^{5+}$, AND ITS INTERACTIONS WITH CALF THYMUS DNA*

Introduction

Electrogenerated chemiluminescence (ECL), a process of light generation initiated by electrochemical reactions, has proven to be a very powerful analytical technique and been widely used in the areas of, for example, DNA probe, immunoassay, biowarfare agent testing, and environmental detection, due to its inherent features such as low background, high sensitivity, and excellent selectivity.[1-4] These applications are predominantly based on the fundamental ECL research work of a variety of inorganic and organic compounds[1,2,5] as well as different types of nanomaterials[6] including semi-conductive quantum dots[7] over the past 45 years since the pioneering ECL studies reported by Kuwana, Hercules, and Bard et al.[8-11] in the mid-1960s. Although ECL can be produced via ion annihilation reactions, which generally require the experiments conducted in dried organic solvent in the absence of molecular oxygen so that a wide potential window (both in positive and in negative directions) can be obtained and the ECL quenching by oxygen can be eliminated,[12] the majority of the ECL applications have been performed in aqueous media via the oxidative-reduction type coreactant ECL reactions[13] involving tris(2,2′-bipyridine)ruthenium(II) cation ($Ru(bpy)_3^{2+}$) or its derivatives as luminophore species and tri-*n*-propylamine (TPrA) or its analogues as the

* Part of this work has been published: Wang, S., Milam, J., Ohlin, A. C., Rambaran, V. H., Clark, E., Ward, W., Seymour, L., Casey, W. H., Holder, A. A. & Miao, W. *Anal. Chem.* **81**, 4068-4075 (2009).

coreactant.[14] This type of coreactant ECL needs the potential scanning or pulsing only in the positive region and the atmosphere effect (i.e., moisture and oxygen) on the ECL production is insignificant under commonly used experimental conditions. As a result, ECL-based detectors have been successfully incorporated into many analytical detection systems, which include flow injection analysis, high-performance liquid chromatography, capillary electrophoresis, and micro total analysis, for the quantification of analytes that could act as either ECL emitters or ECL coreactants.[15,16]

Among a large number of inorganic and organometallic complexes studied, only several reports on ECL with multimetallic systems have appeared, which include Mo,[17-19] W,[19,20] Pt,[21-23] and Pb[24] clusters as well as bimetallic Ru complexes.[25,26] Most of their ECL experiments were conducted in organic or mixed media because of the insolubility and instability of these complexes in an aqueous environment. In contrast to the metallic clusters, where weak ECL emissions were generally observed, bimetallic Ru complexes have demonstrated several times increases in ECL efficiency with respect to the $Ru(bpy)_3^{2+}$ standard,[25,26] making them promising ECL labels for use in analytical applications.

In the present study, the electrochemical and ECL behavior of a trinuclear, mixed-metal complex, $[((phen)_2Ru^{II}(dpp))_2Rh^{III}Cl_2]^{5+}$ (where phen = 1,10-phenanthroline, dpp = 2,3-bis-2-pyridylpyrazine, Figure 3.1), is reported. This complex, like other trinuclear complexes coupling light-absorbing ruthenium centers to reactive metal centers (e.g., $[((bpy)_2Ru(BL))_2MCl_2]^{5+}$, where M = Rh^{III} or Ir^{III} and BL = dpp[27] or 2,2'-bipyrimidine[28]), could offer the ability to control spectroscopic and redox properties important to photochemical applications. Recently, $[((bpy)_2Ru(dpp))_2RhCl_2](PF_6)_5$ complex has

demonstrated the ability to produce H_2 when excited with visible light in acetonitrile/H_2O solution in the presence of dimethylaniline electron donor.[29] Moreover, the photocleaving of DNA and the photochemical inhibition of cell replication of this complex[30,31] suggest strong interactions of the complex with DNA. Therefore, another objective of this study is to quantitatively monitor the intercalations of $[((phen)_2Ru^{II}(dpp))_2Rh^{III}Cl_2]^{5+}$ complex into DNA and to estimate the binding constant of the interactions using quartz crystal microbalance (QCM). This is the very first report of the binding kinetics involving trinuclear Ru-Rh complex and calf thymus DNA through the use of QCM.

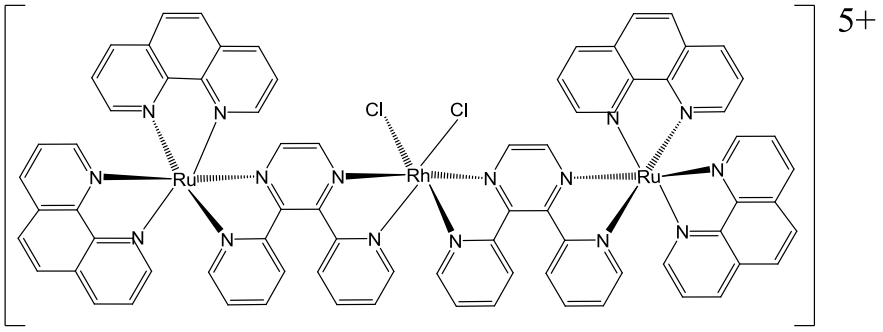

Figure 3.1. Structure of $[((phen)_2Ru(dpp))_2RhCl_2]^{5+}$.

Experimental Section

Chemicals and Materials

Tri-*n*-propylamine (TPrA, 99+%), sulfuric acid (H_2SO_4, 98%), nitric acid (HNO_3, 70%), and 11-mercapto-1-undecanol [$HSCH_2(CH_2)_9CH_2OH$, 97%] from Aldrich (Milwaukee, WI), hydrochloric acid (HCl, 37.5%), hydrogen peroxide (H_2O_2, 30%), and sodium chloride (NaCl, certified A.C.S.) from Fisher (Fairlawn, NJ), sodium hydroxide (NaOH, 98.7%) from J. T. Baker (Phillipsburg, NJ), silver nitrate ($AgNO_3$, 99.5%) and tetrabutylammonium perchlorate (TBAP, 99+%, electrochemical grade) from Fluka

(Milwaukee, WI), acetonitrile (MeCN, 99.93+%, HPLC grade), 2-(dibutylamino)ethanol (DBAE, 99%), calf thymus DNA (ctDNA), and 2-morpholinoethanesulfonic acid (MES, 99+%) from Sigma (St. Louis, MO), and 1-ethyl-3-(3-dimethylaminopropyl) carbodiimide (EDAC) and tris(hydroxymethyl)-aminomethane (Tris) from Pierce (Rockford, IL) were used as received. All aqueous solutions were prepared with deionized-distilled water produced from a Barnstead MP-6A Mega-Pure® system (Barnstead international Dubuque, Iowa).

Synthesis of $[(phen)_2Ru(dpp))_2RhCl_2]^{5+}$ Complexes

Water insoluble $[((phen)_2Ru(dpp))_2RhCl_2](PF_6)_5$ and water soluble $[(phen)_2Ru(dpp))_2RhCl_2]Cl_5$ complexes were synthesized by Dr. Alvin Holder's group in the Department of Chemistry and Biochemistry at the University of Southern Mississippi, using procedures similar to those previously reported.[27,31]

Instrumentation

Cyclic voltammetry (CV) was carried out with a model 660A electrochemical workstation (CH Instruments, Austin, TX). A conventional three-electrode cell was used, with a Pt wire as the counter electrode and an $Ag/AgCl/Cl^-$ (3.0 M KCl) or Ag/Ag^+ (10 mM $AgNO_3$ and 0.10 M TBAP in MeCN) as the reference electrode. Three different types of working electrodes, namely glassy carbon (GC, 3-mm diameter), Pt (2-mm diameter), and gold (Au, 2-mm diameter), were used for CV and ECL measurements. These electrodes were polished with 0.3-0.05-μm alumina slurry, thoroughly rinsed with water, and dried with the Kim wipes facial tissue before each experiment. The electrolyte solution was purged with high purity nitrogen (Nordan Smith, Hattiesburg, MS) for ~10

min and kept under nitrogen atmosphere during the measurement whenever a negative potential range was used.

The ECL signals along with the CV responses were measured simultaneously with a homemade ECL instrument as described previously.[1,32] This instrument combined the 660A electrochemical workstation with a photomultiplier tube (PMT, Hamamatsu R928, Japan) biased at a voltage of -700 V via a high voltage power supply (Model 472A Brandenburg PMT power supply, England), and the photocurrent detected with a high sensitive Keithley 6514 electrometer (Keithley, Cleveland, OH) was converted to a voltage before it was sent to the electrochemical workstation computer. ECL spectra were obtained by collecting the peak ECL intensity of the forward scan (~1.3 V vs Ag/Ag^+ in MeCN) during the cyclic potential cycling at a scan rate of 50 mV/s with 24 pieces of interference filters (Intro, Inc. Socorro, NM) over a spectral range of 360 to 820 nm. These filters had an average half-peak width of 10 nm and a transmittance value of 50% at the specified wavelength.

Fluorescence spectra were recorded with a Spex Fluorolog 2 fluorimeter (Horiba Jobin Yvon Inc., NJ). UV-visible spectroscopic measurements were performed with a Shimadzu UV-2401 PC Spectrometer (Columbia, MD).

QCM experiments were performed on a QCM200 Quartz-crystal Microbalance Digital Controller with a QCM25 5 MHz Crystal Oscillator (Stanford Research Systems, Sunnyvale, CA). A 5 MHz polished gold/Cr-coated AT-cut quartz crystal, with diameters of 2.54 and 1.32 cm for the quartz and the gold, respectively, was used. Data obtained from electrochemical deposition of silver by potential-step experiments from a 5.0 mM

$AgNO_3$ solution in 0.50 M HNO_3 were used to calibrate the QCM instrument,[33] resulting in a sensitivity factor of 51.7 Hz $cm^2/\mu g$ on the basis of the Sauerbrey equation.[34-37]

Immobilization of ctDNA onto Au/QCM Electrodes

AT-cut 5 MHz quartz-gold electrodes were cleaned with freshly prepared piranha solution (98% H_2SO_4/30% H_2O_2, 70/30 in v/v) for ~10 min, followed by washing with copious amounts of distilled water and then ethanol. The piranha solution was handled carefully because of its ability to react violently with organic materials. The Au electrodes were subsequently dried in a stream of N_2 before being transferred into a 1.0 mM ethanol solution of 11-mercapto-1-undecanol for ~24 h. The resulting electrodes were washed with ethanol to remove excess 11-mercapto-1-undecanol and then air-dried. The electrodes were then placed into a 10 mL of 40 mM MES buffered solution (pH 6.4) containing 10 mM EDAC and 1.3 mM ctDNA per nucleotide determined spectrophotometrically by employing an extinction coefficient of 6600 M^{-1} cm^{-1} at 260 nm.[38] This mixture was kept at 4 ℃ for 72 h with addition of ~20 mg of EDAC into the solution every few hours. In this way, covalent immobilization of the ctDNA onto the thiol coated-Au/QCM electrode *via* phosphate ester formation from the condensation reaction between 5′-end of ctDNA and the hydroxyl group of 11-mercapto-1-undecanol can be realized.[39,40] The obtained electrodes were cleaned with 0.20 M Tris-HCl buffer (pH 7.4) and distilled water, and then kept in 0.20 M Tris buffer-HCl (pH 7.4) at 4 ℃ until further use.

ctDNA-$[((phen)_2Ru(dpp))_2RhCl_2]^{5+}$ Binding Constant Measurements

A QCM flow cell (Stanford Research Systems, Sunnyvale, CA) with above mentioned ctDNA immobilized Au/QCM electrode was connected to a peristaltic pump

(VWR International) and used for the ctDNA-$[((phen)_2Ru(dpp))_2RhCl_2]^{5+}$ binding constant measurements. To eliminate the temperature effect on the frequency change of the QCM, the experiment was performed in a small constant temperature room of 25.00 ± 0.01 ℃, and the flow cell as well as the buffer solution (10.00 mL of 0.20 M Tris-HCl, pH 7.4) was kept in a thermo-insulating foam box on an anti-vibration pad. The instrument was pumped with the buffer at a flow rate of 0.44 mL/min until the frequency change of less than 0.1 Hz over 10 min was reached. This was followed by adding μL levels of 1.00 mM $[((phen)_2Ru(dpp))_2RhCl_2]Cl_5$ in 0.20 M Tris-HCl (pH 7.4) to the buffer solution at various time intervals, and the corresponding frequency change was recorded.

Results and Discussion

Cyclic Voltammetry of $[((phen)_2Ru(dpp))_2RhCl_2]^{5+}$ Complex

Figures 3.2a-c show the cyclic voltammograms of 1.0 mM $[((phen)_2Ru(dpp))_2RhCl_2](PF_6)_5$ in MeCN containing 0.10 M TBAP at various reduction potentials using a 2 mm Pt electrode at a scan rate of 50 mV/s. Only one reversible redox process (process 1) with $E_{1/2}$ = 1.21 V vs Ag/Ag^+ that corresponds to the electron transfer of $Ru^{II/III}$ was observed, suggesting that the two Ru^{II} centers are chemically equivalent and largely electronically uncoupled.[41,42] The irreversible reduction of process 2 at -0.73 V vs Ag/Ag^+ can be attributed to a two-electron transfer of Rh^{III} to Rh^{I}, which shows a slightly smaller peak current than that of process 1 as expected. Quasi-reversible process 3 ($E_{1/2}$ = -1.11 V vs Ag/Ag^+; $\Delta E \approx$ 110 mV) and process 4 ($E_{1/2}$ = -1.36 V vs Ag/Ag^+; $\Delta E \approx$ 100 mV) result from a one-electron transfer of the first ligand $dpp^{0/-}$ and the second $dpp^{0/-}$, respectively. This assignment is based on the ratio of peak current

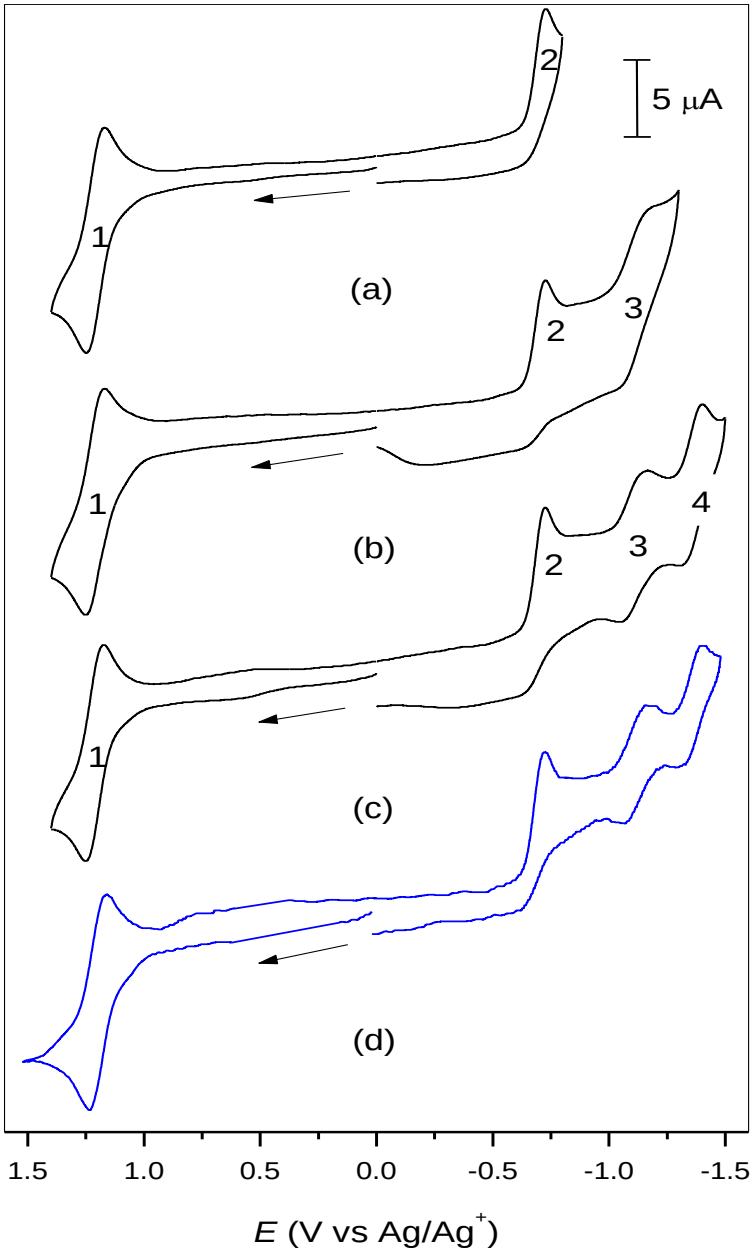

Figure 3.2. Cyclic voltammograms obtained from (a)-(c) 1.0 mM $[((phen)_2Ru(dpp))_2RhCl_2](PF_6)_5$ at various negative potential scanning limits and (d) 1.0 mM $[((bpy)_2Ru(dpp))_2RhCl_2](PF_6)_5$ in MeCN containing 0.10 M TBAP at a 2 mm Pt electrode with a scan rate of 50 mV/s.

(Figure 3.2c, $i_{p2} \approx 2i_{p3} \approx 2i_{p4}$) as well as the comparison of the CVs between $[((phen)_2Ru(dpp))_2RhCl_2](PF_6)$ (Figure 3.2c) and its analogue $[((bpy)_2Ru(dpp))_2RhCl_2](PF_6)_5$[30] (where bpy = 2,2′-bipyridine, Figure 3.2d), where almost identical redox peak potentials are present for respective processes.

The CV of the complex (as chloride) in aqueous solution was conducted at a GC electrode with 0.20 M Tris buffer (pH 7.4) as the supporting electrolyte. In this way, a relatively wide potential window (GC vs Pt and Au) can be obtained, and the data obtained from the neutral pH media could be valuable for the production of intensive ECL in water.[43] Phosphate buffered solution was not chosen because the coordinated chloride ligand of the complex may slowly exchange with phosphate ions. As shown in Figure 3.3a, a large irreversible oxidation peak at +1.48 V vs Ag/AgCl on the forward scan and a relatively small, but broad irreversible reduction wave at -0.78 V vs Ag/AgCl on the reverse scan are observed. The former response must result from the oxidation of the two Ru^{II} species as discussed in MeCN, whereas the later wave appears to be a one-electron reduction of Rh^{III} to Rh^{II} because the ratio of integrated charge involved for the oxidation and reduction is close to 2:1.

ECL Behavior of $[((phen)_2Ru(dpp))_2RhCl_2]^{5+}$ Complex in MeCN and Aqueous Media.

The oxidative-reduction type ECL[44] was used to investigate the ECL behavior of the complex in the presence of coreactant DBAE[45] and TPrA. Figure 3.4 shows CV (solid line) and ECL (dashed line) responses of 0.10 mM $[((phen)_2Ru(dpp))_2RhCl_2](PF_6)_5$ complex with 20.0 mM DBAE in MeCN containing 0.10 M TBAP at a Pt electrode. Peaks 1 and 2 on the CV result from the oxidation of DBAE (0.62 V vs Ag/Ag^+, eq. (3.1)) and the oxidation of $[((phen)_2Ru(dpp))_2RhCl_2]^{5+}$ catalyzed by DBAE (1.30 V vs Ag/Ag^+).

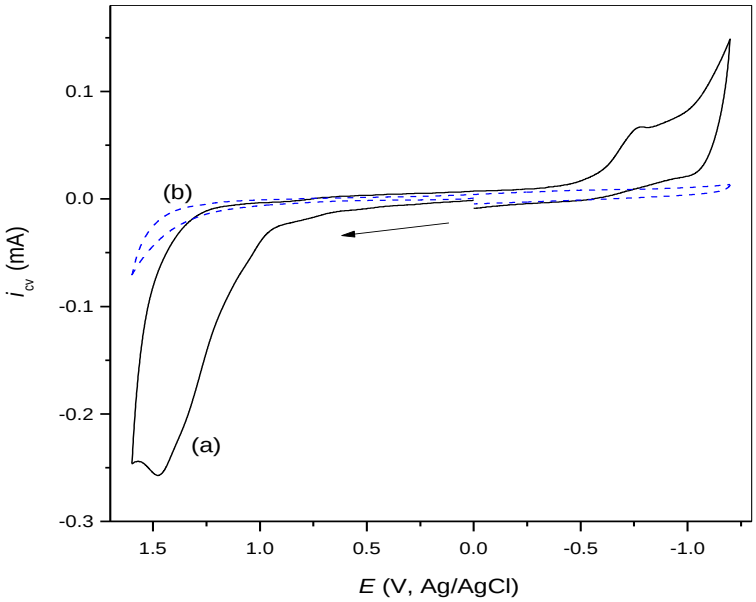

Figure 3.3. Cyclic voltammograms obtained from (a) 5.0 mM $[((phen)_2Ru(dpp))_2RhCl_2]Cl_5$ in 0.20 M Tris buffer (pH 7.4) at a 3 mm GC electrode with a scan rate of 50 mV/s, and (b) blank.

ECL profiles reveal that both forward and reverse scans generate broad ECL peaks around the oxidation peak potential of the emitter. Similar behavior was reported previously for the $Ru(bpy)_3^{2+}$/TPrA system in MeCN,[46,47] although in the present case, noticeable ECL is produced even before the oxidation of $[((phen)_2Ru(dpp))_2RhCl_2]^{5+}$ species (i.e., in the potential range of 0.5 to 0.9 V vs Ag/Ag^+). As shown in Scheme 3.1, this low potential ECL emission, as often seen from the $Ru(bpy)_3^{2+}$/TPrA system in neutral media from GC and Au electrode,[33,48-50] could be originated from the initial electrode oxidation of DBAE (eq.(3.1)), followed by a series of chemical reactions that lead to the formation of excited state Ru_2Rh^* species (eqs. (3.2-3.4), where Ru_2Rh = $[((phen)_2Ru(dpp))_2RhCl_2]^{5+}$, and Ru_2Rh^- results from a one-electron reduction of the Rh center) and light emission (eq. (3.5)).

$$DBAE - e \rightarrow DBAE^{\bullet +} \quad (3.1)$$

$$DBAE^{\bullet +} - H^{+} \rightarrow DBAE^{\bullet} \quad (3.2)$$

$$Ru_2Rh + DBAE^{\bullet} \rightarrow Ru_2Rh^{-} + P_1 \quad (3.3)$$

$$DBAE^{\bullet +} + Ru_2Rh^{-} \rightarrow Ru_2Rh^{*} + DBAE \quad (3.4)$$

$$Ru_2Rh^{*} \rightarrow Ru_2Rh + h\nu \quad (3.5)$$

(where DBAE = $Bu_2NCH_2CH_2OH$, $DBAE^{\bullet +} = Bu_2N^{\bullet +}CH_2CH_2OH$, $DBAE^{\bullet} = Bu_2NC^{\bullet}HCH_2OH$, $P_1 = Bu_2N^{+}{=}CHCH_2OH$, $Ru_2Rh = [((phen)_2Ru(dpp))_2RhCl_2]^{5+}$)

Scheme 3.1. Proposed ECL mechanism of $[((phen)_2Ru(dpp))_2RhCl_2]^{5+}$/DBAE system at low oxidation potential region in MeCN.

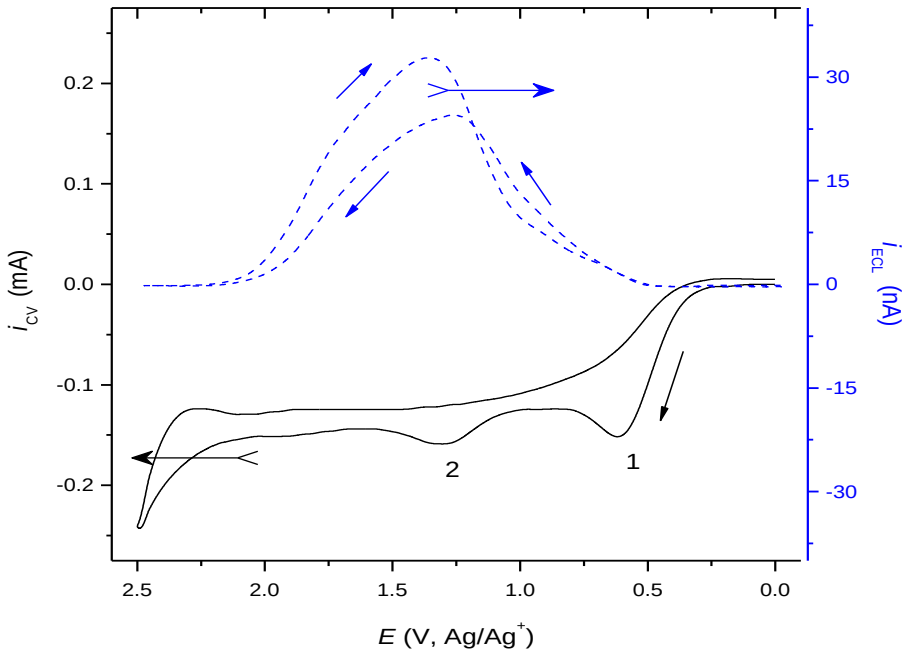

Figure 3.4. CV (solid line) and ECL (dashed line) responses of 0.10 mM $[((phen)_2Ru(dpp))_2RhCl_2](PF_6)_5$ with 0.10 M TBAP and 70 mM DBAE in MeCN at a 2 mm Pt electrode with a scan rate of 50 mV/s.

Similar to the $Ru(bpy)_3^{2+}$/TPrA system, the ECL generation of the main waves in the Ru_2Rh/DBAE system should be also initiated by the electro-oxidation of the emitting complex. That is, upon the anodic potential scanning, DBAE is first oxidized and immediately deprotonated (eq. (3.1-3.2)), followed by catalytic oxidations of Ru_2Rh with DBAE (eqs. (3.6-3.8)). Note that oxidations of Ru_2Rh shown in eqs. (3.6) and (3.7) occur almost at the same electrode potential as revealed by CV (Figure 3.2).

$$Ru_2Rh - e \rightarrow Ru_2Rh^{+} \quad (3.6)$$

$$Ru_2Rh^{+} - e \rightarrow Ru_2Rh^{2+} \quad (3.7)$$

$$Ru_2Rh^{2+} + 2DBAE \rightarrow Ru_2Rh + 2DBAE^{\bullet +} \quad (3.8)$$

Reduced Ru_2Rh species resulting from the reduction of the Rh center of the complex, Ru_2Rh^{-} and Ru_2Rh^{2-}, are then formed via eqs. (3.3) and (3.9).

$$Ru_2Rh^{-} + DBAE^{\bullet} \rightarrow Ru_2Rh^{2-} + P_1 \quad (3.9)$$

The two-electron oxidized and reduced complexes could react with the parent species to produce the one-electron products in the course of diffusion toward the bulk solution (eqs. (3.10-3.11)).

$$Ru_2Rh + Ru_2Rh^{2+} \rightarrow 2Ru_2Rh^{+} \quad (3.10)$$

$$Ru_2Rh + Ru_2Rh^{2-} \rightarrow 2Ru_2Rh^{-} \quad (3.11)$$

In the co-presence of Ru_2Rh^{2+}, Ru_2Rh^{+}, Ru_2Rh^{-}, and Ru_2Rh^{2-}, the excited state species, Ru_2Rh^{*}, could be generated via the following four annihilation reactions (eqs. (3.12-3.14)), although a two-electron transfer to produce an excited state (eq. (3.13)) is unlikely.[25]

$$Ru_2Rh^{2+} + Ru_2Rh^{-} \rightarrow Ru_2Rh^{+} + Ru_2Rh^{*} \quad (3.12)$$

$$Ru_2Rh^{2+} + Ru_2Rh^{2-} \rightarrow Ru_2Rh + Ru_2Rh^{*} \quad (3.13)$$

$$Ru_2Rh^{+} + Ru_2Rh^{-} \rightarrow Ru_2Rh + Ru_2Rh^{*} \quad (3.14)$$

$$Ru_2Rh^{+} + Ru_2Rh^{2-} \rightarrow Ru_2Rh^{-} + Ru_2Rh^{*} \quad (3.15)$$

Finally, the ECL is produced after the emission of light from Ru_2Rh^{*} (eq. (3.5)). A previous ECL study on a bimetallic complex, $[(bpy)_2Ru]_2(bphb)^{4+}$ (bphb = 1,4-bis(4′-methyl-2,2′-bipyridin-4-yl)benzene)], has suggested that the one-electron annihilation reactions are the major ECL contributors.[25] Therefore, in the present case, contributions of eqs. (3.12-3.13) and (3.15) to the overall emission process could be minor.

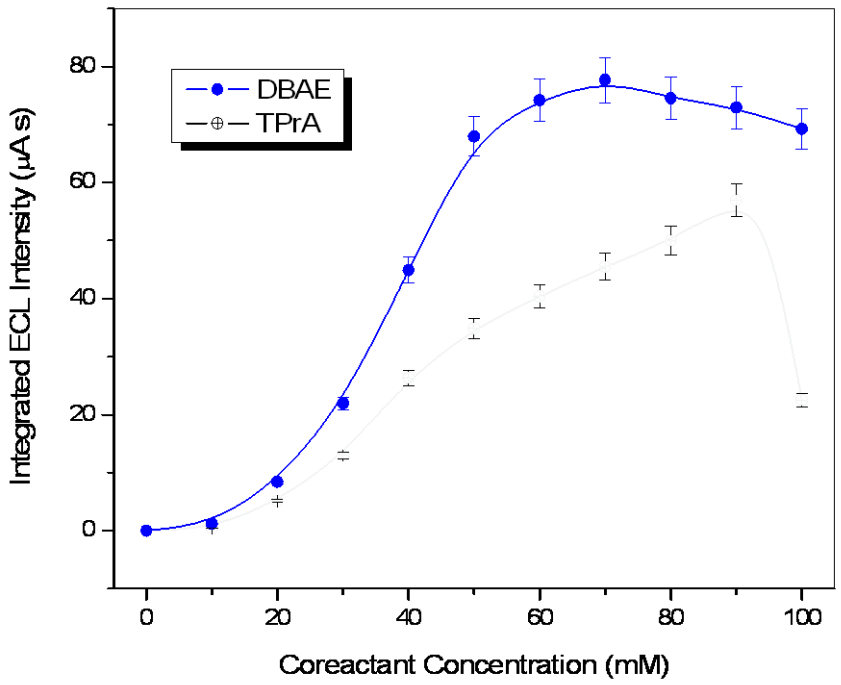

Figure 3.5. Effect of coreactant and its concentration on ECL intensity obtained from 0.10 mM $[((phen)_2Ru(dpp))_2RhCl_2](PF6)_5$ containing 0.10 M TBAP with different concentrations of DBAE and TPrA in MeCN at a 2 mm Pt with a scan rate of 50 mV/s.

Very similar ECL profiles were observed when TPrA was used as the coreactant. However, as shown in Figure 3.5, much stronger ECL intensities are obtained from the DBAE system over an entire coreactant concentration range of 10 to 100 mM, in which the maximum ECL emissions at 70 mM of DBAE and 90 mM of TPrA at a Pt electrode in MeCN are evident. In addition, with respective to TPrA, DBAE produced much smaller background ECL signals in MeCN, resulting in a limit detection of 0.10 μM of the complex using 70 mM DBAE coreactant (eq. (3.16)).

$$\text{Integrated ECL intensity } (\mu A\ s) = 0.901 + 0.574 \times [Ru_2Rh]\ (\mu M) \qquad (3.16)$$
$$([Ru_2Rh] \geq 0.10\ \mu M,\ R^2 = 0.997)$$

The effect of electrode material on the ECL generation was also studied. The relative integrated ECL intensity, obtained from a MeCN solution containing 0.10 M $[((phen)_2Ru(dpp))_2RhCl_2](PF_6)_5$-70 mM DBAE-0.10 M TBAP during the first potential cycle between 0 and 2.5 V vs Ag/Ag^+ at a scan rate of 50 mV/s, at Pt, Au, and GC electrodes had a ratio of 100:100:30. The reason behind still remains unclear.

Two ECL waves, located at 1.00 V and 1.42 V vs Ag/AgCl, are present on the forward scan of the CV from the $[((phen)_2Ru(dpp))_2RhCl_2]Cl_5$/TPrA system in 0.20 M Tris buffer (pH 7.4) at a GC electrode (Figure 3.6a). Under the same experimental conditions, the $Ru(bpy)_3^{2+}$/TPrA system shows very similar ECL responses (Figure 3.6c), which suggests the same ECL mechanisms described previously[48] are probably operative for the two systems. In both cases, essentially the same CVs are obtained as displayed in Figure 3.6b because this process is predominately controlled by the TPrA oxidation (0.10 M) and the catalytic reactions of the ECL emitter (1.0 μM) with TPrA is negligible. Using 1.0 μM $Ru(bpy)_3^{2+}$/0.10 M TPrA as a reference ($\varphi_{ECL} = 1.0$), the 1.0 μM $[((phen)_2Ru(dpp))_2RhCl_2]Cl_5$/0.10 M TPrA system showed an ECL efficiency of ~0.014

on the basis of the integrated ECL intensities. This is unexpected because previously a few bimetallic Ru complexes have demonstrated several times increases in ECL efficiency (i.e., the ratio of the number of photons emitted to the number of annihilations between the oxidized and the reduced forms of the emitter complex) as compared to the $Ru(bpy)_3^{2+}$ standard.[25,26] The complex Ru_2Rh in the present study has also two Ru centers but linked with a Rh-containing bridge (Figure 3.1). This Rh center can be reduced as described above by CV and can function as an electron acceptor. Therefore, the experimentally obtained low ECL efficiency from Ru_2Rh complex could be attributed to the efficient intra-molecular electron-transfer quenching of Ru-based excited states by the Rh center.

A limit detection of 1.0 nM of $[((phen)_2Ru(dpp))_2RhCl_2]Cl_5$ was evaluated with 0.10 M TPrA as the ECL coreactant in 0.20 M Tris buffer neutral media at a GC electrode (eq. (3.17)). This limit of detection is about 100 and 1000 times lower than that obtained from UV-Visible and fluorescence spectroscopy, respectively.

$$\text{Log}\,[i_{ECL}\ (\mu\text{A s})] = 5.57 + 0.645 \times \text{Log}\{[Ru_2Rh]\ (\text{M})\} \qquad (3.17)$$
$$([Ru_2Rh] \geq 1.0\ \text{nM},\ R^2 = 0.999)$$

The ECL emission spectra recorded from the oxidative-reduction process of $[((phen)_2Ru(dpp))_2RhCl_2]^{5+}$-DBAE in MeCN containing 0.10 M TBAP shows a broad emission band between 500 and 850 nm with a maximum at ~640 nm (Figure 3.7). Compared to the fluorescence that shows a broad spectrum at ~695 nm, ECL spectra demonstrate a ~55 nm blue shift (Figure 3.7). This difference is unlikely due to possible problems associated with the ECL and fluorescence instruments (e.g., low resolution) where the spectra were collected, because both instruments were pre-calibrated with the standard $Ru(bpy)_3^{2+}$/TPrA system. Such unusual blue shift behavior has been reported

previously for three aryl-diamide bridged binuclear ruthenium (II) tris(bipyridine) complexes[26] as well as for a series of N,N-dimethylaminophenylethynylarenes,[51] where a blue shift of ~24-65 nm ECL as compared to the fluorescence emissions were observed.

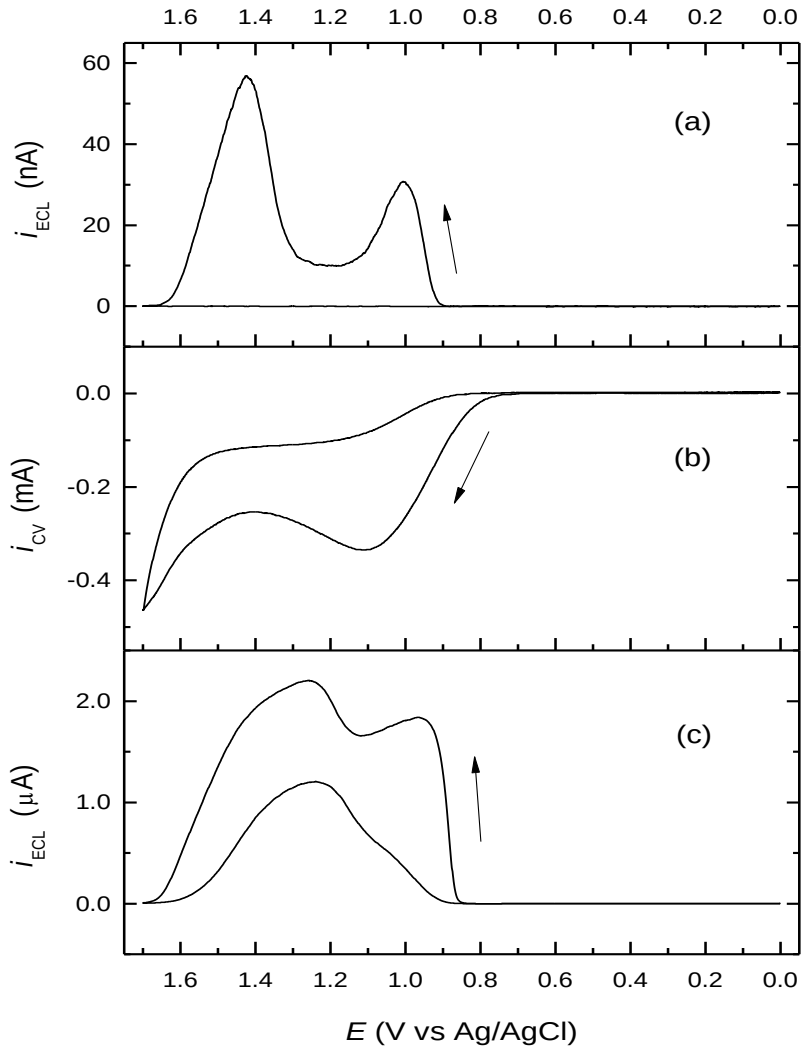

Figure 3.6. ECL responses of (a) 1.0 μM $[((phen)_2Ru(dpp))_2RhCl_2]Cl_5$/0.10 M TPrA and (c) 1.0 μM $Ru(bpy)^{2+}$/0.10 M TPrA in 0.20 M Tris buffer (pH 7.4) at a 3 mm GC electrode at a scan rate of 50 mV/s. CV responses from both systems were essentially the same as displayed in (b).

The formation of the "H-type" excimers[26,51] in the latter case was believed to be responsible for the blue shift. As a result, in our present study, the ECL emissive state may have a unique structure that is formed under the ECL experimental conditions (e.g., via ion annihilations) and is rather different from the photoluminescent state.

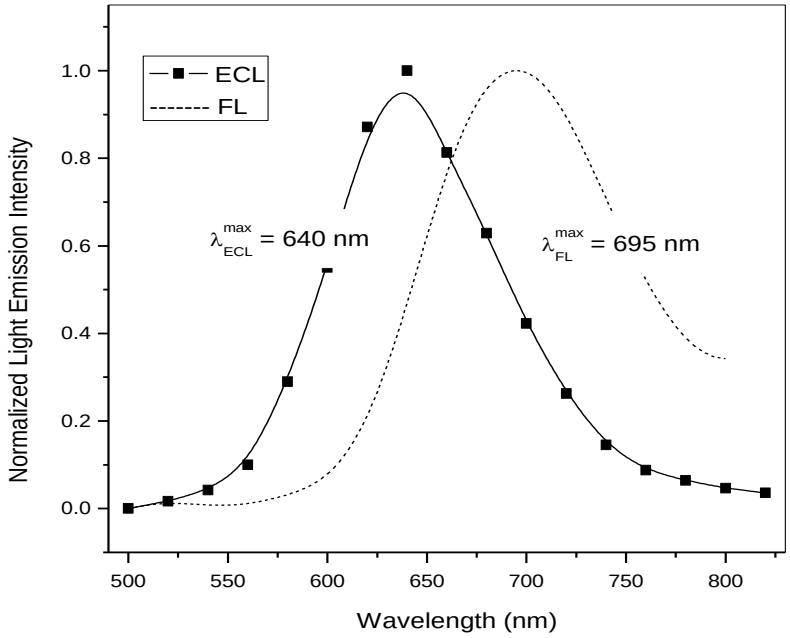

Figure 3.7. ECL emission (squared line) and fluorescence (dotted line) spectra of $[((phen)_2Ru(dpp))_2RhCl_2]^{5+}$ in MeCN. For ECL study a solution of 2.0 mM complex-70 mM DBAE-0.10 M TBAP in MeCN was used with a cyclic potential scanning between 0 and 2.50 V vs Ag/Ag^+ at a 2 mm Pt electrode at a scan rate of 50 mV/s. The fluorescence spectrum was produced with 0.10 μM of the complex in MeCN with an excitation wavelength of 400 nm.

Interaction of $[((phen)_2Ru(dpp))_2RhCl_2]^{5+}$ Complex with ctDNA

QCM has been proven to be very sensitive in measuring nanogram-level mass changes at the surface of a QCM electrode in gas phase and in aqueous solution.[35,52,53] For example, Okahata's group[54,55] has utilized QCM to detect various biomolecule

interactions such as DNA–DNA hybridization,[56,57] DNA–protein interactions,[58,59] sugar–protein interactions,[60-62] and protein–protein interactions[63] in aqueous solution. One of the key principles for the above measurements is the Sauerbrey equation (eq. (3.18)),[34-37] which indicates that the resonance frequency increases linearly upon the decrease of mass on a QCM electrode.

$$\Delta f = -C_f \times \Delta m \qquad (3.18)$$

where Δf is the experimentally measured frequency shift caused by change of a mass per unit area, Δm, to the crystal surface, and C_f is the sensitivity factor which has a calibrated value of 51.7 Hz $cm^2/\mu g$ for our present QCM instrument.[33]

In this study, the ctDNA-$[((phen)_2Ru(dpp))_2RhCl_2]^{5+}$ interactions in 0.20 M Tris-HCl buffer (pH 7.4) were monitored with QCM at a constant temperature of 25.00 ± 0.01 ℃ after additions of certain amounts of the complex into a flow QCM system that contains a ctDNA immobilized Au/QCM electrode. As shown in Figure 3.8a, with addition of the complex into the solution, the frequency drops accordingly, suggesting the intercalations of the complex into the DNA. This is confirmed by a control experiment (Figure 3.8b), where relatively high concentrations of $Ru(bpy)_3^{2+}$ (1-100 μM) were added to a separate flow system with freshly prepared ctDNA-Au/QCM electrode. No frequency changes are observed as expected because $Ru(bpy)_3^{2+}$ has been known to have no interactions with ctDNA.

An alternative plot of Figure 3.8a is shown in Figure 3.9a, where changes in mass (Δm) were calculated from Eq. (18), and the x-axis is the complex concentration in the flow system. Clearly, at the high concentration, intercalation of the complex into the DNA approaches a saturated-status. Assuming the interaction process meets the

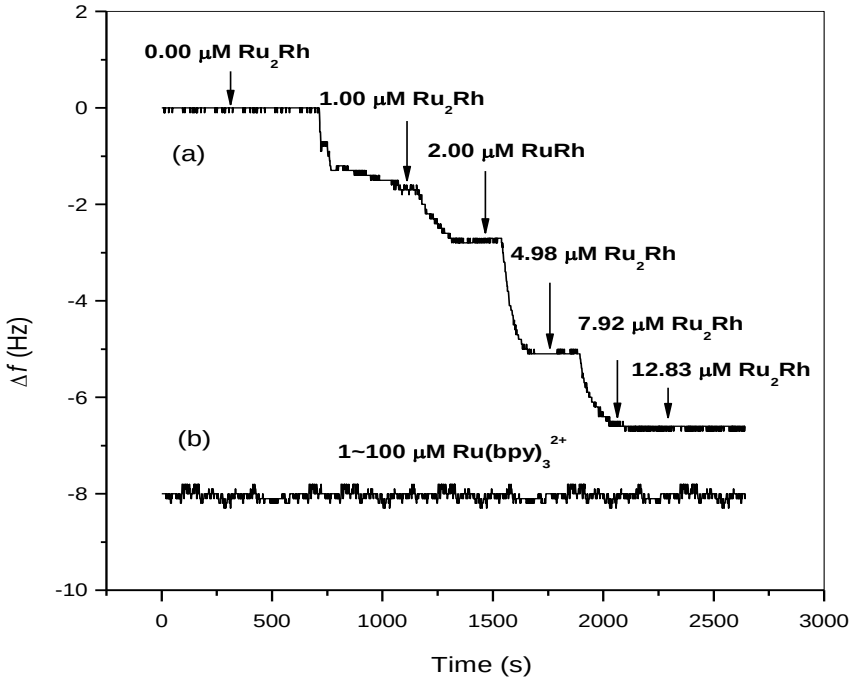

Figure 3.8. QCM frequency changes versus time for (a) intercalations of $[((phen)_2Ru(dpp))_2RhCl_2]^{5+}$ complex into ctDNA immobilized on a Au-coated QCM electrode in 0.20 M Tris buffer (pH 7.4) solution at 25.00 ± 0.01 ℃, and (b) as (a) but the complex was replaced with $Ru(bpy)_3^{2+}$. Concentrations are labeled as the final ones in the buffer and the flow rate of 0.44 mL/min was used.

requirements of the Langmuir isotherm,[64,65] the binding constant (i.e., equilibrium constant, K_b) can be expressed as:

$$ctDNA|_{QCM} + Ru_2Rh \rightleftharpoons ctDNA\text{-}Ru_2Rh|_{QCM} \quad (3.19a)$$

$$K_b = \frac{[ctDNA\text{-}Ru_2Rh|_{QCM}]}{[ctDNA|_{QCM}][Ru_2Rh]} \quad (3.19b)$$

where $[ctDNA|_{QCM}]$ and $[Ru_2Rh]$ represent the surface concentration of ctDNA on Au/QCM and the solution concentration of $[((phen)_2Ru(dpp))_2RhCl_2]^{5+}$ complex in the

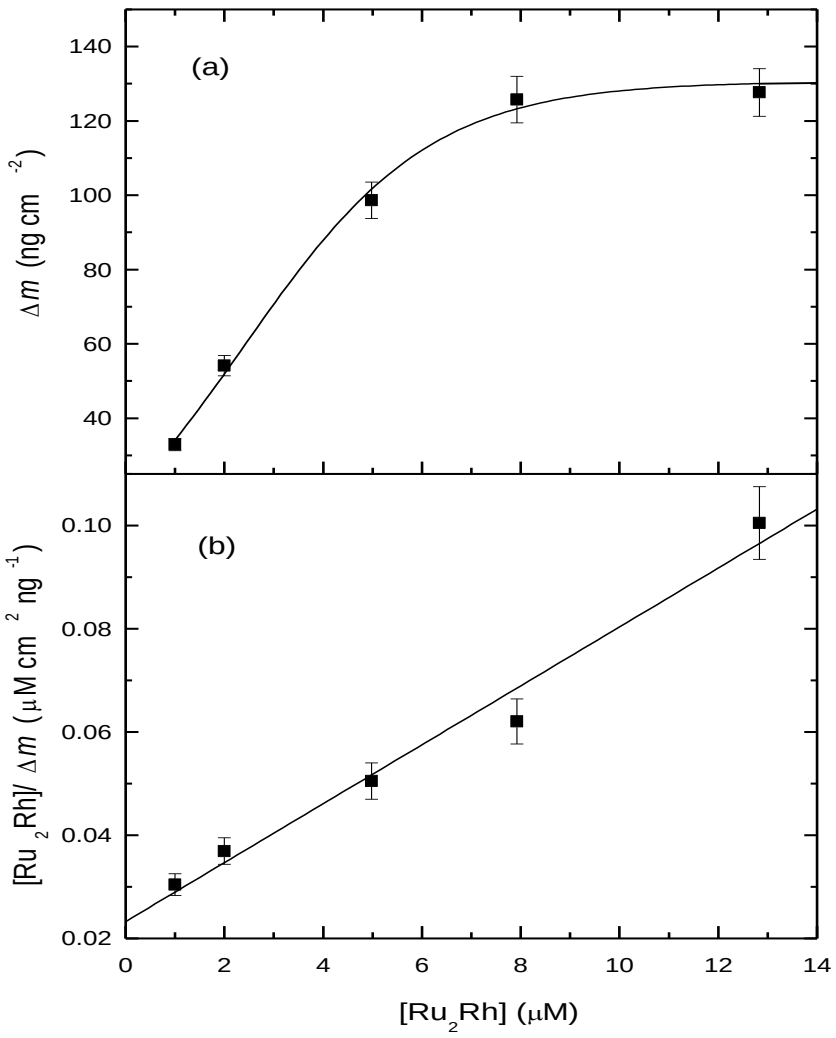

Figure 3.9. Langmuir isotherms obtained from the interactions between $[((phen)_2Ru(dpp))_2RhCl_2]^{5+}$ complex in 0.20 M Tris buffer (pH 7.4) and ctDNA immobilized on a Au-coated QCM electrode at 25.00 ± 0.01 ˚C. (a) Non-linear regression between Δ*m* and [Ru_2Rh], (b) linear regression between [Ru_2Rh]/Δ*m* and [Ru_2Rh].

buffer, respectively. Thus, the relationship between the instant mass change (Δm), the maximum mass change (Δm_{max}), the solution concentration of the complex, and the binding constant (K_b) can be described as follows:

$$\Delta m = \Delta m_{max} \frac{[Ru_2Rh]K_b}{1 + K_b[Ru_2Rh]} \qquad (\text{at } 25 \pm 0.1\ ^\circ C) \tag{3.20a}$$

Eq. (3.20a) can be rearranged to give Eq. (3.20b):

$$\frac{[Ru_2Rh]}{\Delta m} = \frac{1}{\Delta m_{max} K_b} + \frac{[Ru_2Rh]}{\Delta m_{max}} \tag{3.20b}$$

That is, $[Ru_2Rh]/\Delta m$ versus $[Ru_2Rh]$ should give a straight line, in which $1/(\Delta m_{max} K_b)$ will be the intercept and $1/(\Delta m_{max})$ will be the slope. Figure 3.9b depicts such a plot, which results in an intercept of 2.33×10^{-2} μM cm^2 ng^{-1} and a slope of 5.71×10^{-3} cm^2 ng^{-1}. Accordingly, Δm_{max} = 175 ng cm^{-2} and $K_b = 2.5\times10^5$ M^{-1} are obtained. This K_b value compares favorably with that of $K_{b(EtBr)} = 1.2\times10^5$ M^{-1} for the binding of ethidium bromide (EtBr) to salmon testes DNA in a QCM experiment.[58,66] $K_{b(EtBr)}$ values of 2.6×10^5 M^{-1}, 5×10^5 M^{-1}, and 1.9×10^5 M^{-1} were also obtained with other techniques such as equilibrium dialysis,[67] surface plasmon resonance,[68] and UV-visible spectrophotometry,[69] respectively. The consistence of the QCM based binding constant $K_{b(EtBr)}$ with those measured from other methods suggests that QCM could be a reliable technique for the measurement of binding constant for complex intercalations with double-stranded DNAs.

Conclusions

The electrochemical and electrogenerated chemiluminescent behavior of a mixed-metal supramolecular complex, $[((phen)_2Ru(dpp))_2RhCl_2]^{5+}$, was studied in MeCN and

aqueous solutions. In MeCN, a reversible, overlapping redox process of $Ru^{II/III}$ and an irreversible reduction of $Rh^{III/I}$, followed by two quasi-reversible $dpp^{0/-}$ couples, were observed. In aqueous solution, however, the $Ru^{II/III}$ process became irreversible and only one-electron transfer was involved in the reduction of Rh^{III}. ECL produced with both DBAE and TPrA coreactant suggested that mechanisms similar to the $Ru(bpy)_3^{2+}$/TPrA system in respective solvent should be followed. About 55 nm blue shift of ECL to its fluorescence and 1.4 % of ECL efficiency relative to the standard $Ru(bpy)_3^{2+}$/TPrA system were obtained. Interactions of the complex with ctDNA were monitored with a flow-cell based QCM in Tris buffer, which provided a binding constant of 2.5×10^5 M^{-1} on the basis of the Langmuir isotherm.

References

1. Miao, W. Electrogenerated Chemiluminescence and Its Biorelated Applications. *Chem. Rev.* **108**, 2506-2553 (2008).
2. Richter, M. M. Electrochemiluminescence (ECL). *Chem. Rev.* **104**, 3003-3036 (2004).
3. Bard, A. J. (ed.) *Electrogenerated Chemiluminescence* (Marcel Dekker, Inc., New York, 2004).
4. Xu, X.-H. N. & Zu, Y. Electrochemiluminescence detection in bioanalysis, in *New Frontiers in Ultrasensitive Bioanalysis* (ed. Xu, X.-H. N.), 235-267 (John Wiley & Sons, Inc., Hoboken, NJ, 2007).
5. Richter, M. M. Metal chelate systems, in *Electrogenerated Chemiluminescence* (ed. Bard Allen, J.), 321-358, Chapter 7 (Marcel Dekker, Inc, New York, 2004).
6. Qi, H., Peng, Y., Gao, Q. & Zhang, C. Applications of Nanomaterials in Electrogenerated Chemiluminescence Biosensors. *Sensors* **9**, 674-695 (2009).
7. Bard, A. J., Ding, Z. & Myung, N. Electrochemistry and electrogenerated chemiluminescence of semiconductor nanocrystals in solutions and in films. *Structure and Bonding (Berlin, Germany)* **118**, 1-57 (2005).
8. Kuwana, T., Epstein, B. & Seo, E. T. Electrochemical generation of solution luminescence. *J. Phys. Chem.* **67**, 2243-4 (1963).
9. Santhanam, K. S. V. & Bard, A. J. Chemiluminescence of electrogenerated 9,10-diphenylanthracene anion radical. *J. Am. Chem. Soc.* **87**, 139-140 (1965).
10. Hercules, D. M. Chemiluminescence Resulting from Electrochemically Generated Species. *Science* **145**, 808 (1964).
11. Visco, R. E. & Chandross, E. A. Electroluminescence in Solutions of Aromatic Hydrocarbons. *J. Am. Chem. Soc.* **86**, 5350 (1964).

12. Fan, F. R. F. Experimental Techniques of Electrogenerated Chemiluminescence, in *Electrogenerated Chemiluminescence* (ed. Bard, A. J.), 23-100, Chapter 2 (Marcel Dekker, Inc., New York, 2004).

13. Rubinstein, I. & Bard, A. J. Electrogenerated chemiluminescence. 37. Aqueous ecl systems based on tris(2,2'-bipyridine)ruthenium(2+) and oxalate or organic acids. *J. Am. Chem. Soc.* **103**, 512-16 (1981).

14. Miao, W. & Choi, J.-P. Coreactants, in *Electrogenerated Chemiluminescence* (ed. Bard, A. J.), 213-272, Chapter 5 (Marcel Dekker, Inc., New York, 2004).

15. Yin, X.-B., Dong, S. & Wang, E. Analytical applications of the electrochemiluminescence of tris(2,2'-bipyridyl) ruthenium and its derivatives. *TrAC, Trends in Anal. Chem.* **23**, 432-441 (2004).

16. Danielson, N. D. Analytical Application: Flow injection, Liquid Chromatography, and Capillary Electrophoresis, in *Electrogenerated Chemiluminescence* (ed. Bard, A. J.), 397-444, Chapter 9 (Marcel Dekker, Inc., New York, 2004).

17. Ouyang, J., Zietlow, T. C., Hopkins, M. D., Fant, F. R. F., Gray, H. B. & Bard, A. J. Electrochemistry and electrogenerated chemiluminescence of tetrachlorotetrakis(trimethylphosphine) dimolybdenum. *J. Phys. Chem.* **90**, 3841-4 (1986).

18. Maverick, A. W. & Gray, H. B. Luminescence and redox photochemistry of the molybdenum(II) cluster Mo6Cl142. *J. Am. Chem. Soc.* **103**, 1298-300 (1981).

19. Maverick, A. W., Najdzionek, J. S., MacKenzie, D., Nocera, D. G. & Gray, H. B. Spectroscopic, electrochemical, and photochemical properties of molybdenum(II) and tungsten(II) halide clusters. *J. Am. Chem. Soc.* **105**, 1878-82 (1983).

20. Mussell, R. D. & Nocera, D. G. Partitioning of the electrochemical excitation energy in the electrogenerated chemiluminescence of hexanuclear molybdenum and tungsten clusters. *Inorg. Chem.* **29**, 3711-17 (1990).

21. Vogler, A. & Kunkely, H. Electrochemiluminescence of tetrakis(diphosphite)diplatinate(II). *Angew. Chem.* **96**, 299-300 (1984).

22. Kim, J., Fan, F. F., Bard, A. J., Che, C. M. & Gray, H. B. Electrogenerated chemiluminescence. On the electrogenerated chemiluminescence (ECL) of tetrakis(pyrophosphito)diplatinate(II), $Pt_2(P_2O_5H_2)_4^{4-}$. *Chem. Phys. Lett.* **121**, 543-6 (1985).

23. Kane-Maguire, N. A. P., Wright, L. L., Guckert, J. A. & Tweet, W. S. Photoluminescence and electrogenerated chemiluminescence of palladium(0) and platinum(0) complexes of dibenzylideneacetone and tribenzylideneacetylacetone. *Inorg. Chem.* **27**, 2905-7 (1988).

24. Singh, P. & Richter, M. M. Electrogenerated chemiluminescence of Pb(II)-bromide complexes. *Inorg. Chim. Acta* **357**, 1589-1592 (2004).

25. Richter, M. M., Bard, A. J., Kim, W. & Schmehl, R. H. Electrogenerated Chemiluminescence. 62. Enhanced ECL in Bimetallic Assemblies with Ligands That Bridge Isolated Chromophores. *Anal. Chem.* **70**, 310-318 (1998).

26. Li, M., Liu, J., Zhao, C. & Sun, L. Aryl-diamide bridged binuclear ruthenium (II) tris(bipyridine) complexes: Synthesis, photophysical, electrochemical and electrochemiluminescence properties. *J. Organomet. Chem.* **691**, 4189-4195 (2006).

27. Molnar, S. M., Jensen, G. E., Vogler, L. M., Jones, S. W., Laverman, L., Bridgewater, J. S., Richter, M. M. & Brewer, K. J. Photochemical Properties of Mixed-Metal Supramolecular Complexes. *J. Photochem. Photobio., A* **80**, 315-322 (1994).

28. Nallas, G. N. A., Jones, S. W. & Brewer, K. J. Bipyrimidine-Bridged Mixed-Metal Trimetallic Complexes of Ruthenium(II) with Rhodium(III) or Iridium(III), $\{[(bpy)_2Ru(bpm)]_2MCl_2\}^{5+}$. *Inorg. Chem.* **35**, 6974-6980 (1996).

29. Elvington, M., Brown, J., Arachchige, S. M. & Brewer, K. J. Photocatalytic Hydrogen Production from Water Employing A Ru, Rh, Ru Molecular Device for Photoinitiated Electron Collection. *J. Am. Chem. Soc.* **129**, 10644-10645 (2007).

30. Holder, A. A., Swavey, S. & Brewer, K. J. Design aspects for the development of mixed-metal supramolecular complexes capable of visible light induced photocleavage of DNA. *Inorg. Chem.* **43**, 303-308 (2004).

31. Holder, A. A., Zigler, D. F., Tarrago-Trani, M. T., Storrie, B. & Brewer, K. J. Photobiological Impact of $[\{(bpy)_2Ru(dpp)\}_2RhCl_2]Cl_5$ and $[\{(bpy)_2Os(dpp)\}_2RhCl_2]Cl_5$ [bpy = 2,2'-Bipyridine; dpp = 2,3-Bis(2-pyridyl)pyrazine] on Vero Cells. *Inorg. Chem.* **46**, 4760-4762 (2007).

32. Rosado, D. J., Jr., Miao, W., Sun, Q. & Deng, Y. Electrochemistry and Electrogenerated Chemiluminescence of All-trans Conjugated Polymer Poly[distyrylbenzene-b-(ethylene Oxide)]s. *J. Phys. Chem. B* **110**, 15719-15723 (2006).

33. Wang, S., Neshkova, M. T. & Miao, W. EQCM study of the ECL quenching of the tris(2,2'-bipyridyl)ruthenium(II)/tris-n-propylamine system at a Au electrode in the presence of chloride ions. *Electrochim. Acta* **53**, 7661-7667 (2008).

34. Buttry, D. A. & Ward, M. D. Applications of the Quartz Crystal Microbalance to Electrochemistry, in *Electroanal. Chem.* (ed. Bard, A. J.), 1-85 (Marcle Dekker, New York, 1991).

35. Buttry, D. A. & Ward, M. D. Measurement of interfacial processes at electrode surfaces with the electrochemical quartz crystal microbalance. *Chem. Rev.* **92**, 1355-79 (1992).

36. Sauerbrey, G. The use of quartz oscillators for weighing thin layers and for microweighing. *Zeitschrift fuer Physik* **155**, 206-22 (1959).

37. Ward, M. D. Principles and applications of the electrochemical quartz crystal microbalance, in *Physical Electrochemistry* (ed. Rubinstein, I.), 293-338 (Dekker, New York, 1995).

38. Saunders, G. C. & Parkes, H. C. (eds.) *Analytical Molecular Biology: Quality and Validation* (Royal Society of Chemistry, 1999).

39. Tombelli, S., Minunni, M. & Mascini, M. A Surface Plasmon Resonance biosensor for the determination of the affinity of drugs for nucleic acids. *Anal. Lett.* **35**, 599-613 (2002).

40. Naylor, R. & Gilham, P. T. Studies on some interactions and reactions of oligonucleotides in aqueous solution. *Biochemistry (Mosc).* **5**, 2722-8 (1966).

41. Ammar, F. & Saveant, J. M. Convolution potential sweep voltammetry. II. Multistep Nernstian waves. *J. Electroanal. Chem. Interfacial Electrochem.* **47**, 215-21 (1973).

42. Saveant, J.-M. *Elements of Molecular and Biomolecular Electrochemistry: An Electrochemical Approach to Electron Transfer Chemistry* (John Wiley & Sons, Inc., Hoboken, New Jersey., 2006).

43. Knight, A. W. & Greenway, G. M. Relationship between structural attributes and observed electrogenerated chemiluminescence (ECL) activity of tertiary amines as potential analytes for the tris(2,2-bipyridine)ruthenium(II) ECL reaction - a review. *Analyst* **121**, 101R-106R (1996).

44. Chang, M.-M., Saji, T. & Bard, A. J. Electrogenerated chemiluminescence. 30. Electrochemical oxidation of oxalate ion in the presence of luminescers in acetonitrile solutions. *J. Am. Chem. Soc.* **99**, 5399-403 (1977).

45. Liu, X., Shi, L., Niu, W., Li, H. & Xu, G. Environmentally friendly and highly sensitive ruthenium(II) tris(2,2'-bipyridyl) electrochemiluminescent system using 2-(dibutylamino)ethanol as co-reactant. *Angew. Chem. Int. Ed.* **46**, 421-424 (2007).

46. Miao, W. & Bard, A. J. Electrogenerated Chemiluminescence. 80. C-Reactive Protein Determination at High Amplification with $[Ru(bpy)_3]^{2+}$-Containing Microspheres. *Anal. Chem.* **76**, 7109-7113 (2004).

47. Miao, W. & Bard, A. J. Electrogenerated Chemiluminescence. 77. DNA Hybridization Detection at High Amplification with $[Ru(bpy)_3]^{2+}$-Containing Microspheres. *Anal. Chem.* **76**, 5379-5386 (2004).

48. Miao, W., Choi, J.-P. & Bard, A. J. Electrogenerated Chemiluminescence 69: The Tris(2,2'-bipyridine)ruthenium(II), $(Ru(bpy)_3^{2+})$/Tri-n-propylamine (TPrA) System Revisited-A New Route Involving $TPrA^{\cdot+}$ Cation Radicals. *J. Am. Chem. Soc.* **124**, 14478-14485 (2002).

49. Zu, Y. & Li, F. Characterization of the low-oxidation-potential electrogenerated chemiluminescence of tris(2,2'-bipyridine)ruthenium(II) with tri-n-propylamine as coreactant. *Anal. Chim. Acta* **550**, 47-52 (2005).

50. Zheng, H. & Zu, Y. Emission of Tris(2,2'-bipyridine)ruthenium(II) by Coreactant Electrogenerated Chemiluminescence: From O_2-Insensitive to Highly O_2-Sensitive. *J. Phys. Chem. B* **109**, 12049-12053 (2005).

51. Ho, T.-I., Elangovan, A., Hsu, H.-Y. & Yang, S.-W. Highly Fluorescent N,N-Dimethylaminophenylethynylarenes: Synthesis, Photophysical Properties, and Electrochemiluminescence. *J. Phys. Chem. B* **109**, 8626-8633 (2005).

52. Ricci, F., Volpe, G., Micheli, L. & Palleschi, G. A review on novel developments and applications of immunosensors in food analysis. *Anal. Chim. Acta* **605**, 111-129 (2007).

53. Steinem, C., Janshoff, A. & Editors. *Piezoelectric Sensors. [In: Springer Ser. Chem. Sens. Biosens., 2007; 5]* (2007).

54. Okahata, Y., Mori, T., Furusawa, H. & Nihira, T. in *Springer Series on Chemical Sensors and Biosensors* 341-369 (Springer, 2007).

55. Okahata, Y., Niikura, K., Furusawa, H. & Matsuno, H. A highly sensitive 27 MHz quartz-crystal microbalance as a device for kinetic measurements of molecular recognition on DNA strands. *Anal. Sci.* **16**, 1113-1119 (2000).

56. Okahata, Y., Matsunobu, Y., Ijiro, K., Mukae, M., Murakami, A. & Makino, K. Hybridization of nucleic acids immobilized on a quartz crystal microbalance. *J. Am. Chem. Soc.* **114**, 8299-300 (1992).

57. Caruso, F., Rodda, E., Furlong, D. N., Niikura, K. & Okahata, Y. Quartz Crystal Microbalance Study of DNA Immobilization and Hybridization for Nucleic Acid Sensor Development. *Anal. Chem.* **69**, 2043-2049 (1997).

58. Okahata, Y., Niikura, K., Sugiura, Y., Sawada, M. & Morii, T. Kinetics Studies of Sequence-Specific Binding of GCN4-bZIP Peptides to DNA Strands Immobilized on a 27-MHz Quartz-Crystal Microbalance. *Biochemistry* **37**, 5666-5672 (1998).

59. Matsuno, H., Niikura, K. & Okahata, Y. Design and Characterization of Asparagine- and Lysine-Containing Alanine-Based Helical Peptides That Bind Selectively to A.T Base Pairs of Oligonucleotides Immobilized on a 27 MHz Quartz Crystal Microbalance. *Biochemistry* **40**, 3615-3622 (2001).

60. Ebara, Y. & Okahata, Y. In situ surface-detecting technique by using a quartz-crystal microbalance. Interaction behaviors of proteins onto a phospholipid monolayer at the air-water interface. *Langmuir* **9**, 574-6 (1993).

61. Ebara, Y. & Okahata, Y. A Kinetic Study of Concanavalin A Binding to Glycolipid Monolayers by Using a Quartz-Crystal Microbalance. *J. Am. Chem. Soc.* **116**, 11209-12 (1994).

62. Mori, T., Sekine, Y., Yamamoto, K. & Okahata, Y. Enzymatic preparation of biotinylated naturally-occurring sialylglycan and its molecular recognition on a quartz-crystal microbalance. *Chem. Commun.*, 2692-2693 (2004).

63. Matsuno, H., Furusawa, H. & Okahata, Y. Kinetic study of phosphorylation-dependent complex formation between the kinase-inducible domain (KID) of CREB and the KIX domain of CBP on a quartz crystal microbalance. *Chem. Eur. J.* **10**, 6172-6178 (2004).

64. Langmuir, I. Constitution and fundamental properties of solids and liquids. I. Solids. *J. Am. Chem. Soc.* **38**, 2221-95 (1916).

65. Langmuir, I. The adsorption of gases on plane surfaces of glass, mica and platinum. *J. Am. Chem. Soc.* **40**, 1361-1402 (1918).

66. Okahata, Y., Ijiro, K. & Matsuzaki, Y. A DNA-lipid cast film on a quartz-crystal microbalance and detection of intercalation behaviors of dye molecules into DNAs in an aqueous solution. *Langmuir* **9**, 19-21 (1993).

67. Bresloff, J. L. & Crothers, D. M. Equilibrium studies of ethidium-polynucleotide interactions *Biochemistry* **20**, 3547-3553 (1981).

68. Tombelli, S., Minunni, M. & Mascini, M. A surface plasmon resonance biosensor for the determination of the affinity of drugs for nucleic acids. *Anal. Lett.* **35**, 599-613 (2002).

69. Yielding, L. W., Yielding, K. L. & Donoghue, J. E. Ethidium binding to deoxyribonucleic acid: spectrophotometric analysis of analogs with amino, azido, and hydrogen substituents. *Biopolymers* **23**, 83-110 (1984).

CHAPTER IV

ECL DETERMINATION OF C-REACTIVE PROTEIN WITH CARBOXYL CdSe/ZnS CORE/SHELL QUANTUM DOTS*

Introduction

Quantum dots (QDs) are nanometer-scale semiconductor crystals with unique optical, spectroscopic, electronic, and electrochemical properties.[1-8] QDs provide broad absorption (UV→ near IR) and narrow size- and composition-tunable emission ($\Delta\lambda_{1/2}$ = 20–40 nm), exceptional brightness and photostability when compared to organic dyes and fluorescent (FL) proteins.[1,9] QDs also offer a versatile nanoscale scaffold for designing multifunctional nanoparticles with imaging and therapeutic functions.[1] As a result, in recent years QDs have been intensively studied as a new class of nanoparticle probe for molecular, cellular, and *in vivo* imaging, as well as for multiplexing FL chemical sensing and biosensing.[1,10-11]

Electrochemical and ECL studies of QDs were first reported in 2002 for Si QDs, where ECL was generated from both annihilation and coreactant systems in MeCN.[12] Since then, a number of compound QDs (e.g., CdS, CdTe, and CdSe/ZnSe) have been shown to produce ECL under various conditions including in solutions and in solid-films.[13-14] Most of these ECL studies, however, were conducted in organic media and their emissions were produced by either ion annihilation or cathodic reductions in the presence of persulfate or H_2O_2.[8,13] For bioanalytical applications, it is highly desirable to have QDs ECL produced in aqueous media[15-17] with a coreactant upon anodic potential scanning[18-19] so that the system is biocompatible and the effect of oxygen reduction from

* Part of this work was presented in: *Abstracts, 60th Southeast Regional Meeting of the American Chemical Society, Nashville, TN, United States, November 12-15*, SERM-559 (2008).

air and solution media on ECL production can be eliminated. Furthermore, because the solution phase QDs often suffer from low solubility, low concentration, and small diffusion coefficient, experimental designs with QDs biosensing films could provide enhanced electrochemical and ECL signals, resulting in high sensitivity and low detection limit for the determination of the analyte of interest.

Recently, a series of carboxylated water-soluble CdSe/ZnS core/shell QDs coated with polyethylene glycol (PEG) polymer (referred to as CdSe/ZnS/PEG-COOH) have become commercially available.[20] These QDs, with FL λ_{max} values from 525 to 800 nm, show extremely high FL efficiencies and narrow FL spectra. Thus, unlike traditional $Ru(bpy)_3^{2+}$ type ECL labels that have a typical ECL emission at 620 nm, CdSe/ZnS/PEG-COOH QDs could be excellent ECL labels for multiplexing biomolecules detection when several different sizes of QDs with distinct ECL spectra are conjugated with target species and analyzed with ECL technology. Previously, bioinorganic conjugates prepared with CdSe/ZnS core-shell QDs and antibodies/proteins have shown potential applications in fluoro-immunoassays.[5,21-23]

In this chapter, "oxidative-reduction" type coreactant ECL[24] of the CdSe/ZnS/PEG-COOH QDs ("Qdot 625") will be investigated in aqueous media. The Qdot 625 will be then used as an ECL label for sandwich-type immunoassay of C-reactive protein (CRP) at a partially transparent gold electrode prepared from a recordable Au compact disk (CD). CRP has long been regarded as an inflammatory biomarker and cardiovascular risk factor.[25-31] As a result, the presently reported QDs-based CRP measurements could have potential applications in clinic analysis of CRP in human serum.

Experiment Section

Chemicals and Materials

Tri-*n*-propylamine (TPrA, 99+%), sulfuric acid (H_2SO_4, 98%), nitric acid (HNO_3, 70%), sodium borohydride ($NaBH_4$, > 99%), concentrated ammonium hydroxide (30%), ethanolamine (98+%), and 1-methyl-imidazole (99%) from Aldrich (Milwaukee, WI); hydrochloric acid (HCl, 37.5%), hydrogen peroxide (H_2O_2, 30%), and sodium chloride (NaCl, certified A.C.S.), sodium citrate, and methanol (spectroanalyzed grade) from Fisher (Fairlawn, NJ); sodium hydroxide (NaOH, 98.7%) from J. T. Baker (Phillipsburg, NJ); 2-(dibutylamino)ethanol (DBAE, 99%), N-hydroxysuccinimide (NHS), C-reactive protein (CRP, from human plasma), anti-human C-reactive protein (anti-CRP, developed in rabbit, ~90 mg/mL), and bovine serum albumin (BSA, 98-99 %) from Sigma (St. Louis, MO); ethylenedinitrilotetraacetic acid (EDTA) from EM (Gibbstown, NJ); avidin (NeutrAvidin), pH phosphate-buffered saline (PBS buffer, 0.10 M sodium phosphate-0.15 M sodium chloride, pH 7.4), sulfo-NHS-LC-biotin, and SuperBlock blocking buffer in PBS, and 1-ethyl-3-(3-dimethylaminopropyl) carbodiimide (EDAC) from Pierce (Rockford, IL); hydrogen tetrachloroaurate ($HAuCl_4$, 99.999%) from GFS (Powell, OH); and (3-aminopropyl)triethoxysilane from Gelest (Morrisville, PA) were used as received. Streptavidin-coated superparamagnetic polystyrene beads (referred to as magnetic beads or MB, 1.0 μm in diameter, 10 mg/mL aqueous suspension with ~9.5×10^6 beads/μL), and Qdot 625 carboxyl quantum dots (8 μM solution in 50 mM borate, pH 9.0) were purchased from Dynal Biotech (Lake Success, NY) and Invitrogen (Eugene, OR), respectively. Recordable CDs (MAM-A Thermal Gold CD-R) from CD Dimensions

(Deep River, CT) were used in this work. Indium tin oxide (ITO) electrodes (R_s = 8-12 Ω) were obtained from Delta Technologies (Stillwater, MN).

Unless otherwise stated, all aqueous solutions were prepared with deionized-distilled water produced from a Barnstead MP-6A Mega-Pure® system (Barnstead international Dubuque, Iowa), and all experiments were carried out at a room temperature of 24±1 °C.

Instruments

Unless otherwise stated, all electrochemistry and ECL experiments were performed with a model 660A electrochemical workstation (CH Instruments, Austin, TX) and homebuilt ECL instrument as described in previous chapters. For solution phase electrochemical and ECL studies of QDs, a conventional three-electrode cell was used, with a Pt wire as the counter electrode and an Ag/AgCl/Cl^- (3.0 M KCl) as the reference electrode. Working electrodes used in this part were glassy carbon (GC, 3-mm diameter), Pt (2-mm diameter), and gold (Au, 2-mm diameter) disks. These electrodes were polished with 0.3-0.05-μm alumina slurry, thoroughly rinsed with water, and dried with the Kimwipes facial tissue before each experiment. For QDs-based sandwich-type CRP detection, a homemade Teflon electrochemical cell was used (Figure 4.1), in which a transparent working electrode (e.g., Au nanoparticle-coated ITO or Au/CD electrode) was sandwiched between a piece of polycarbonate and the Teflon cell body. The Teflon opening close to the working electrode had a diameter of 4.0 mm, and the O-ring had an external diameter of 7.0 mm. Because the CV and ECL were performed in positive potential regions, degassing of oxygen with nitrogen was not needed.

ECL spectra of Qdot 625 were obtained by collecting the peak ECL intensity of the forward scan (0-1.5 V vs Ag/AgCl in 80 nM Qdot 625-70 mM DBAE-0.10 M PBS, pH 7.4) during the cyclic potential cycling using a ~1 ×1 cm^2 Pt flag electrode as the working electrode at a scan rate of 50 mV/s with 24 pieces of interference filters (Intro, Inc. Socorro, NM) over a spectral range of 360 to 820 nm. These filers had an average half-peak width of 10 nm and a transmittance value of 50% at the specified wavelength.

Fluorescence spectra were recorded with a PTI QM fluorimeter (Photon Technology International, Birmingham, NJ). UV-visible spectroscopic measurements were performed with a Shimadzu UV-2401 PC Spectrometer (Columbia, MD).

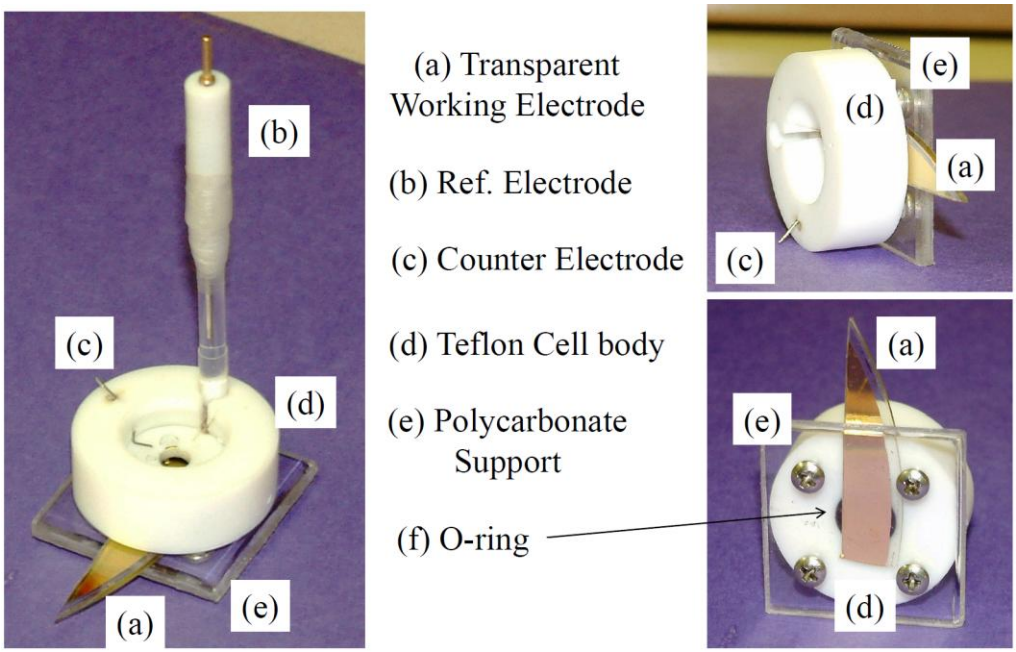

Figure 4.1 Electrochemical cell used for QDs-based sandwich type CRP detection.

Fluorescence spectra were recorded with a PTI QM fluorimeter (Photon Technology International, Birmingham, NJ). UV-visible spectroscopic measurements were performed with a Shimadzu UV-2401 PC Spectrometer (Columbia, MD).

Immobilization of avidin on the surface of QDs

A layer of avidin was covalently attached to the surface of Qdot 625 via the formation of amide bonds (i.e. CdSe/ZnS/PEG-CO-NH-avidin) by adding 10 μL of 8.0 μM of Qdot 625 into 1.5 mL of freshly prepared 25 μM avidin in a 0.10 M 1-methyl-imidazole buffer (pH = 7.5) containing 0.10 M EDAC and rotating the mixture at ~40 rpm for 1 hour. The newly formed avidin-coated Qdot 625 was separated from any unreacted avidin using a 100 kDa molecular weight cutoff (MWCO) membrane (Amicon Ultra-4, Millipore). The mixture was centrifuged at 5,000~10,000 rpm for 5 minutes and washed with 1 mL of 1X "B & W buffer" (1X binding & washing buffer, which consists of 5 mM Tris-HCl (pH 7.5)-0.5 mM EDTA-0.1 M NaCl) three times. The finally obtained QD/avidin was resuspended in 1.5 mL of 1X "B & W buffer" solution, resulting in a QD/avidin concentration of ~53 nM. This solution was kept at ~4 ℃ prior to use.

Biotinylation of Anti-CRP

Similar procedures described in the literature were followed.[32-33] Briefly, a 17-molar fold excess of water soluble sulfo-NHS-LC-biotin (MW = 556.6 g/mol) was used to react with the anti-CRP (assuming that the antibody has a molecular weight of 150 kDa/mol) in order to make sure proper biotin labeling. A 44 μL of 90 mg/mL anti-CRP (~0.6 mM) in 1-methyl-imidazole solution (pH 7.5) was added to a 1.5 mL micro-centrifuge tube containing a 440 μL of 1 mM aqueous biotin solution. The mixture was incubated at room temperature with rotation at 20 rpm with a Dynal sample mixer (Dynal Biotech Inc.) for one hour. The unbound biotin molecules were subsequently removed by gel filtration with a Sephadex G-25 PD-10 desalting column (Amersham Pharmacia Biotech, Piscataway, NJ). The final product with a concentration of ~2.0 mg/mL

biotinylated anti-CRP (~13.3 μM) in 1.5 mL of 1-methyl-imidazole buffer solution (pH 7.5) was stored at ~4 ℃ prior to use (assuming a 75% of gel filtration yield).

Attachment of Biotinylated Anti-CRP to the Surface of MB and QD/avidin

The streptavidin-coated magnetic beads were thoroughly washed with 1 mL of 2X "B & W buffer" (2× binding & washing buffer, which consists of 10 mM Tris-HCl (pH 7.5)-1 mM EDTA-0.2 M NaCl) twice and 1 mL of 1X "B & W buffer" once before attaching biotinylated anti-CRP using similar procedures described in the literature.[33] Experimentally, freshly washed 1-μm solid MB corresponding to 200 μL of the original MB suspension was immersed in 1.5 mL of ~2.0 mg/mL biotinylated anti-CRP solution, and the mixture was then rotated with a Dynal sample mixer at ~40 rpm for one hour. As a result, a saturated layer of anti-CRP is expected to be formed on the surface of MB, since streptavidin and biotin interactions are very strong and specific. Newly formed anti-CRP↔MB conjugates were separated from the solution mixture with a magnet (Dynal MPC®-S), followed by washing with 1X "B & W buffer" three times, transferred to a new 1.5 mL microcentrifuge tube, and re-suspended in 200 μL of 1-methyl-imidazole buffer (pH 7.5) solution so that possible biotinylated anti-CRP absorption on the wall of the previous tube can be avoided.

Likewise, the immobilization of anti-CRP onto the surface of QD/avidin was obtained by mixing 12 μL of 2.0 mg/mL biotinylated anti-CRP and 200 μL of ~53 nM avidin-coated Qdot 625 and rotating the mixture at ~40 rpm for one hour. Because the molar ratio of added QD/avidin to biotinylated anti-CRP was ~7:1 and the avidin-biotin interaction is strong and specific, there should not be any free anti-CRP left in the solution. Therefore, undesired interference from free anti-CRP on the subsequent CRP is

avoided. As will be discussed later, the unbound QD/avidin in the solution will not affect the final CRP detection.

Sandwich-Type QD/Avidin↔Anti-CRP⟨CRP⟩Anti-CRP↔MB Aggregates Formation

A 20 μL of QD/avidin↔anti-CRP, 130 μL of a blocking agent, e.g., 2.0% BSA in 0.10 M 1-methyl-imidazole buffer (pH 7.5), and 5 μL of anti-CRP↔MB conjugates, together with 20 μL of an appropriated concentration of pure CRP were used to produce the sandwich type QD/avidin↔anti-CRP⟨CRP⟩anti-CRP↔MB aggregates. Up to 25 μL of 0.10 M 1-methyl-imidazole buffer (pH 7.5) was also added to the above mixture to make an overall volume of 200 μL. The antibody-antigen reactions were carried out at room temperature for 3 hours with frequent gentle shaking. Newly produced sandwich type aggregates, along with any unbound anti-CRP↔MB conjugates, were separated magnetically from the solution medium containing free unbound QD/avidin↔anti-CRP and QD/avidin, washed gently with 200 μL of 1X "B & W buffer" three times, followed by magnetic separation. The aggregates were finally resuspended in a 0.50 mL solution of 50 mM DBAE-0.10 M PBS (pH 7.5) buffer solution for ECL measurements. Figure 4.2 schematically illustrates the formed sandwich type aggregates located on the electrode surface.

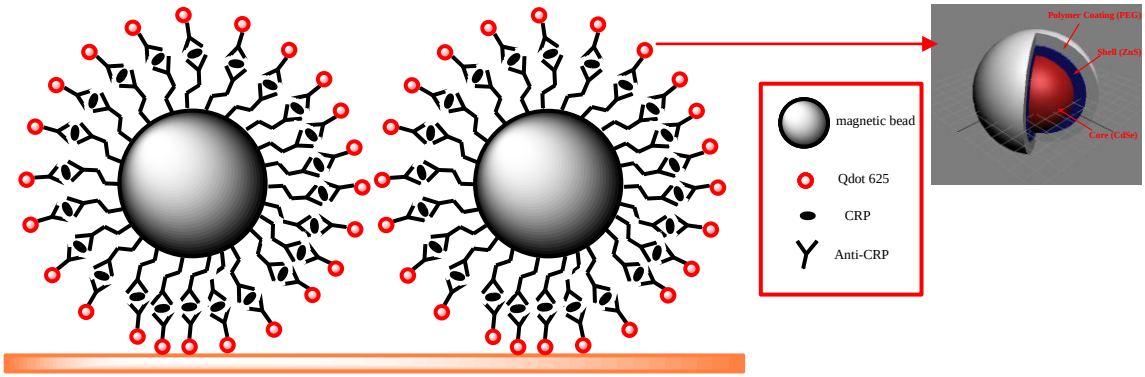

Figure 4.2. Sandwich type QD/avidin↔anti-CRP⟨CRP⟩anti-CRP↔MB aggregates on the surface of an electrode.

Preparation of Au nanoparticle coated ITO electrodes

This was done by following the procedures as in reference 34. Briefly, Au nanoparticles (GNP) were synthesized by chemical reduction of $HAuCl_4$ with sodium citrate and $NaBH_4$. The formed GNPs were characterized with UV-Visible spectroscopy and had an estimated size of ~6 nm[34-35] (Figure 4.3).

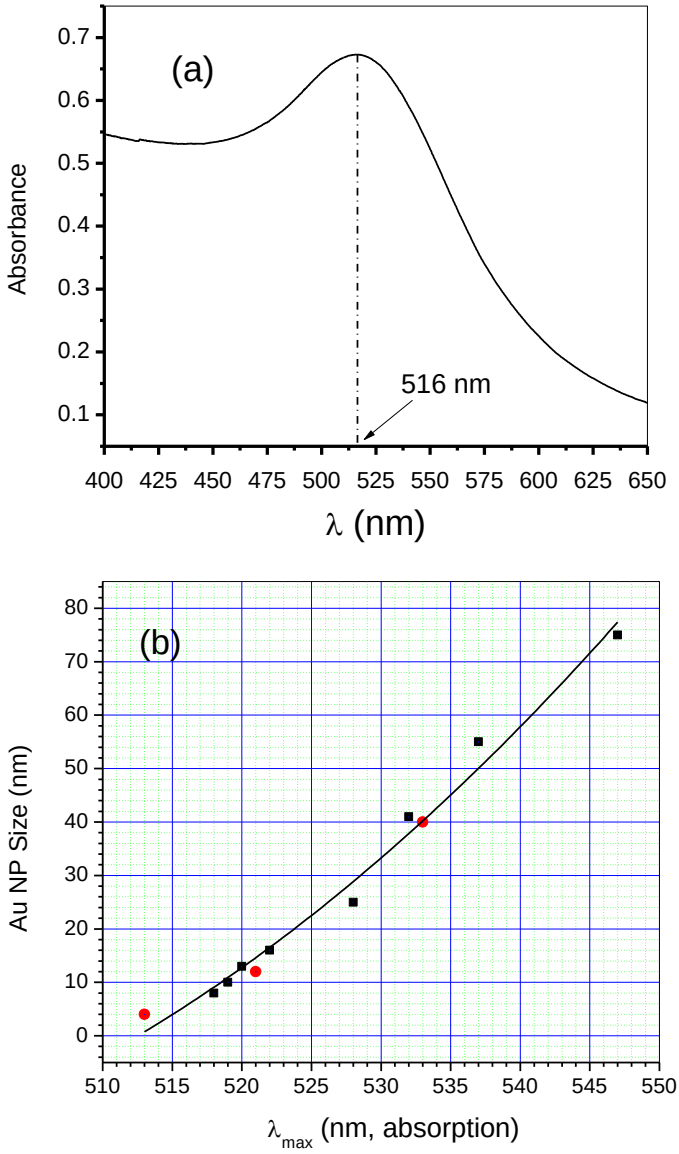

Figure 4.3. (a) UV-Visible spectra of Au nanoparticles, (b) correlation between the Au nanoparticle size and the maximum absorption of UV-visible spectra of Au nanoparticles.[35]

As shown in Figure 4.4A, clean and dried ITO electrodes were treated with ammonium hydroxide, followed by silanization reactions with (3-aminopropyl)-triethoxysilane. The attachment of GNPs was achieved by immersing the silanized substrates in the GNP colloid solutions. Figure 4.4B shows the UV-Visible spectra and

photographs of ITO electrodes before and after the immobilization of GNPs. ITO coated with GNPs becomes reddish.

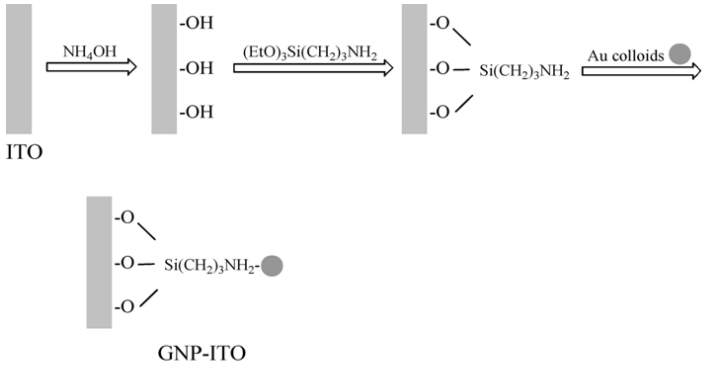

(A)

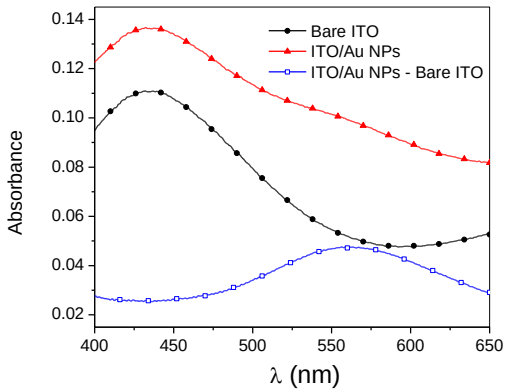

(a)

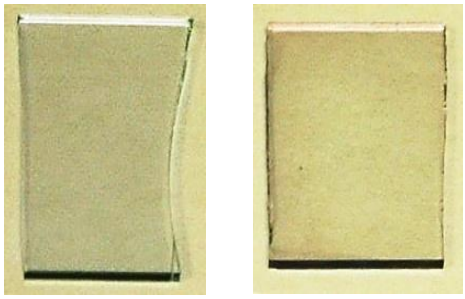

Bare ITO GNPs/ITO

(b)

(B)

Figure 4.4. (A) Schematic of preparation of GNPs-modified ITO electrode;[34] (B) (a) UV-Visible spectra, and (b) photographs of ITO electrodes before and after the immobilization of GNPs.

Preparation of Au CD Electrodes

Partially transparent Au working electrodes were prepared with recordable Au CDs, as reported previously.[36-38] As shown in Figure 4.5, a typical Au CD includes a 50-100 nm thickness of Au film that is coated with one or two layers of polymer films. Beneath the Au film is a dye-photosensitive layer sitting on the top of a polycarbonate disk. A Au CD was first cut to small pieces with dimensions of ~1.5×3.5 cm^2 before dipped into a concentrated nitric acid solution for few minutes, and the protective film was subsequently peeled off. The Au/CD electrode was finally washed with a large amount of water and dried with a hot gun before further use.

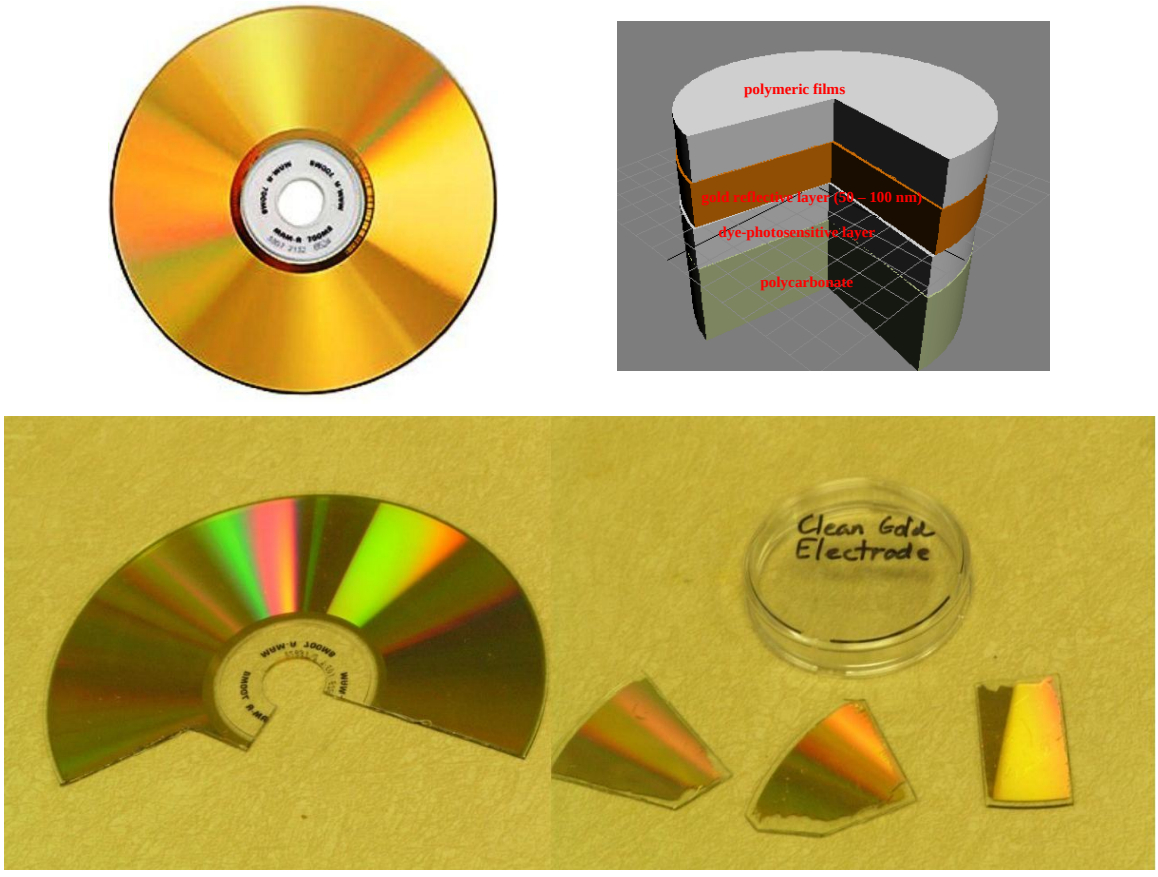

Figure 4.5. A recordable Au CD, its composition, and its use as Au/CD electrodes for QD-based ECL biosensing.

Results and discussion

Absorption and FL Spectra of Qdot 625

Figure 4.6 shows the absorption (blue line) and FL spectra (red line) of Qdot 625 in PBS buffer (pH 7.5), where the absorption spectra exhibit two strong absorption peaks at 571 and 610 nm, and the FL spectra has a narrow peak at 625 nm. As displayed in the inset of Figure 4.6, the FL peak intensity varies linearly with Qdot 625 concentration over the range of 8 pM to 80 nM in PBS buffer solution (pH = 7.5), and levels off at higher concentrations due to probably the inner filter effect or self quenching.

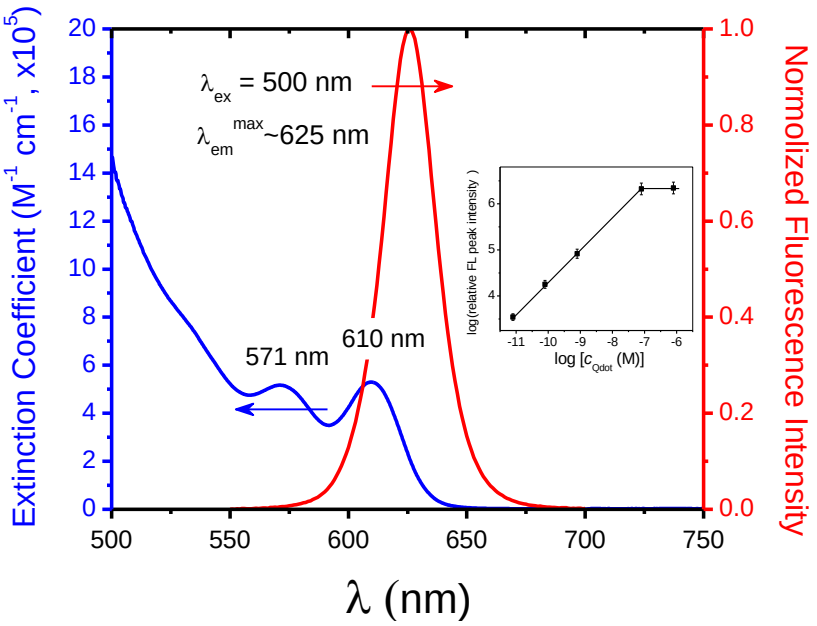

Figure 4.6. Absorption and FL emission spectra of 80 nM Qdot 625 in 0.10 M PBS buffer (pH 7.5) with an excitation at 500. Inset: relationship between FL peak intensity and Qdot 625 concentration.

Electrochemical and ECL Behavior of Qdot 625 in Aqueous Media

The oxidative-reduction type ECL was used to investigate the ECL behavior of Qdot 625 in the presence of coreactant DBAE[39] and TPrA. Figure 4.7 shows CV (dash

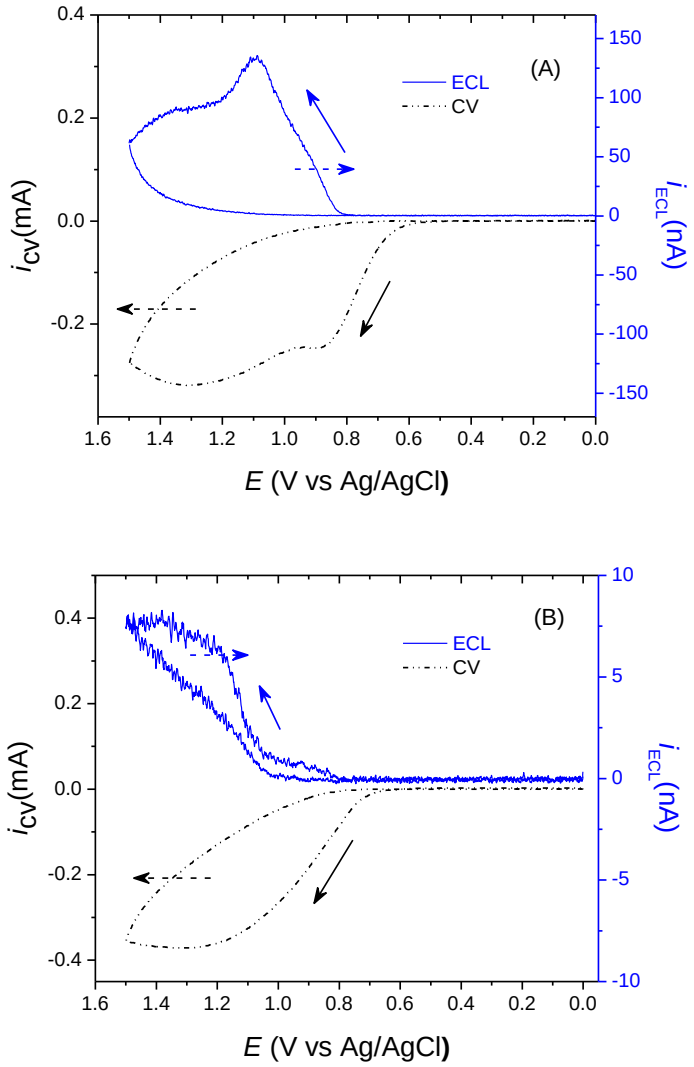

Figure 4.7. CV (dashed line) and ECL (solid line) responses of 80 nM Qdot 625 in 0.10 M PBS (pH 7.5) with (A) 50 mM DBAE and (B) 100 mM TPrA at a 3-mm GC electrode with a scan rate of 50 mV/s.

line) and ECL (solid line) responses of 80 nM Qdot 625 in 0.10 M PBS (pH 7.5) with 50.0 mM DBAE (Figure 4.7A) and 100 mM TPrA (Figure 4.7B) at a GC electrode. In both cases, ECL emissions appear at the same potential of ~0.80 V vs Ag/AgCl, which is about 200 mV and 150 mV more positive compared with the oxidation potentials for DBAE (~+0.60 V vs Ag/AgCl) and TPrA (~+0.65 V vs Ag/AgCl), respectively. These

data suggest that ECL can be generated only when both ECL emitter Qdot 625 and ECL coreactant DBAE or TPrA are oxidized at the electrode. In other words, Qdot 625 starts to oxidize at ~+0.80 V vs Ag/AgCl and has an estimated oxidation peak potential at ~+1.0 V vs Ag/AgCl, if the process is electrochemically reversible.[40] Note that the direct CV measurement of the oxidation (or reduction) potential of Qdot 625 in solution is difficult because the parent concentration of Qdot 625 (8 μM) is much lower than that needed for conducting a good CV (~1 mM). Another important feature of the ECL emission is that under the present experimental conditions, Qdot 625 ECL produced with DBAE is ~165 times stronger than that with TPrA. This implies that the $TPrA^{\bullet}$ free radical produced via the EC reaction mechanism[41] cannot effectively reduce Qdot 625 to its $(Qdot\ 625)^{\bullet-}$. That is, the reduction potential for Qdot 625 is probably close to that for the $TPrA^{\bullet}$ free radical of ~-1.7 V vs Ag/AgCl.[42] Therefore, the reducing energy of the $DBAE^{\bullet}$ free radical must be sufficiently strong for the reduction of Qdot 625 (i.e., < -1.7 V vs Ag/AgCl). This deduction will be further supported by the data shown in Chapter V, where 9,10-diphenylanthracene (DPA) [$E_{1/2}$(ox) = +1.29 V, $E_{1/2}$(red) = -1.96 V vs. SCE][42] shows strong ECL emissions with DBAE but almost no ECL with TPrA.

Figure 4.8 shows the effects of the working electrode material and the coreactant concentration of DBAE on the Qdot 625 ECL intensity. When [DBAE] < 30 mM, the Au electrode has the highest ECL responses among the three tested electrodes; when 30 mM < [DBAE] < 90 mM, the obtained ECL intensity increases in the order of GC >> Au > Pt. The maximum ECL is obtained at GC electrode when [DBAE] ≈ 53 mM, where a ratio of 11 : 3 : 1 in ECL intensity can be evaluated for GC, Au, and Pt electrodes, respectively. The overall tendency of ECL intensity is consistent with the amount of coreactant

oxidation at different electrodes in CV (not shown), which is believed to be related to the hydrophobicity of the electrode surface as well as the formation of a Pt oxide layer during the anodic potential scanning[43-44] (see also Chapter 2).

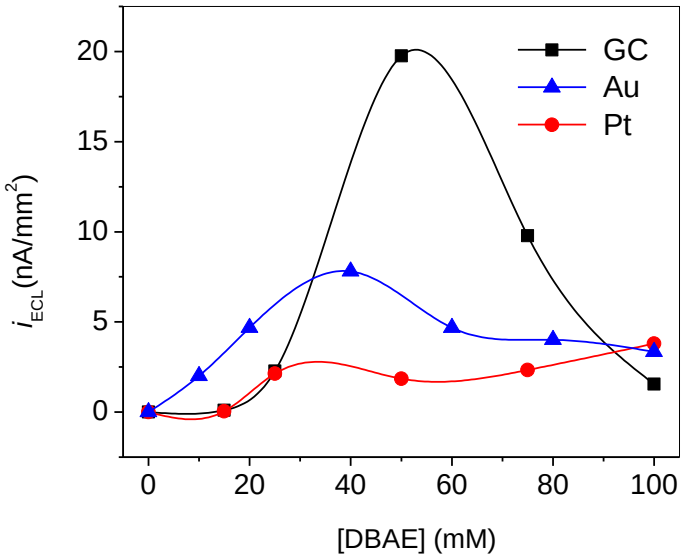

Figure 4.8. Effects of working electrode material and the concentration of coreactant DBAE on Qdot 625 ECL intensity for a 80 nM Qdot 625-0.10 M PBS (pH 7.5) solution at a scan rate of 50 mV/s.

ECL Spectra of Qdot 625

Figure 4.9 shows the ECL spectra of Qdot 625 obtained from an aqueous PBS solution (pH 7.5) containing 80 nM Qdot 625 and 75 mM DBAE at a large Pt flag electrode of ~1 ×1 cm^2. This broad ECL spectrum has only one peak at the FL emission maximum of 625 nm (see Figure 4.1). It is believed that PL spectroscopies mainly probe the interior of the QD and provide information about the electronic transition (band gap) of material, whereas electrochemistry and ECL studies mainly probe the QD surface[8] (Figure 4.10). Thus, the present data suggest that Qdot 625 is largely well-passivated (e.g., the CdSe core is well coated with the ZnS shell) and the undesired red-shifted ECL

emission observed frequently from other QDs is nearly absent.[45-47] The bump of the ECL spectra at ~695 nm may indicate the non-perfect passivation of Qdot 625, which can be explained with the two simulated curves. Figure 4.11 illustrates the passivation status of Qdot 625.

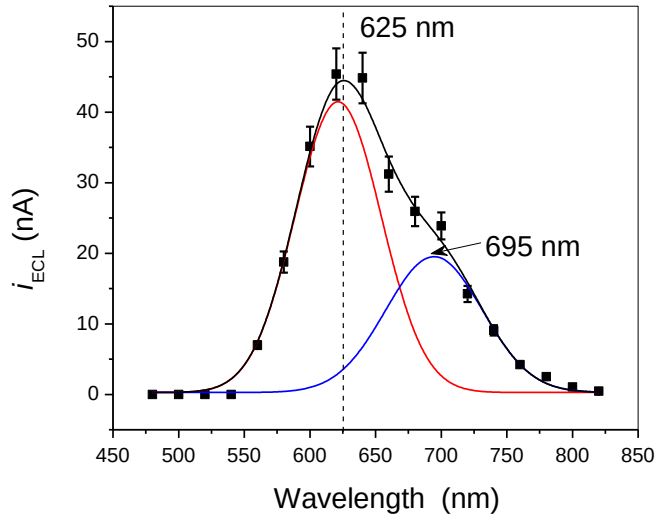

Figure 4.9. ECL emission spectra of Qdot 625 with 75 mM DBAE in 0.10 M PBS buffer solution (pH 7.5) at ~1 ×1 cm^2 Pt electrode with a scan rate of 50 mV/s.

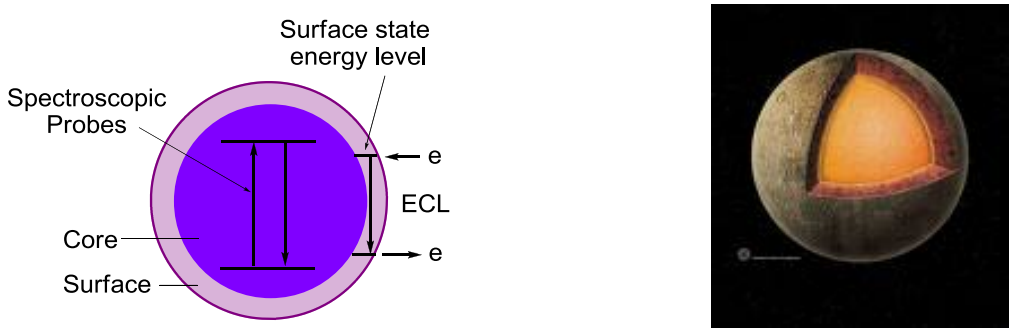

Figure 4.10. Schematic representation of photoluminescence and ECL in QDs.

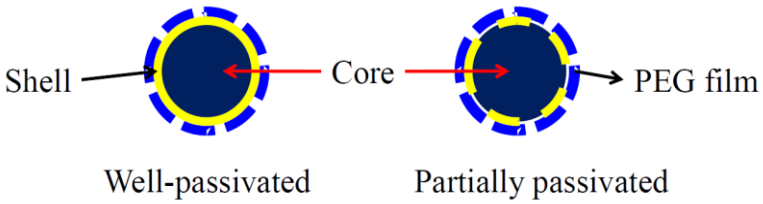

Figure 4.11. Illustration of the passivation status of Qdot 625.

Proposed ECL Mechanism of Qdot 625 Using DBAE as a Coreactant

Based on the data presented above, the ECL mechanism of Qdot 625 using DBAE as a coreactant in a neutral aqueous medium can be proposed as shown in Scheme 4.1. Up on the anodic potential scanning, DBAE oxidizes at the electrode (~0.60 V vs Ag/AgCl) to form a $DBAE^{\bullet+}$ cation radical (eq. (4-1)) that deprotonates to for a $DBAE^{\bullet}$ free radical (eq. (4-2)). Due to the sufficient reducing energy, the newly produced $DBAE^{\bullet}$ free radical reduces Qdot 625 to $(Qdot\ 625)^{\bullet-}$ near the electrode surface (eq. (4-1)). When the electrode is scanned to more positive potentials ($\sim\geq$ +0.80 V vs Ag/AgCl), Qdot 625 gets oxidized (eq. (4-4)). The excited state (Qdot 625)* can be generated via two reaction pathways: the positively charged $(Qdot\ 625)^{\bullet+}$ species annihilates either $(Qdot\ 625)^{\bullet-}$ (eq. (4-5)) or $DBAE^{\bullet}$ free radical (eq. (4-6)). Depending on the passivation status of the Qdot 625, ECL emissions at different wavelengths can be produced. For well-passivated Qdot 625, the ECL emission matches the FL emission (eq. (4-7a)). For partially passivated Qdot 625, however, a ~70 nm red-shifted ECL emission with respect to its FL is observed (eq. (4-7b)). Because the partially passivated QDs have a relatively small energy gap at the surface that is probed by ECL as compared with the band gap of the core that is probed by FL, ECL emits at a relatively longer wavelength. Note that the shell of the QDs (ZnS) does not interfere with the light emission of the core (CdSe) in the

visible range (400-700 nm), because the band gap of ZnS has a much large value that corresponds to a emission at a much short wavelength (e.g., in the UV region).[4,48]

$$DBAE - e \rightarrow DBAE^{\bullet +} \quad (4.1)$$

$$DBAE^{\bullet +} - H^{+} \rightarrow DBAE^{\bullet} \quad (4.2)$$

$$CdSe/ZnS/PEG + DBAE^{\bullet} \rightarrow (CdSe/ZnS/PEG)^{\bullet -} + P1 \quad (4.3)$$

$$CdSe/ZnS/PEG - e \rightarrow (CdSe/ZnS/PEG)^{\bullet +} \quad (4.4)$$

$$(CdSe/ZnS/PEG)^{\bullet +} + (CdSe/ZnS/PEG)^{\bullet -} \rightarrow (CdSe/ZnS/PEG)^{*} + CdSe/ZnS/PEG \quad (4.5)$$

$$(CdSe/ZnS/PEG)^{\bullet +} + DBAE^{\bullet} \rightarrow (CdSe/ZnS/PEG)^{*} + P1 \quad (4.6)$$

$$(CdSe/ZnS/PEG)^{*}_{well\text{-}passivated} \rightarrow CdSe/ZnS/PEG + h\nu\ (\sim 625\ nm) \quad (4.7a)$$

$$(CdSe/ZnS/PEG)^{*}_{partially\text{-}passivated} \rightarrow CdSe/ZnS/PEG + h\nu\ (\sim 695\ nm) \quad (4.7b)$$

(where: DBAE = $(n\text{-Bu})_2NCH_2CH_2OH$; $DBAE^{\bullet +} = (n\text{-Bu})_2N^{\bullet +}CH_2CH_2OH$
$DBAE^{\bullet} = (n\text{-Bu})_2NC^{\bullet}HCH_2OH$; P1 = $(n\text{-Bu})_2N^{+}{=}CHCH_2OH$
CdSe/ZnS/PEG = Qdot 625)

Scheme 4.1 Proposed ECL mechanism of Qdot/DBAE system at low oxidation potential region in PBS buffer (pH 7.5).

ECL determination of CRP with QDs

Assay format and electrode selection. It is well-known that for the MB-coated $Ru(bpy)_3^{2+}$/TPrA system, ECL can be recorded with a photo-detector installed above the electrochemical cell.[13,41,49] However, for our current MB-coated QDs/DBAE system, ECL emissions were found to be acquired only from the bottom of the cell as illustrated in Figure 4.12. This suggests that the ECL emission initiates from the direct electrochemical oxidation of QDs that contact the electrode, which is consistent with the ECL behavior observed from the solution (see Section 4.3.2 and Scheme 4.1). Note that

MBs are opaque and non-conductive. Consequently, the selection and preparation of a suitable transparent working electrode becomes crucial for sensitive ECL detection. The indium tin oxide-coated glass (ITO) electrode has been widely used in variety of electronics that include electronic conductivity and optical transparency (~70-80% transmittance). However, studies have shown that due to the large overpotential of TPrA oxidation and the instability at high anodic potentials, ITO electrodes can only produce a very low ECL efficiency for the $Ru(bpy)_3^{2+}$/TPrA system.[34] With the attachment of Au nanoparticles on the surface of an ITO electrode, significant enhancement in the ECL intensity of the $Ru(bpy)_3^{2+}$/TPrA system was recently reported.[34] The preparation of such an electrode, however, is very complex and time-consuming. As described in Chapter II, Au electrodes are excellent for the ECL generation of the $Ru(bpy)_3^{2+}$/TPrA system in aqueous solutions (Figure 2.1). When a Au film becomes very thin, partial transparency may become possible. Given that a 50-100 nm Au layer is commonly used in a recordable Au CD, we decided to test its suitability as an ECL electrode after removal of the top protection layer[50] when the ECL measurements were performed with the $Ru(bpy)_3^{2+}$/TPrA standard. Figure 4.13 shows the ECL responses from different electrodes for 1.0 μM $Ru(bpy)_3^{2+}$/0.10 M TPrA-0.10 M phosphate buffer (pH 7.4) using an electrochemical cell shown in Figure 4.1, where the PMT detector was installed under the cell. Clearly, ECL produced from a bare Au/CD (Figure 4.13a) is stronger than that from an ITO coated with 6-nm Au nanoparticles (Figure 4.14b). Also, no delay in ECL production is found at the Au/CD. The data suggest that bare Au/CD electrodes should serve our present QDs ECL study well.

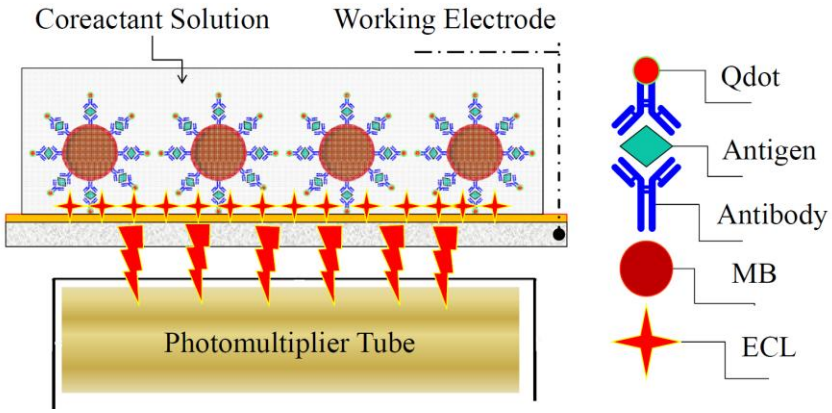

Figure 4.12. ECL assay format using QDs coated MB.

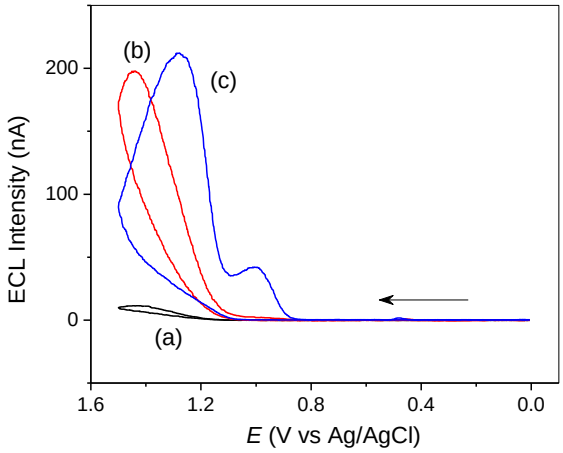

Figure 4.13. ECL responses of 1.0 μM $Ru(bpy)_3^{2+}$/0.10 M TPrA-0.10 M phosphate buffer (pH 7.4) obtained from (a) a bare ITO, (b) an ITO coated with 6 nm Au nanoparticles, and (c) a Au/CD electrode with a scan rate of 50 mV/s.

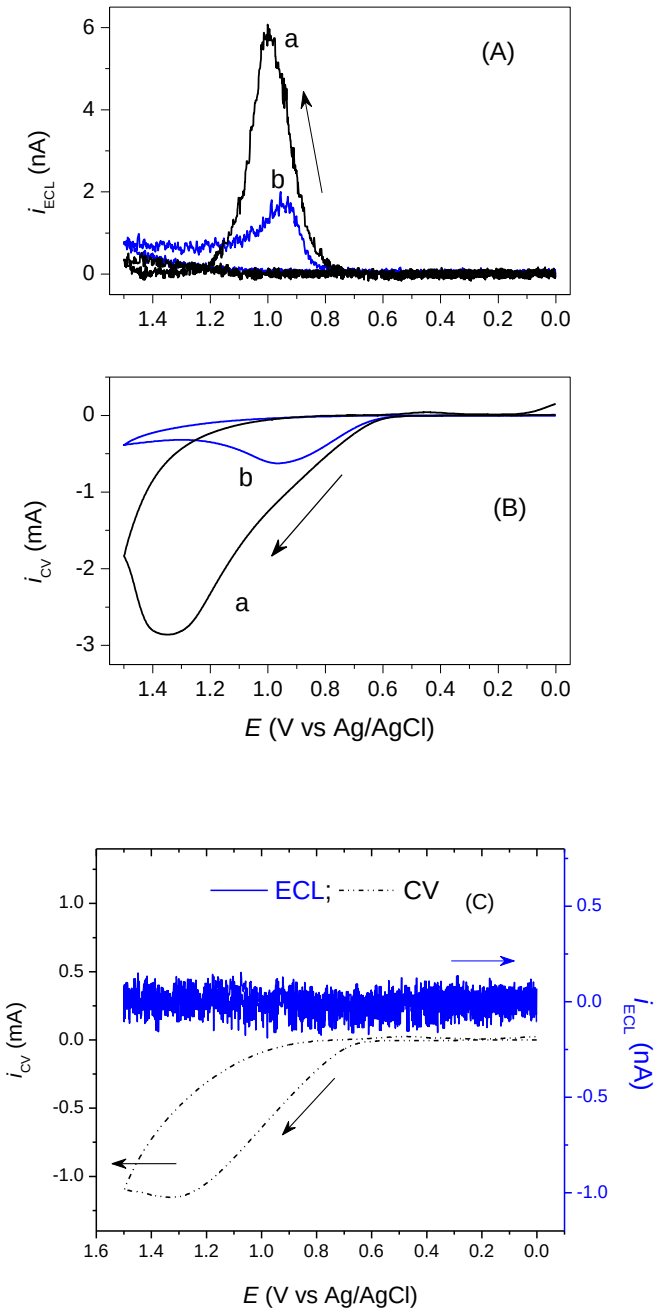

Figure 4.14. Responses of (A) ECL and (B) CV obtained from QD/avidin↔anti-CRP⟨CRP⟩anti-CRP↔MB aggregates on (a) Au/CD and (b) ITO coated with 6-nm Au nanoparticles electrodes in the presence of 50 mM DBAE-0.10 M phosphate buffer (pH 7.4) for an added [CRP] = 10 μg/mL with a scan rate of 50 mV/s. (c) Background CV and ECL of 50 mM DBAE-0.10 M phosphate buffer (pH 7.4) at a Au/CD electrode.

CRP determination. Figure 4.14 shows the responses of ECL (Figure 4.14A) and CV (Figure 4.14B) obtained from QD/avidin↔anti-CRP⟨CRP⟩anti-CRP↔MB aggregates on Au/CD (Figures 4.14A(a) and B(a)) and ITO coated with 6-nm Au nanoparticles electrodes (Figures 4.14A(b) and B(b)) in the presence of 50 mM DBAE-0.10 M phosphate buffer (pH 7.4) for an added [CRP] = 10 μg/mL. Similar to the results shown in Figure 4.13, the Au/CD electrode gives much stronger ECL emissions than the Au nanoparticle-coated ITO electrode. This is because the oxidation of DBAE is much easier at the Au/CD electrode as revealed in Figure 14B. No background ECL was observed at the Au/CD electrode (Figure 14C), suggesting that the detection limit of the analyte could be very low.

A linear relationship between the ECL peak intensity and the CRP concentration over a range of 1.0-10.0 μM/mL is displayed in Figure 15, with a limit of detection of 1.0 μM/mL. For apparently healthy people, a mean value of ~1.9 μM/mL CRP has been reported previously.[25-31] Therefore, our present method is sensitive enough for the determination of CRP in human serum samples.

Because the ECL can only be generated from the oxidized QDs, it is essential for the sandwich-type aggregates to directly contact with the electrode, so that optimized ECL responses are acquired. In other words, a monolayer aggregates on the electrode is preferred. Assuming the aggregates are closely-packed on the electrode surface (Figure 14.16), then two aggregates (≈ 2 MBs sizes) should occupy the area of $4r^2\sqrt{3}$, where r is the radius of each aggregate (or MB). A 5.0 μL of MBs (1 μm-diameter, ~9.5×10^6 MBs/μL) (see Experimental section) should use an area of ~41 mm^2. This value is close to the apparent Au/CD electrode area of ~39 mm^2 estimated from the size of the O-ring

(an internal diameter of ~7 mm). That is, under present experimental conditions, the formation of a monolayer aggregates on the Au/CD electrode is expected. This is supported experimentally by the data shown in Figure 4.17, where the ECL intensity of the aggregates is found to be linearly proportional to the number of MBs used (expressed as the electrode surface coverage). In this experiment, an ECL response from the following sandwich-type aggregates was regarded to be corresponded to a 100% of the electrode coverage: a 5.0 μL of anti-CRP↔MBs conjugated with 20 μL of 10 μg/mL CRP in the presence of an excess amount of QD/avidin↔anti-CRP.

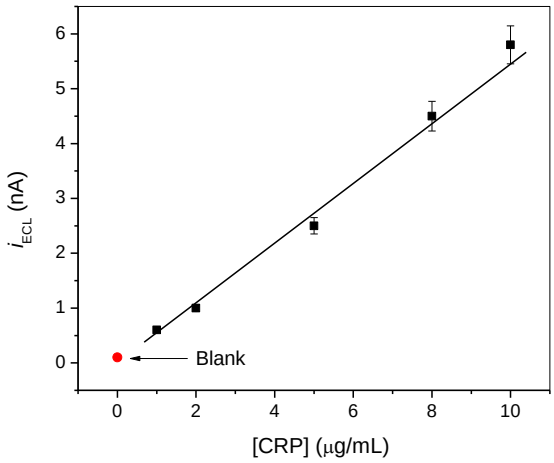

Figure 4.15. ECL response as a function of added CRP concentration obtained from QD ("Qdot 625")/avidin↔anti-CRP⟨CRP⟩anti-CRP↔MB aggregates on a Au/CD electrode in the presence of 50 mM DBAE-0.10 M phosphate buffer (pH 7.4) at a scan rate of 50 mV/s.

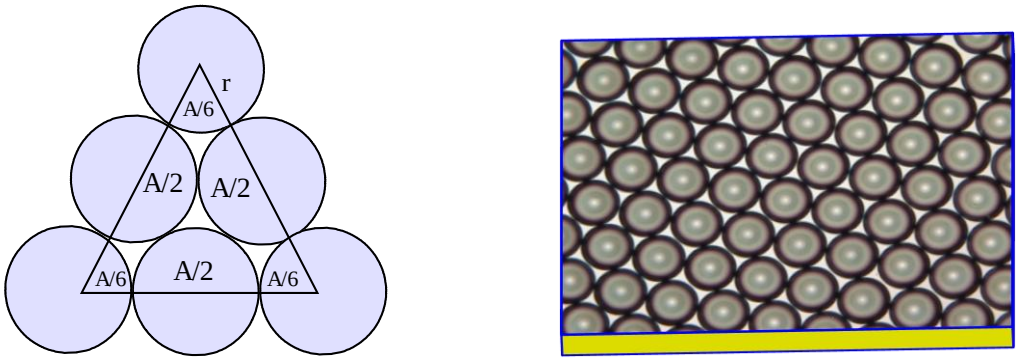

(a) (b)

Figure 4.16. A close-packed plane: (a) illustration of the area calculation, (b) demonstration of MBs closely packed on the surface of a Au/CD electrode.

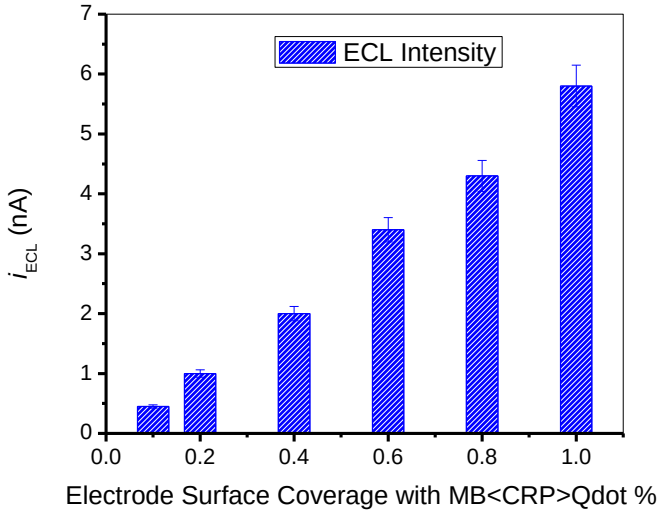

Figure 4.17. ECL response as a function of the electrode surface coverage with QD ("Qdot 625")/avidin↔anti-CRP⟨CRP⟩anti-CRP↔MB aggregates on a Au/CD electrode in the presence of 50 mM DBAE-0.10 M phosphate buffer (pH 7.4) at a scan rate of 50 mV/s. The added [CRP] = 10 μg/mL.

Conclusions

ECL of core/shell semiconductor CdSe/ZnS QDs coated with a carboxyl polymer layer ("Qdot 625") was studied in aqueous solutions using TPrA and DBAE as ECL coreactants. Upon the anodic potential scanning, strong ECL emissions were observed at GC electrode within the potential range of ~0.8 to 1.5 V vs Ag/AgCl when DBAE was used as the coreactant. The ECL behavior of the Qdot 625 was found to be strongly dependent on the types and concentrations of ECL coreactants as well as the nature of the working electrode. The ECL emission measured with the solution-phase Qdot 625/DBAE/GC electrode system had an apparent peak value of ~625 nm that matched well with the FL data. The Qdot 625 was used as an ECL label for sandwich-type immunoassays of CRP at Au/CD electrodes. A limit of detection of 1.0 μg/mL CRP could allow the developed method to be directly employed for the determination of CRP in human serum samples.

References

1. Smith, A. M., Duan, H., Mohs, A. M. & Nie, S. Bioconjugated quantum dots for in vivo molecular and cellular imaging. *Adv. Drug Del. Rev.* **60**, 1226-1240 (2008).

2. Smith, A. M. & Nie, S. Semiconductor Nanocrystals: Structure, Properties, and Band Gap Engineering. *Acc. Chem. Res.* **43**, 190-200 (2010).

3. Bawendi, M. G., Steigerwald, M. L. & Brus, L. E. The quantum mechanics of larger semiconductor clusters ("quantum dots"). *Annu. Rev. Phys. Chem.* **41**, 477-496 (1990).

4. Dabbousi, B. O., Rodriguez-Viejo, J., Mikulec, F. V., Heine, J. R., Mattoussi, H., Ober, R., Jensen, K. F. & Bawendi, M. G. (CdSe)ZnS Core−Shell Quantum Dots: Synthesis and Characterization of a Size Series of Highly Luminescent Nanocrystallites. *J. Phys. Chem. B* **101**, 9463-9475 (1997).

5. Mattoussi, H., Mauro, J. M., Goldman, E. R., Anderson, G. P., Sundar, V. C., Mikulec, F. V. & Bawendi, M. G. Self-Assembly of CdSe-ZnS Quantum Dot Bioconjugates Using an Engineered Recombinant Protein. *J. Am. Chem. Soc.* **122**, 12142-12150 (2000).

6. Murray, C. B., Kagan, C. R. & Bawendi, M. G. Synthesis and characterization of monodisperse nanocrystals and close-packed nanocrystal assemblies. *Annu. Rev. Mater. Sci.* **30**, 545-610 (2000).

7. Murray, C. B., Norris, D. J. & Bawendi, M. G. Synthesis and characterization of nearly monodisperse CdE (E = sulfur, selenium, tellurium) semiconductor nanocrystallites. *J. Am. Chem. Soc.* **115**, 8706-8715 (1993).

8. Bard, A. J., Ding, Z. & Myung, N. Electrochemistry and electrogenerated chemiluminescence of semiconductor nanocrystals in solutions and in films. *Structure and Bonding (Berlin, Germany)* **118**, 1-57 (2005).

9. Resch-Genger, U., Grabolle, M., Cavaliere-Jaricot, S., Nitschke, R. & Nann, T. Quantum dots versus organic dyes as fluorescent labels. *Nat Meth* **5**, 763-775 (2008).

10. Frasco, M. F. & Chaniotakis, N. Semiconductor quantum dots in chemical sensors and biosensors. *Sensors* **9**, 7266-7286 (2009).

11. Frasco, M. F. & Chaniotakis, N. Bioconjugated quantum dots as fluorescent probes for bioanalytical applications. *Anal. Bioanal. Chem.* **396**, 229-240 (2010).

12. Ding, Z., Quinn Bernadette, M., Haram Santosh, K., Pell Lindsay, E., Korgel Brian, A. & Bard Allen, J. Electrochemistry and electrogenerated chemiluminescence from silicon nanocrystal quantum dots. *Science* **296**, 1293-7 (2002).

13. Miao, W. Electrogenerated Chemiluminescence and Its Biorelated Applications. *Chem. Rev.* **108**, 2506-2553 (2008).

14. Qi, H., Peng, Y., Gao, Q. & Zhang, C. Applications of Nanomaterials in Electrogenerated Chemiluminescence Biosensors. *Sensors* **9**, 674-695 (2009).

15. Jie, G., Liu, B., Pan, H., Zhu, J. & Chen, H. CdS nanocrystal-based electrochemiluminescence biosensor for the detection of low-density lipoprotein by increasing sensitivity with gold nanoparticle amplification. *Anal. Chem.* **79**, 5574 (2007).

16. Jie, G., Zhang, J., Wang, D., Cheng, C., Chen, H.-Y. & Zhu, J.-J. Electrochemiluminescence Immunosensor Based on CdSe Nanocomposites. *Anal. Chem.* **80**, 4033-4039 (2008).

17. Huang, H., Jie, G., Cui, R. & Zhu, J.-J. DNA aptamer-based detection of lysozyme by an electrochemiluminescence assay coupled to quantum dots. *Electrochem. Commun.* **11**, 816-818 (2009).

18. Liu, X. & Ju, H. Coreactant Enhanced Anodic Electrochemiluminescence of CdTe Quantum Dots at Low Potential for Sensitive Biosensing Amplified by Enzymatic Cycle. *Anal. Chem.* **80**, 5377-5382 (2008).

19. Zhang, L., Zou, X., Ying, E. & Dong, S. Quantum dot electrochemiluminescence in aqueous solution at lower potential and its sensing application. *J. Phys. Chem. C* **112**, 4451-4454 (2008).

20. Invitrogen, http://www.invitrogen.com/site/us/en/home.html.

21. Goldman, E. R., Balighian, E. D., Mattoussi, H., Kuno, M. K., Mauro, J. M., Tran, P. T. & Anderson, G. P. Avidin: A Natural Bridge for Quantum Dot-Antibody Conjugates. *J. Am. Chem. Soc.* **124**, 6378-6382 (2002).

22. Goldman, E. R., Balighian, E. D., Kuno, M. K., Labrenz, S., Tran, P. T., Anderson, G. P., Mauro, J. M. & Mattoussi, H. Luminescent quantum dot-adaptor protein-antibody conjugates for use in fluoroimmunoassays. *Phys. Status Solidi B* **229**, 407-414 (2002).

23. Goldman, E. R., Clapp, A. R., Anderson, G. P., Uyeda, H. T., Mauro, J. M., Medintz, I. L. & Mattoussi, H. Multiplexed Toxin Analysis Using Four Colors of Quantum Dot Fluororeagents. *Anal. Chem.* **76**, 684-688 (2004).

24. Chang, M.-M., Saji, T. & Bard, A. J. Electrogenerated chemiluminescence. 30. Electrochemical oxidation of oxalate ion in the presence of luminescers in acetonitrile solutions. *J. Am. Chem. Soc.* **99**, 5399-403 (1977).

25. de Ferranti, S. & Rifai, N. C-reactive protein and cardiovascular disease: a review of risk prediction and interventions. *Clin. Chim. Acta* **317**, 1-15 (2002).

26. Haidari, M., Javadi, E., Sadeghi, B., Hajilooi, M. & Ghanbili, J. Evaluation of C-reactive protein, a sensitive marker of inflammation, as a risk factor for stable coronary artery disease. *Clin. Biochem.* **34**, 309-315 (2001).

27. Heilbronn, L. K. & Clifton, P. M. C-reactive protein and coronary artery disease: influence of obesity, caloric restriction and weight loss. *Journal of Nutritional Biochemistry* **13**, 316-321 (2002).

28. Onat, A., Sansoy, V., Yildirim, B., Keles, I., Uysal, O. & Hergenc, G. C-reactive protein and coronary heart disease in Western Turkey. *Am. J. Cardiol.* **88**, 601-607 (2001).

29. Rifai, N. C-reactive protein and coronary heart disease: diagnostic and therapeutic implications for primary prevention. *Cardiovasc. Toxicol.* **1**, 153-157 (2001).

30. Rifai, N. & Ridker, P. M. High-sensitivity C-reactive protein: a novel and promising marker of coronary heart disease. *Clin. Chem.* **47**, 403-411 (2001).

31. Wanner, C. & Metzger, T. C-reactive protein a marker for all-cause and cardiovascular mortality in haemodialysis patients. *Nephrol. Dial. Transplant.* **17**, 29-32 (2002).

32. Miao, W. & Bard, A. J. Electrogenerated chemiluminescence. 72. Determination of immobilized DNA and C-reactive protein on Au(111) electrodes using tris(2,2'-bipyridyl)ruthenium(II) labels. *Anal. Chem.* **75**, 5825-5834 (2003).

33. Miao, W. & Bard, A. J. Electrogenerated Chemiluminescence. 80. C-Reactive Protein Determination at High Amplification with $[Ru(bpy)_3]^{2+}$-Containing Microspheres. *Anal. Chem.* **76**, 7109-7113 (2004).

34. Chen, Z. & Zu, Y. Gold Nanoparticle-Modified ITO Electrode for Electrogenerated Chemiluminescence: Well-Preserved Transparency and Highly Enhanced Activity. *Langmuir* **23**, 11387-11390 (2007).

35. Kim, C. K., Kalluru, R. R., Singh, J. P., Fortner, A., Griffin, J., Darbha, G. K. & Ray, P. C. Gold-nanoparticle-based miniaturized laser-induced fluorescence probe for specific DNA hybridization detection: studies on size-dependent optical properties. *Nanotechnology* **17**, 3085 (2006).

36. Angnes, L., Richter, E. M., Augelli, M. A. & Kume, G. H. Gold Electrodes from Recordable CDs. *Anal. Chem.* **72**, 5503-5506 (2000).

37. Lowinsohn, D., Richter, E. M., Angnes, L. & Bertotti, M. Disposable gold electrodes with reproducible area using recordable CDs and toner masks. *Electroanalysis* **18**, 89-94 (2006).

38. Richter, E. M., Munoz, R. A. A., Bertotti, M. & Angnes, L. Heat-transference of toner masks onto conductive substrates: A rapid and easy way to produce microelectrode ensembles. *Electrochem. Commun.* **9**, 1091-1096 (2007).

39. Liu, X., Shi, L., Niu, W., Li, H. & Xu, G. Environmentally friendly and highly sensitive ruthenium(II) tris(2,2'-bipyridyl) electrochemiluminescent system using 2-(dibutylamino)ethanol as co-reactant. *Angew. Chem., Internation. Ed.* **46**, 421-424 (2007).

40. Note: this is estimated with DigiSim electrochemical simulation software.

41. Bard, A. J. & Faulkner, L. R. *Electrochemical Methods: Fundamentals and Applications* (John Wiley & Sons, Inc., New York, 2001).

42. Lai, R. Y. & Bard, A. J. Electrogenerated Chemiluminescence. 70. The Application of ECL to Determine Electrode Potentials of Tri-n-propylamine, Its Radical Cation, and Intermediate Free Radical in MeCN/Benzene Solutions. *J. Phys. Chem. A* **107**, 3335-3340 (2003).

43. Zu, Y. & Bard, A. J. Electrogenerated Chemiluminescence. 66. The Role of Direct Coreactant Oxidation in the Ruthenium Tris(2,2')bipyridyl/Tripropylamine System and the Effect of Halide Ions on the Emission Intensity. *Anal. Chem.* **72**, 3223-3232 (2000).

44. Zu, Y. & Bard, A. J. Electrogenerated chemiluminescence. 67. Dependence of light emission of the tris(2,2'-bipyridyl)ruthenium(II)/tripropylamine system on electrode surface hydrophobicity. *Anal. Chem.* **73**, 3960-3964 (2001).

45. Bae, Y., Myung, N. & Bard, A. J. Electrochemistry and Electrogenerated Chemiluminescence of CdTe Nanoparticles. *Nano Lett.* **4**, 1153-1161 (2004).

46. Myung, N., Bae, Y. & Bard, A. J. Effect of Surface Passivation on the Electrogenerated Chemiluminescence of CdSe/ZnSe Nanocrystals. *Nano Lett.* **3**, 1053-1055 (2003).

47. Myung, N., Lu, X., Johnston, K. P. & Bard, A. J. Electrogenerated Chemiluminescence of Ge Nanocrystals. *Nano Lett.* **4**, 183-185 (2004).

48. Cheng, C. & Yan, H. Bandgap of the core-shell CdSe/ZnS nanocrystal within the temperature range 300-373 K. *Physica E* **41**, 828-832 (2009).

49. Debad, J. D., Glezer, E. N., Leland, J. K., Sigal, G. B. & Wohlsadter, J. Clinical and biological Applications of ECL, in *Electrogenerated Chemiluminescence* (ed. Bard, A. J.), 359-396, Chapter 8 (Marcel Dekker, Inc., New York, 2004).

50. Angnes, L., Richter, E. M., Augelli, M. A. & Kume, G. H. Gold Electrodes from Recordable CDs. *Anal. Chem.* **72**, 5503-5506 (2000).

CHAPTER V

TOWARD SIMULTANEOUSLY MULTIPLEXED DETECTION OF BIO-MOLECULES USING ELECTROGENERATED CHEMILUMINESCENCE*

Introduction

ECL is superior to photoluminescence owing to its high sensitivity, very low background, and good temporal and spatial control capability.[1,2] For example, compared with fluorescence (FL) methods, ECL does not need a light source, which effectively frees the ECL from scattered-light and luminescent impurity interferences. In addition, the specificity of the ECL reaction associated with an ECL label and a coreactant decreases problems with side reactions (e.g., self-quenching). This is supported by several recent studies,[3-5] where different immunoassays based on enzyme-linked immunosorbent assay (ELISA), chemiluminescence (CL), ECL, and FL were compared, and ECL-based immunoassays were found to have excellent reproducibility and sensitivity over other assays. ECL has now been proven to be a very powerful analytical technique and been widely used in flow injection analysis, high-performance liquid chromatography, and capillary electrophoresis for the detection of, e.g., oxalate, alkylamines, nucleic acids and proteins.[6-15] Although a large number of chemiluminescent reagents such as polyaromatic hydrocarbons (e.g., 9,10-diphenylanthracene (DPA, Figure 5.1a), rubrene (RUB, Figure 5.1b)) and metal complexes (e.g., $Ru(bpy)_3^{2+}$, Figure 5.1c) have been applied in ECL reactions,[16-18] $Ru(bpy)_3^{2+}$ type species are obviously the most widely used ECL emitting reagents in the

* Part of this work was presented in: Miao, W. & Wang, S. *PITTCON*, 130-3 (March 2-7, 2008, New Orleans, LA).

detection and quantification of analyte of interest, due to their superior properties in the ECL production, which include high sensitivity, high efficiency, and good stability under moderate conditions in aqueous solution.[19]

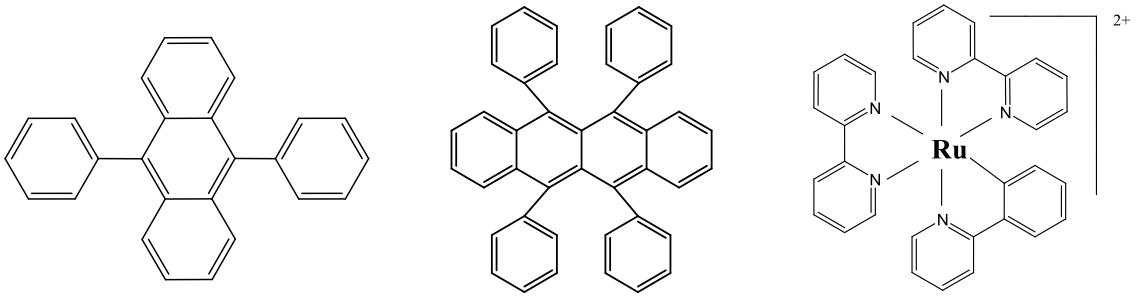

(a) (b) (c)

Figure 5.1. Molecular structures of (a) 9,10-diphenylanthracene (DPA), (b) rubene (RUB), and (c) $Ru(bpy)_3^{2+}$.

Multiplexing permits greater throughput, minimizes sample volume and handling, decreases assay cost and increases the amount of information obtainable from each sample. Various approaches for conducting multiplexed assays have been described using, for example, FL microspheres or QD probes,[20-24] electrochemical microelectrode arrays,[25] and mass spectrometric immunoassays.[26] Although ECL offers many advantages over other detection techniques, its development in multiplexed analysis is very limited. Most recently, Walt's group[27] described a bead-based platform that exploited ECL to detect three antigens simultaneously by individually imaging fluorescently encoded microbeads located in a microwell array. Similar imaging-based ECL assays have been commercialized by Meso Scale Diagnostics.[28] In both cases, ECL signals are imaged from attached $Ru(bpy)_3^{2+}$ labels in the presence of TPrA.

In this chapter, the basic principle and the proof for the concept of multiplexed ECL detection in solution will be presented.

General Principles of Multiplexing ECL Assays

Multiplexed ECL detection of biomolecules may be realized as illustrated in Figure 5.2. Different ECL labels with distinctive ECL emission wavelengths (λ) are loaded separately into different sets of micro-/nanobeads or micro-/nanocapsules. Each set of ECL labels are then coated with one type of specific antibodies (Figure 5.2a) or target single-stranded (ss) DNAs (Figure 5.2b). Similarly, different types of antibodies or probe ssDNAs are separately immobilized onto one type of micro-/nanosized magnetic beads (MBs). Aggregates are formed when ECL label loaded beads mix with MBs in the presence of the analytes. The aggregates are separated magnetically from the solution suspension, where unbound ECL labels remain. ECL spectra are subsequently recorded from the solution containing dissolved or released ECL labels (from the aggregates) and added coreactant. The type and the amount of target analytes can be verified and determined from the ECL peak positions and intensities, respectively (Figure 5.2c). Traditionally, only one or few labels can be attached directly to one target biomolecule, so that nonspecific adsorption can be avoided and the bioactivity of the target biomolecule remains. In the present configuration, each ECL label carrier is loaded with a large amount of ECL labels (e.g., ~10^9 $Ru(bpy)_3^{2+}$ molecules per 10-μm polystyrene bead).[29]

Requirements of ECL labels

Ideally, prospective ECL labels used in this study should meet the following five criteria: (1) high ECL efficiencies so that high sensitivity and low detection limits can be obtained; (2) sufficiently soluble in organic solvents but completely insoluble in aqueous solutions when micro-/nanosized PSBs are used as ECL label carriers. In this way, ECL

labels can be effectively loaded into PSBs and remain within them during a series of water-phase processes such as avidin coating and DNA hybridization; (3) well distinguishable emission wavelengths to enable the spectra-based ECL signal separation and the individual species quantification; (4) ECL can be generated from different labels under the same experimental conditions; and (5) oxygen from air and trace amounts of water (from preceding aqueous reactions etc.) in organic solvent should not affect the ECL production, which would allow the developed technique to be widely used under relatively unrestricted conditions.

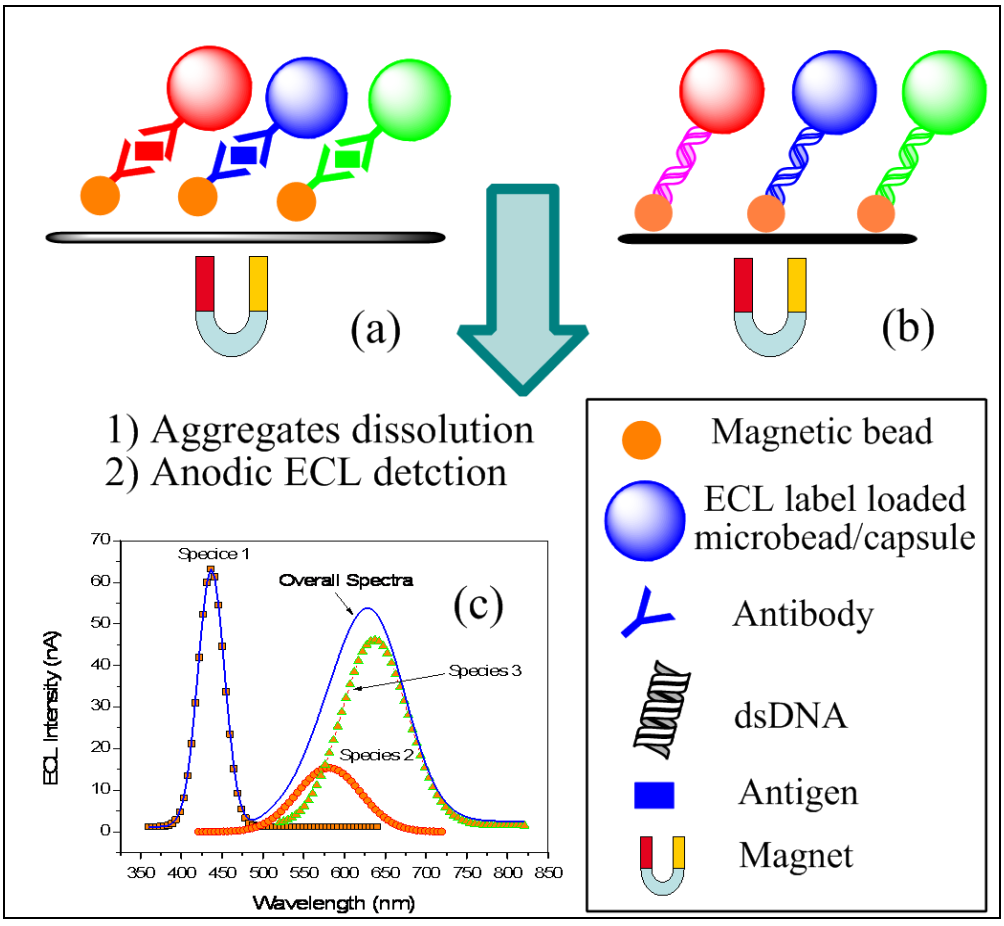

Figure 5.2. General principle of multiplexing ECL assays. (a) ECL immunoassays, (b) ECL DNA probes, and (c) ECL spectra from mixed ECL labels.

Principle of Effective Loading of Hydrophobic ECL Labels into PSBs

Figure 5.3 shows an example of such a process, where PSBs modified with carboxyl groups are swollen in an organic solvent with dissolved ECL labels. The water-insoluble ECL labels diffuse into the polymer matrix, and are entrapped when the solvent is removed from the beads by vacuum evaporation or transferred to an aqueous phase medium. Because the ECL intensity is generally proportional to the ECL label concentration, the ECL labels should be sufficiently loaded into each bead. Note that different ECL labels are to be separately loaded into different sets of PSBs, i.e., each bead contains only one type of ECL labels. Therefore, it avoids the problem of ECL label partitioning. It is also not an issue where the labels are located in the beads, because ECL tests will be conducted after the beads/ECL labels dissolve in MeCN. However, labels adsorbed on PSB surfaces should be washed away so that the surface functional groups can be used. This is followed by the centrifugation separation of PSB/ECL labels from free labels in the solution. Finally, the beads can be either dried under vacuum or suspended in water to remove residual solvent.

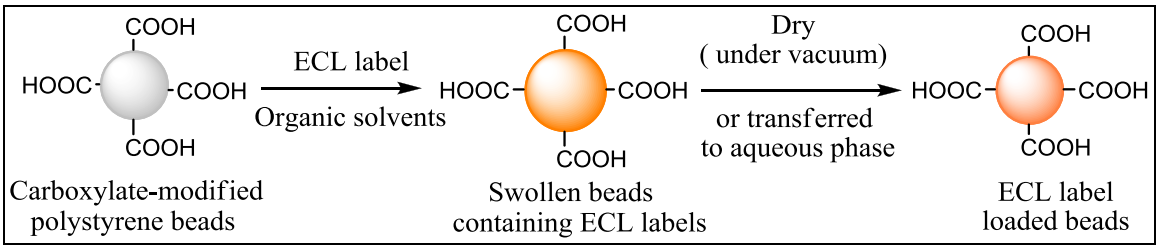

Figure 5.3. Internal loading of ECL labels into polystyrene beads.

Experimental Section

Chemicals and materials

Tris(2,2′-bipyridyl)ruthenium dichloride hexahydrate ($Ru(bpy)_3Cl_2.6H_2O$), tri-*n*-propylamine (TPrA, 99+%), rubrene (RUB), and 1-methyl-imidazole (99%) from Aldrich (Milwaukee, WI); lithium tetrakis(pentafluorophenyl) borate ($Li[B(C_6F_5)_4]\cdot nEt_2O$, n=2-3) from Boulder Scientific Co. (Mead, CO); hydrochloric acid (HCl, 37.5%), hydrogen peroxide (H_2O_2, 30%), pH phosphate-buffered saline (PBS buffer, 0.10 M sodium phosphate-0.15 M sodium chloride, pH 7.4), methanol (spectroanalyzed grade), and sodium chloride (NaCl, certified A.C.S.) from Fisher (Fairlawn, NJ); sodium hydroxide (NaOH, 98.7%) from J. T. Baker (Phillipsburg, NJ); silver nitrate ($AgNO_3$, 99.5%), 9,10-diphenylanthracene (DPA), and tetra-*n*-butylammonium perchlorate (TBAP, 99+%, electrochemical grade) from Fluka (Milwaukee, WI); acetonitrile (MeCN, 99.93+%, HPLC grade), 2-(dibutylamino)ethanol (DBAE, 99%), and N-hydroxysuccinimide (NHS) from Sigma (St. Louis, MO); tetrahydrofuran (THF, GR) and ethylenediaminetetraacetic acid (EDTA) from EM (Gibbstown, NJ); tris(hydroxymethyl)-aminomethane (Tris), and avidin (NeutrAvidin) from Pierce (Rockford, IL) were used as received. Carboxylated polystyrene microspheres/beads (PSB, 10-μm diameter, 2.6% (w/w) aqueous suspension with ~6.5×10^4 beads/μL) and streptavidin-coated superparamagnetic polystyrene beads (MBs) were purchased from Dynal Biotech (Lake Success, NY).

Unless otherwise stated, all aqueous solutions were prepared with deionized-distilled water produced from a Barnstead MP-6A Mega-Pure® system (Barnstead international Dubuque, Iowa).

Synthesis of Hydrophobic $Ru(bpy)_3^{2+}$ ECL Labels

Because $Ru(bpy)_3Cl_2$ is soluble in aqueous and organic solutions, tris-(2,2'-bipyridyl)ruthenium(II) tetrakis(pentafluorophenyl)borate ($Ru(bpy)_3[B(C_6F_5)_4]_2$) was chosen as the ECL label in this project. $Ru(bpy)_3[B(C_6F_5)_4]_2$ is soluble in organic solvents but completely insoluble in aqueous solutions. This complex, as shown below, can be effectively loaded into polystyrene beads in an organic solution and remained within the beads during a series of modifications of the beads in aqueous solution. On the other hand, $Ru(bpy)_3[B(C_6F_5)_4]_2$, like $Ru(bpy)_3Cl_2$, has shown a similar ECL efficiency.[15] The synthesis of $Ru(bpy)_3[B(C_6F_5)_4]_2$ was carried out by a metathesis reaction between $Ru(bpy)_3Cl_2$ and $Li[B(C_6F_5)_4]\cdot nEt_2O$ (n = 2-3) in aqueous solution. The sediment was washed with water, recrystallized in an acetonitrile/water solution, and dried under vacuum.[15]

Effective loading of the ECL labels into polystyrene beads

10-μm diameter carboxylated polystyrene beads were detached from a ~1.0 mL of a 2.6% (w/w) polystyrene bead suspension by an Eppendorf 5415D centrifuge (Brinkmann Instruments, Inc., Westbury, NY) at 10,000 rpm for 5 min, and washed once with ~1 mL of water. The beads were dried under vacuum at ~60 ℃ for 1 h, followed by addition of ~1.5 mL of the ECL labels, $Ru(bpy)_3[B(C_6F_5)_4]_2$, DPA, or RUB-saturated (~0.7 mM, ~1.0 mM, or ~0.5 mM, respectively) 5% THF-95% MeOH (v/v) solution into a 1.5-mL microcentrifuge tube containing PSBs. The mixture was rotated with a Dynal sample mixer (Dynal Biotech Inc.) at 20 rpm for 2 h, followed by centrifugation and washing with 50% MeOH-50% H_2O (v/v) twice.

Immobilization of Avidin on the Surface of Ru(II) ⊂PSB, DPA ⊂PSB, and RUB ⊂PSB

Ru(II)⊂PSB, DPA⊂PSB, and RUB⊂PSB were separately immobilized with a layer of avidin through the formation of amide bonds [e.g., Ru(II)⊂PSB-CONH-avidin] by mixing the beads with 1.5 mL of freshly prepared 25 μM avidin in a 0.10 M 1-methyl-imidazole buffer (pH 7.5) and then adding 0.10 M EDAC and 0.10 M NHS and rotating the mixture at ~40 rpm for 1 h. The newly formed avidin-coated Ru(II)⊂PSB, DPA⊂PSB, and RUB⊂PSB (referred to as Ru(II)⊂PSB/avidin, DPA⊂PSB/avidin, and RUB⊂PSB/avidin, respectively) were centrifuged from the reaction solution at 5-10,000 rpm for 5 min and washed with 1 mL of 1X "B/W buffer" (1X binding/washing buffer, 5.0 mM Tris-HCl (pH 7.5) + 0.5 mM EDTA + 1.0 M NaCl) 3 times. The final avidin-coated three types of PSBs were individually resuspended in a 1X B/W buffer solution that had the same volume as the starting PSB suspension (0.10-1.0 mL) and kept at ~4 ℃ until use. Approximately, 6.5×10^4 Ru(II) (DPA or RUB)⊂PSB /avidin beads/μL can thus be estimated, with the assumption of no loss of the beads during the preparation of Ru(II) (DPA or RUB)⊂PSB /avidin.

ECL and Electrochemical Measurements

CV and ECL measurements were conducted with the same instruments described in previous chapters. Briefly, a model 660A electrochemical workstation (CH Instruments, Austin, TX) was combined with a homebuilt ECL detection system for CV as well as ECL experiments. What unique in this chapter was that nearly all CV and ECL tests were carried out in acetonitrile solutions. As a result, 0.10 M TBAP as the supporting electrolyte and a Ag/Ag^+ (10 mM $AgNO_3$-50 mM TBAP in MeCN) as the reference electrode were used. Because all electrochemical reactions occurred in positive potential regions, degassing of oxygen with nitrogen was found to be unnecessary, which

significantly simplified the procedures and reduced the time frame of assay. For ECL spectra acquisitions, a set of 24 pieces of interference filters (Intro, Inc. Socorro, NM) with a spectral range of 360 to 820 nm were used; the filter was sandwiched between the PMT detector biased at -700 V and the bottom of an electrochemical/ECL cell. The working electrode in this case was changed to a large Pt flag electrode with dimensions of ~1 ×1 cm^2, so that the loss in ECL light intensity after passing the filter (~50% transmittance and $\Delta\lambda_{1/2}$ = 10 nm on an average at the specified wavelength) can be compensated. The obtained partially overlapped spectra were deconvoluted with OriginPro 8 (OriginLab, Northampton, MA) or PeakFit[30] software. All measurements were conducted at a room temperature of 24 ± 1 ℃, unless otherwise stated.

Results and discussion

Selection of ECL Labels and ECL Coreactant

MeCN was used as the ECL testing solvent because of its good solubility for PSBs and its wide potential window. Moreover, strong ion annihilation ECL was observed from many metal chelates as well as polycyclic aromatic hydrocarbons, since these compounds can be reversibly oxidized and reduced in MeCN. For example, the ECL efficiency Φ_{ECL} (via ion annihilation) for $Ru(bpy)_3^{2+}$ [$E_{1/2}$(ox) = +1.35 V, $E_{1/2}$(red) = -1.32 V vs. SCE],[31] DPA [$E_{1/2}$(ox) = +1.29 V, $E_{1/2}$(red) = -1.96 V vs. SCE],[32] and RUB [$E_{1/2}$(ox) = +0.82 V, $E_{1/2}$(red) = -1.56 V vs. SCE in 1:1 MeCN/PhH][32] were reported to be 5%,[33] 25%,[34] and 25%,[35,36] respectively. Note that 25% efficiency for DPA represents the theoretical maximum for ECL from DPA singlets.[34] Their ECL emissions are also well separated: λ_{max} ($Ru(bpy)_3^{2+}$) ~620 nm, λ_{max} (DPA) ~420 nm, and λ_{max} (RUB) ~540 nm.[37] As expected, immediately after the oxidation of coreactant DBAE [E_p = 0.61 V vs

Ag/Ag^+ (10 mM), Figure 5.4a], $Ru(bpy)_3^{2+}$, DPA and RUB can all be oxidized and react with strong reducing species, $DBAE^{\bullet}$ free radicals generated from oxidized coreactant, to form excited state species that emit light (Figure 5.5).[18,38,39] Note that TPrA [E_p = 0.76 V vs Ag/Ag^+, Figure 5.4b] is not suitable for the present systems; it produces significantly high ECL background [~35 nA vs ~3 nA from DBAE (Figure 5.4a), or vs ±0.5 nA from the PMT darkcurrent[40]], presumably due to "inverse photoemission."[41] Also, only very weak ECL is generated from the DPA/TPrA system (Figure 5.5A), probably due to the reducing energy of $TPrA^{\bullet}$ free radical (~-1.7 V vs SCE)[32] being lower than that needed for the reduction of DPA to $DPA^{\bullet-}$ [$E_{1/2}$(red) = -1.96 V vs. SCE].[31] This suggests that the electrode potential of $DBAE^{\bullet}$ free radical should be <-1.96 V vs SCE. As a result, when a relatively high concentration of DBAE (e.g., 80-100 mM) is used, $Ru(bpy)_3^{2+}$, DPA, and RUB are all excellent ECL emitters (Figure 5.5). Note that these ECL labels, unlike their oxidized or reduced species, are very stable and can coexist in a solution with DBAE; no cross reaction occurs with each other. Figure 5.5B(d) shows an overall ECL profile obtained from a mixture solution of the above three labels. The appearance of each ECL profile (Figures 5.5B (a)-(c)) is consistent with its oxidation potential. When the three labels coexist in 0.10 M DBAE MeCN solution, the potential range of the ECL wave covers all three individual labels, and the ECL peak current is approximately the sum of the three individuals. This demonstrates that simultaneous detection of three different ECL labels, hence three analytes, is highly probable (see following section for more details).

Figure 5.6 shows the effect of electrode materials on the ECL intensity as a function of DBAE concentration in 0.10 M TBAP MeCN with a scan rate of 50 mV/s.

ECL peak values from the first cycle of potential scanning were used. In the case of $Ru(bpy)_3^{2+}$ emitter (Figure 5.6a), ECL responses are larger at Pt than those at Au.

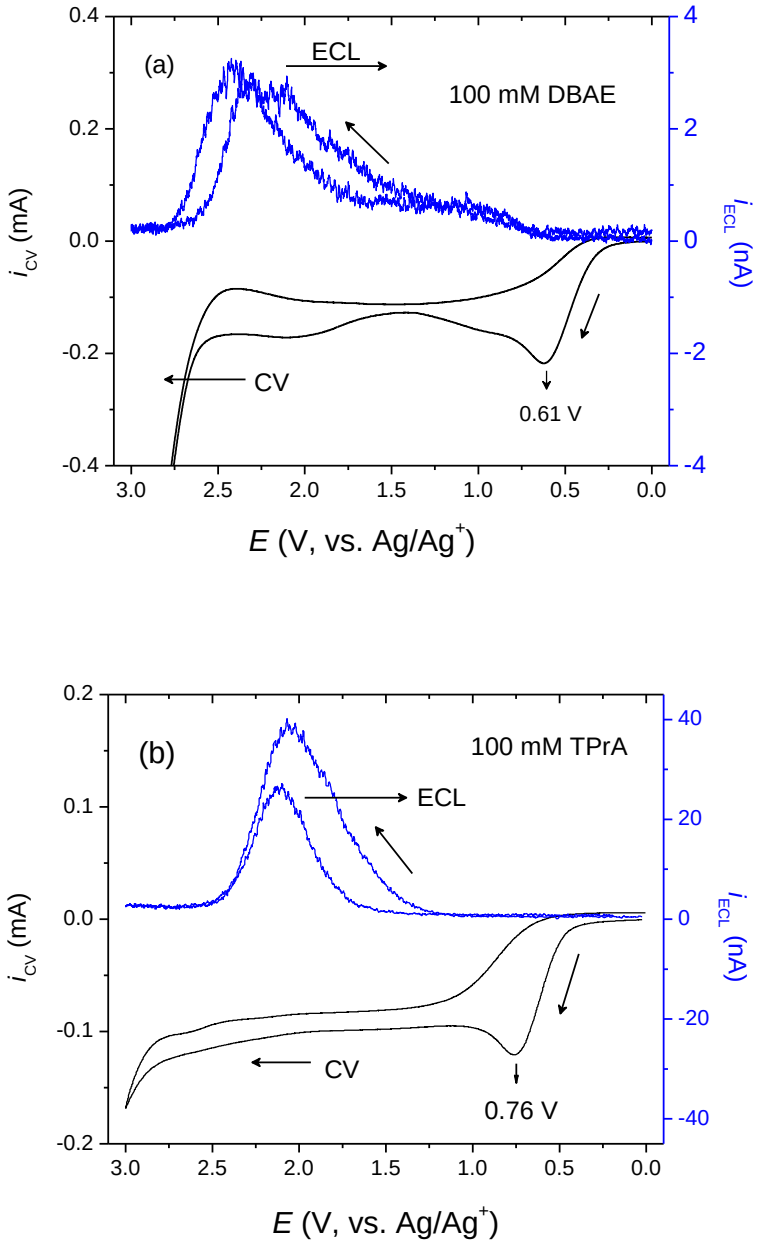

Figure 5.4. CV and ECL responses of 0.10 M coreactant (a) DBAE and (b) TPrA in MeCN containing 0.10 M TBAP at a 2-mm diameter Pt electrode with a scan rate of 50 mV/s.

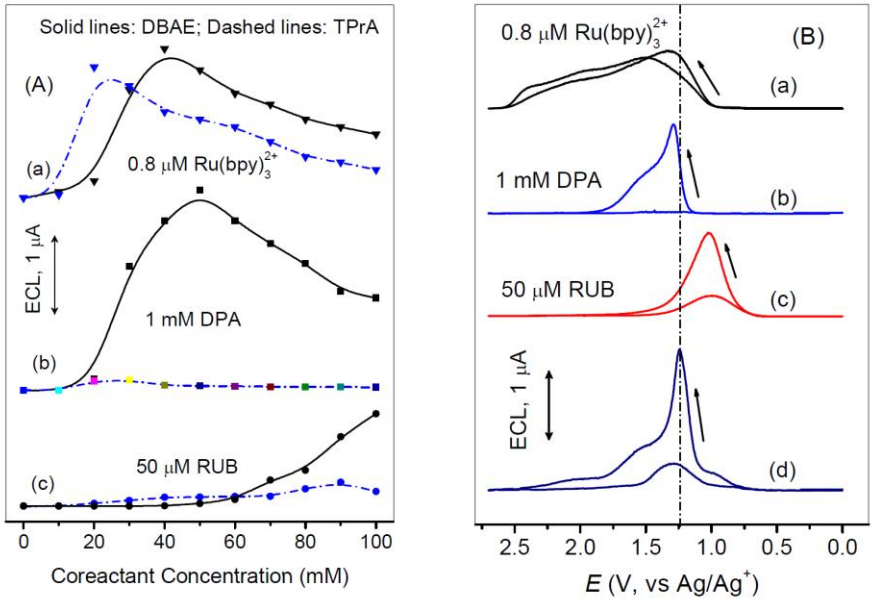

Figure 5.5. (A) Coreactant [TPrA] and [DBAE] effect on ECL intensity of (a) 0.8 μM $Ru(bpy)_3^{2+}$, (b) 1.0 mM DPA, and (c) 50 μM RUB; (B) ECL profiles of (a) 0.8 μM $Ru(bpy)_3^{2+}$, (b) 1.0 mM DPA, (c) 50 μM RUB, and (d) (a)+(b)+(c) using 0.10 M DBAE as the coreactant in MeCN containing 0.10 M TBAP on 2 mm Pt at a scan rate of 50 mV/s.

The GC electrode is not suitable for the system because no ECL can be produced after the initial cycling, presumably due to dramatic changes in the surface properties (e.g., a polymer film formation on the electrode). For both DPA (Figure 5.5b) and RUB systems (Figure 5.6c), the produced ECL signals increase with the following order: GC << Pt < Au. That is, the Au electrode seems slightly better than Pt for the ECL generation. However, as shows in Figure 5.6d, the ECL background is also electrode dependent, in which the GC electrode has the lowest responses within the entire DBAE concentration range of 10 to 100 mM, whereas the Au electrode has the highest blank signals. The exact reason for this remains unclear, but it is presumably due to "inverse photoemission".[41] This behavior is surprisingly different from that obtained from a Au/CD electrode using

DBAE as a coreactant (Figure 4.14C). Solvent as well as Au crystal structure may have played certain roles. Thus, Pt is the most suitable electrode material for ECL generation.

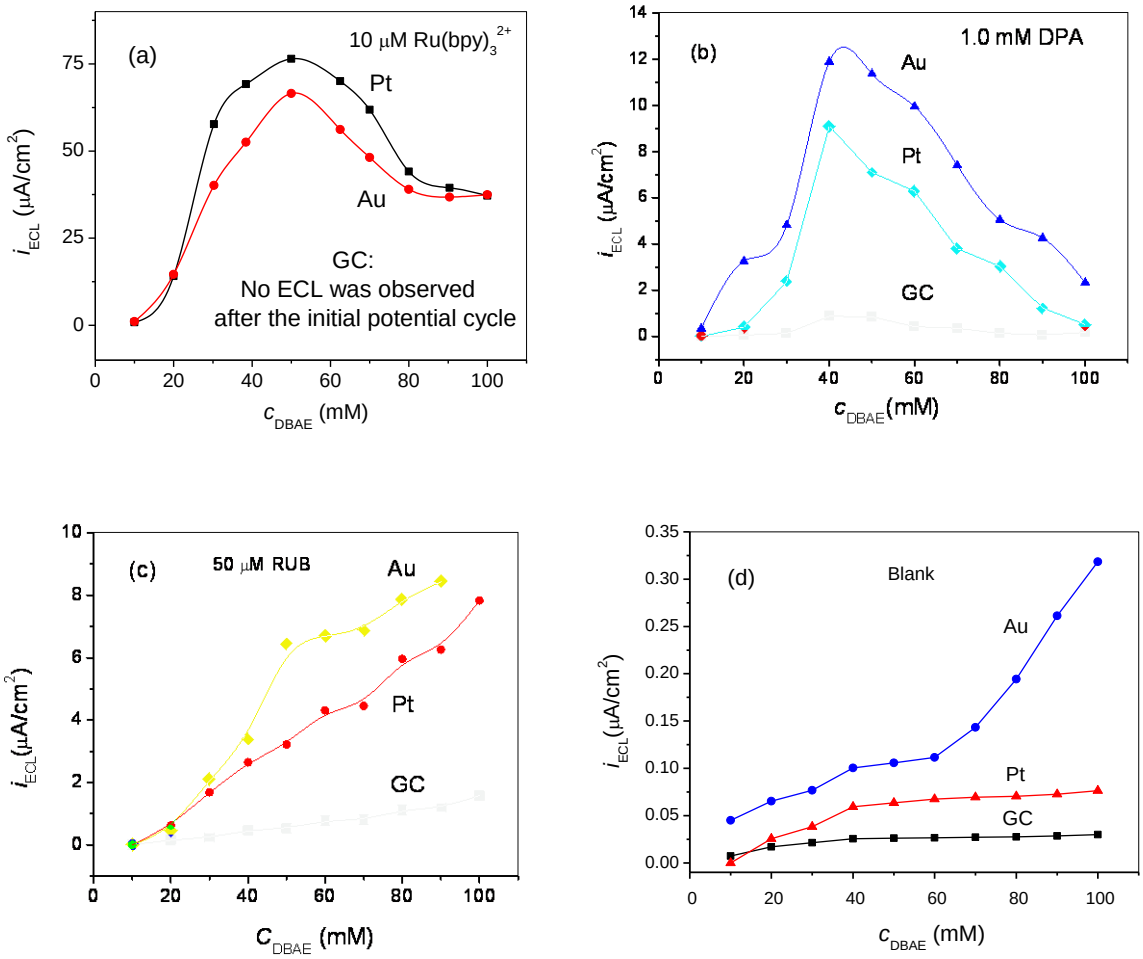

Figure 5.6. Effect of the electrode material on ECL intensity obtained from (a) 10 μM $Ru(bpy)_3^{2+}$, (b) 1.0 mM DPA, and (c) 50 μM RUB in 0.10 M TBAP MeCN at different concentrations of DBAE at a scan rate of 50 mV/s; (d) Blank ECL responses.

ECL spectra and their deconvolution

Figure 5.7 shows the ECL spectra of the three individual emitters in 0.10 M DBAE-0.10 M TBAP MeCN at a Pt electrode. The maximum ECL emissions from $Ru(bpy)_3^{2+}$, DPA, and RUB appear at ~635, ~440, and ~560 nm, respectively. Figure 5.8 shows the

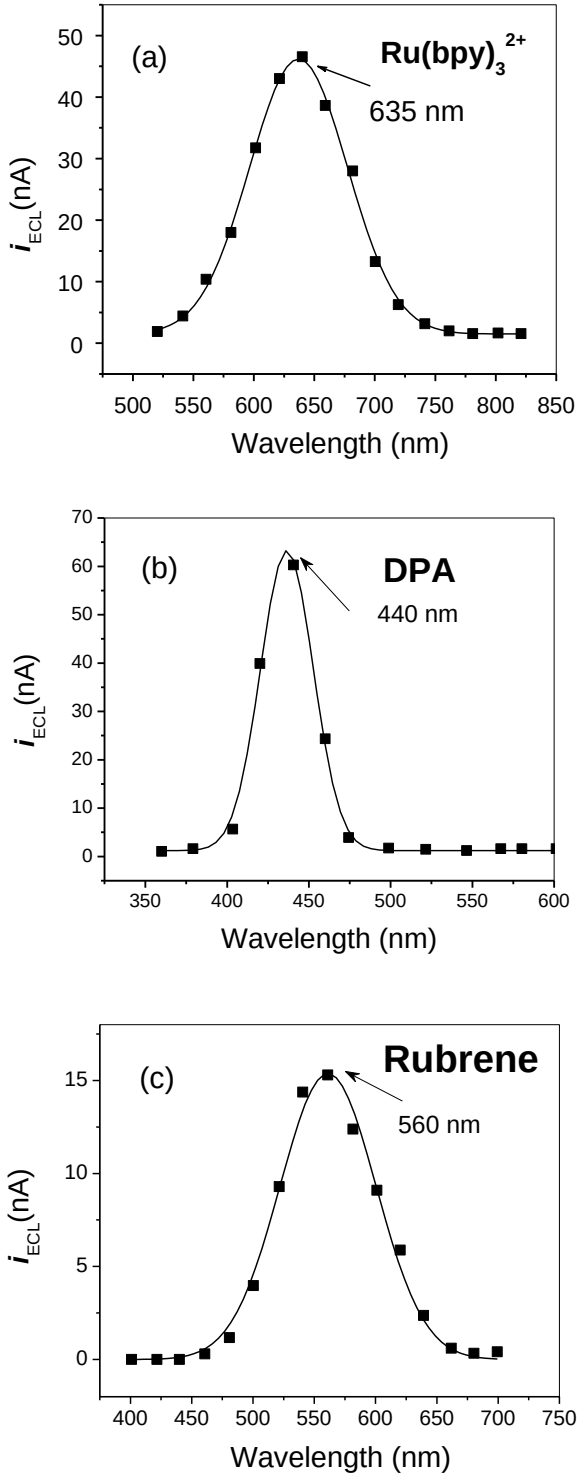

Figure 5.7. ECL spectra obtained in 0.10 M DBAE-0.10 M TBAP MeCN containing (a) 4.0 μM $Ru(bpy)_3^{2+}$, (b) 1.0 mM DPA, and (c) 50 μM RUB at a Pt flag electrode at a scan rate of 50 mV/s.

ECL spectra from mixed ECL labels in MeCN containing 0.10 M DBAE. Identification and deconvolution of partially overlapped peaks can be readily undertaken with a commercially available digital simulation or spectral fitting program, such as OriginPro 8.0 and PeakFit®[30] programs. Such a spectral simulation or fitting is constrained by the known ECL emissions including λ_{max} values. Therefore, errors introduced by deconvolution of experimentally obtained spectra, which contain essentially no background, are small. This can be seen from Figure 5.8, where experimentally obtained data are well fitted with the three individual emission waves.

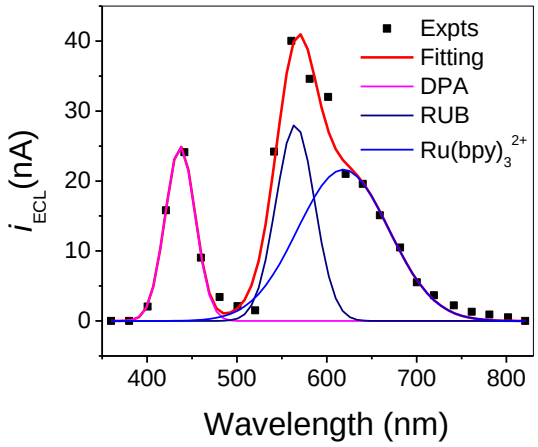

Figure 5.8. ECL spectra of $Ru(bpy)_3^{2+}$ (0.40 μM), DPA (0.50 mM) and RUB (50 μM) mixture in MeCN containing 0.10 M DBAE-0.10 M TBAP at a Pt flag electrode with a scan rate of 50 mV/s.

Investigations on the relationship between the ECL peak intensity and its added concentration in the presence of two other ECL labels were also conducted (Figure 5.9). In all three cases, linear correlations between the concentration of an ECL label and its fitted ECL peak intensity are evident.

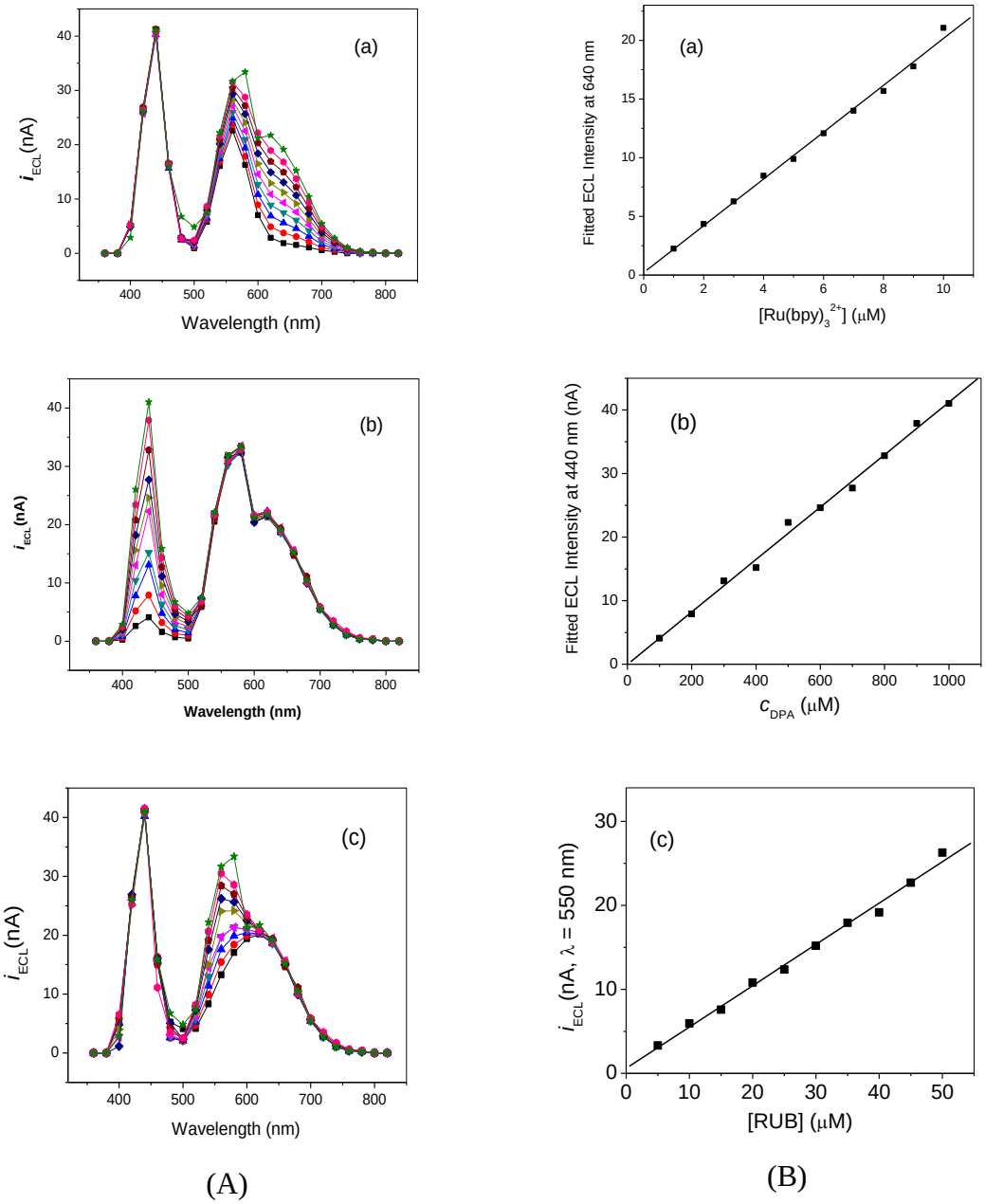

Figure 5.9. (A) ECL spectra from solutions containing three ECL labels, and (B) ECL peak intensity as a function of the concentration of an added ECL label when two others concentrations remained constant. Concentration changes corresponded to (a) $Ru(bpy)_3^{2+}$, (b) DPA, and (c) RUB in MeCN with 0.10 M DBAE-0.10 M TBAP at a Pt flag electrode with a scan rate 50 mV/s. All data in (B) were obtained from fitted ECL spectra at respective λ_{max}. The CV was scanned between 0 and 2.50 V vs Ag/Ag^+.

Spectral fitting of severely overlapped peaks in high resolution X-ray photoelectron spectroscopy has been widely used for many years.[42] Although three ECL labels are used in the present studies, at least two more ECL labels with λ_{max} values of ~490 nm and 700 nm could be added to the current system, resulting in five target analytes simultaneously detectable over a common ECL detector spectral range of 400-850 nm. There is, however, no certain number of ECL labels required to realize the multiplexing detection.

Verification of Effective Loading of ECL Labels into PSBs

Figure 5.10 shows the fluorescent images of PSBs loaded with $Ru(bpy)_3[B(C_6F_5)_4]_2$ (Figure 5.10a), DPA (Figure 5.10b), and RUB (Figure 5.10c). The images were taken with a Nikon Eclipse TE 300 inverted microscope (Nikon Instruments Inc., Melville, NY) with a UV light excitation.

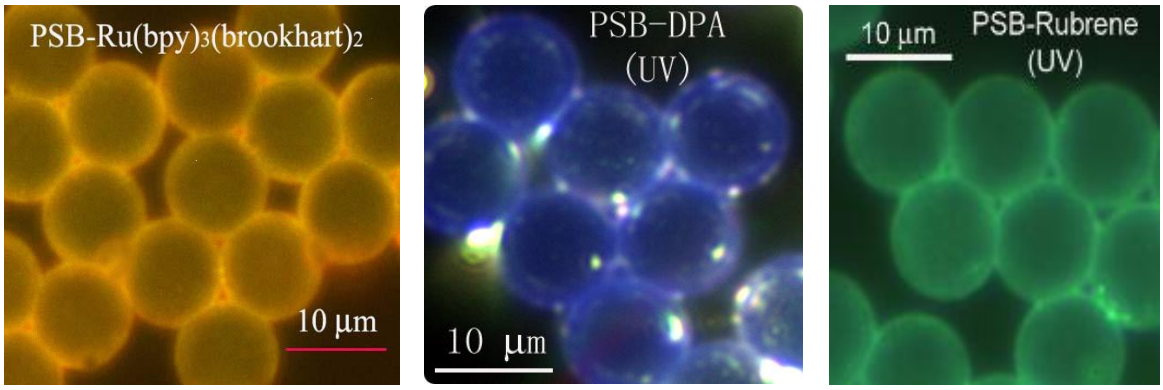

(a) (b) (c)

Figure 5.10. Fluorescent images of 10-µm diameter carboxylate polystyrene beads loaded with (a) $Ru(bpy)_3[B(C_6F_5)_4]_2$, (b) DPA, and (c) RUB.

A typical loading capacity of ~7.5×10^9 $Ru(bpy)_3[B(C_6F_5)_4]_2$ molecules,[15] ~16×10^9 DPA molecules, and ~9.0×10^9 RUB per 10-µm PSB were estimated on the basis of the ECL data obtained from Ru(II)⊂PSB, DPA⊂PSB, and RUB⊂PSB dissolved in MeCN

and their respective standard solutions using TPrA (for $Ru(bpy)_3[B(C_6F_5)_4]_2$)[15] or DBAE (for DPA and RUB) as the coreactant.

Characterization of Avidin-Coated PSBs Preloaded with ECL Labels

The avidin coated beads, i.e., Ru(II)⊂PSB/avidin, DPA⊂PSB/avidin, and RUB⊂PSB/avidin, were mixed with diluted fluorescein biotin solution, washed with 1X "B/W buffer", and air dried. This was followed by a fluorescent imaging examination. A characteristic bright green, evenly distributed image on the surface of each bead was seen, whereas only light imaging was observed from the control experiment, where non-avidin-coated Ru(II)⊂PSB, DPA⊂PSB, and RUB⊂PSB beads were used (images not shown). This result confirms that a thin layer of avidin had been covalently attached to the ECL label loaded PSBs.

Conclusions

ECL behavior of three hydrophobic luminophores, $Ru(bpy)_3[B(C_6F_5)_4]_2$, DPA, and RUB, with distinctive emission wavelengths was explored in MeCN solution using DBAE and TPrA as the oxidative-reduction type coreactant. Their ECL intensities were found to be dependent on the material of the working electrode as well as the type and the concentration of coreactant. In MeCN with DBAE as the coreactant and Pt as the working electrode, the partially overlapped ECL spectra from a mixed ECL-label solution can be well deconvoluted. The ECL peak value obtained from the digital simulation or fitting was found to be linearly proportional to the concentration of the emitter. These data suggest that using different ECL labels loaded PSBs that combine with respective MBs, ECL based multiplexing detection of biomolecules is feasible.

References

1. Bard, A. J. (ed.) *Electrogenerated Chemiluminescence* (Marcel Dekker, Inc., New York, 2004).
2. Miao, W. Electrogenerated Chemiluminescence and Its Biorelated Applications. *Chem. Rev.* **108**, 2506-2553 (2008).
3. Fichorova, R. N., Richardson-Harman, N., Alfano, M., Belec, L., Carbonneil, C., Chen, S., Cosentino, L., Curtis, K., Dezzutti, C. S., Donoval, B., Doncel, G. F., Donaghay, M., Grivel, J.-C., Guzman, E., Hayes, M., Herold, B., Hillier, S., Lackman-Smith, C., Landay, A., Margolis, L., Mayer, K. H., Pasicznyk, J.-M., Pallansch-Cokonis, M., Poli, G., Reichelderfer, P., Roberts, P., Rodriguez, I., Saidi, H., Sassi, R. R., Shattock, R. & Cummins, J. J. E. Biological and Technical Variables Affecting Immunoassay Recovery of Cytokines from Human Serum and Simulated Vaginal Fluid: A Multicenter Study. *Anal. Chem.* **80**, 4741-4751 (2008).
4. Toedter, G., Hayden, K., Wagner, C. & Brodmerkel, C. Simultaneous Detection of Eight Analytes in Human Serum by Two Commercially Available Platforms for Multiplex Cytokine Analysis. *Clin. Vaccine Immunol.* **15**, 42-48 (2008).
5. Chowdhury, F., Williams, A. & Johnson, P. Validation and comparison of two multiplex technologies, Luminex and Mesoscale Discovery, for human cytokine profiling. *J. Immunol. Methods* **340**, 55-64 (2009).
6. Martin, A. F. & Nieman, T. A. Glucose quantitation using an immobilized glucose dehydrogenase enzyme reactor and a tris(2,2'-bipyridyl)ruthenium(II) chemiluminescent sensor. *Anal. Chim. Acta* **281**, 475-81 (1993).
7. Choi, H. N., Cho, S.-H., Park, Y.-J., Lee, D. W. & Lee, W.-Y. Sol-gel-immobilized Tris(2,2'-bipyridyl)ruthenium(II) electrogenerated chemiluminescence sensor for high-performance liquid chromatography. *Anal. Chim. Acta* **541**, 49-56 (2005).
8. Arora, A., Eijkel, J. C. T., Morf, W. E. & Manz, A. A Wireless Electrochemiluminescence Detector Applied to Direct and Indirect Detection for

Electrophoresis on a Microfabricated Glass Device. *Anal. Chem.* **73**, 3282-3288 (2001).

9. Lee, W.-Y. & Nieman, T. A. Evaluation of Use of Tris(2,2'-bipyridyl)ruthenium(III) as a Chemiluminescent Reagent for Quantitation in Flowing Streams. *Anal. Chem.* **67**, 1789-96 (1995).
10. Rubinstein, I., Martin, C. R. & Bard, A. J. Electrogenerated chemiluminescent determination of oxalate. *Anal. Chem.* **55**, 1580-2 (1983).
11. Downey, T. M. & Nieman, T. A. Chemiluminescence detection using regenerable tris(2,2'-bipyridyl)ruthenium(II) immobilized in Nafion. *Anal. Chem.* **64**, 261-8. (1992).
12. Noffsinger, J. B. & Danielson, N. D. Generation of chemiluminescence upon reaction of aliphatic amines with tris(2,2'-bipyridine)ruthenium(III). *Anal. Chem.* **59**, 865-8 (1987).
13. O'Connell, C. D., Juhasz, A., Kuo, C., Reeder, D. J. & Hoon, D. S. B. Detection of tyrosinase mRNA in melanoma by reverse transcription-PCR and electrochemiluminescence. *Clin. Chem.* **44**, 1161-1169 (1998).
14. Miao, W. & Bard, A. J. Electrogenerated Chemiluminescence. 80. C-Reactive Protein Determination at High Amplification with $[Ru(bpy)_3]^{2+}$-Containing Microspheres. *Anal. Chem.* **76**, 7109-7113 (2004).
15. Miao, W. & Bard, A. J. Electrogenerated Chemiluminescence. 77. DNA Hybridization Detection at High Amplification with $[Ru(bpy)_3]^{2+}$-Containing Microspheres. *Anal. Chem.* **76**, 5379-5386 (2004).
16. Vinyard, D. J., Su, S. & Richter, M. M. Electrogenerated Chemiluminescence of 9,10-Diphenylanthracene, Rubrene, and Anthracene in Fluorinated Aromatic Solvents. *J. Phys. Chem. A* **112**, 8529-8533 (2008).
17. Moret, S. & Conte, L. S. Polycyclic aromatic hydrocarbons in edible fats and oils: occurrence and analytical methods. *J. Chromatogr. A* **882**, 245-253 (2000).

18. Miao, W., Choi, J.-P. & Bard, A. J. Electrogenerated Chemiluminescence 69: The Tris(2,2'-bipyridine)ruthenium(II), ($Ru(bpy)_3^{2+}$)/Tri-n-propylamine (TPrA) System Revisited-A New Route Involving $TPrA^{\cdot+}$ Cation Radicals. *J. Am. Chem. Soc.* **124**, 14478-14485 (2002).

19. Honda, K., Yoshimura, M., Rao, T. N. & Fujishima, A. Electrogenerated Chemiluminescence of the Ruthenium Tris(2,2')bipyridyl/Amines System on a Boron-Doped Diamond Electrode. *J. Phys. Chem. B* **107**, 1653-1663 (2003).

20. Martins, T. B., Augustine, N. H. & Hill, H. R. Development of a multiplexed fluorescent immunoassay for the quantitation of antibody responses to group A streptococci. *J. Immunol. Methods* **316**, 97-106 (2006).

21. Martins, T. B., Burlingame, R., von Muehlen, C. A., Jaskowski, T. D., Litwin, C. M. & Hill, H. R. Evaluation of multiplexed fluorescent microsphere immunoassay for detection of autoantibodies to nuclear antigens. *Clin. Diagn. Lab. Immunol.* **11**, 1054-1059 (2004).

22. Martins, T. B., Pasi, B. M., Pickering, J. W., Jaskowski, T. D., Litwin, C. M. & Hill, H. R. Determination of cytokine responses using a multiplexed fluorescent microsphere immunoassay. *Am. J. Clin. Pathol.* **118**, 346-353 (2002).

23. Zajac, A., Song, D., Qian, W. & Zhukov, T. Protein microarrays and quantum dot probes for early cancer detection. *Colloids Surf., B* **58**, 309-314 (2007).

24. Pickering, J. W., Martins, T. B., Greer, R. W., Schroder, M. C., Astill, M. E., Litwin, C. M., Hildreth, S. W. & Hill, H. R. A multiplexed fluorescent microsphere immunoassay for antibodies to pneumococcal capsular polysaccharides. *Am. J. Clin. Pathol.* **117**, 589-596 (2002).

25. Dill, K., Montgomery, D. D., Ghindilis, A. L., Schwarzkopf, K. R., Ragsdale, S. R. & Oleinikov, A. V. Immunoassays based on electrochemical detection using microelectrode arrays. *Biosens. Bioelectron.* **20**, 736-742 (2004).

26. Kiernan, U. A., Nedelkov, D. & Nelson, R. W. Multiplexed Mass Spectrometric Immunoassay in Biomarker Research: A Novel Approach to the Determination of a Myocardial Infarct. *J. Proteome Res.* **5**, 2928-2934 (2006).

27. Deiss, F., La Fratta, C. N., Symer, M., Blicharz, T. M., Sojic, N. & Walt, D. R. Multiplexed Sandwich Immunoassays Using Electrochemiluminescence Imaging Resolved at the Single Bead Level. *J. Am. Chem. Soc.* **131**, 6088-6089 (2009).

28. Meso Scale Discovery, www.mesoscale.com.

29. Pittman, T. L., Thomson, B. & Miao, W. Ultrasensitive detection of TNT in soil, water, using enhanced electrogenerated chemiluminescence. *Anal. Chim. Acta* **632**, 197-202 (2009).

30. PeakFit, http://www.sigmaplot.com/products/peakfit/peakfit.php.

31. Tokel, N. E. & Bard, A. J. Electrogenerated chemiluminescence. IX. Electrochemistry and emission from systems containing tris(2,2'-bipyridine)ruthenium(II) dichloride. *J. Am. Chem. Soc.* **94**, 2862-3 (1972).

32. Lai, R. Y. & Bard, A. J. Electrogenerated Chemiluminescence. 70. The Application of ECL to Determine Electrode Potentials of Tri-n-propylamine, Its Radical Cation, and Intermediate Free Radical in MeCN/Benzene Solutions. *J. Phys. Chem. A* **107**, 3335-3340 (2003).

33. Wallace, W. L. & Bard, A. J. Electrogenerated chemiluminescence. 35. Temperature dependence of the ECL efficiency of tris(2,2'-bipyridine)rubidium(2+) in acetonitrile and evidence for very high excited state yields from electron transfer reactions. *J. Phys. Chem.* **83**, 1350-1357 (1979).

34. Maness, K. M. & Wightman, R. M. Electrochemiluminescence in low ionic strength solutions of 1,2-dimethoxyethane. *J. Electroanal. Chem.* **396**, 85-95 (1995).

35. Fleet, B., Keliher, P. N., Kirkbright, G. F. & Pickford, C. J. Analytical usefulness of electrochemiluminescence for the determination of microgram amounts of aromatic hydrocarbons. *Analyst* **94**, 847-54 (1969).

36. Forry, S. P. & Wightman, R. M. Organic ECL systems, in *Electrogenerated Chemiluminescence* (ed. Bard Allen, J.), 273-320, Chapter 6 (Marcel Dekker, Inc, New York, 2004).

37. Richter, M. M. Electrochemiluminescence (ECL). *Chem. Rev.* **104**, 3003-3036 (2004).

38. Liu, X., Shi, L., Niu, W., Li, H. & Xu, G. Environmentally friendly and highly sensitive ruthenium(II) tris(2,2'-bipyridyl) electrochemiluminescent system using 2-(dibutylamino)ethanol as co-reactant. *Angew. Chem. Int. Ed.* **46**, 421-424 (2007).

39. Wang, S., Milam, J., Ohlin, A. C., Rambaran, V. H., Clark, E., Ward, W., Seymour, L., Casey, W. H., Holder, A. A. & Miao, W. Electrochemical and Electrogenerated Chemiluminescent Studies of a Trinuclear Complex, $[((phen)_2Ru(dpp))_2RhCl_2]^{5+}$, and Its Interactions with Calf Thymus DNA. *Anal. Chem.* **81**, 4068-4075 (2009).

40. Miao, W. Electrogenerated Chemiluminescence, in *Handbook of Electrochemistry* (ed. Zoski, C. G.), 541-590, Chapter 13 (Elsevier, HR Amsterdam, 2007).

41. Ouyang, J. & Bard, A. J. Inverse photoemission spectroscopy at the platinum/acetonitrile interface with several redox couples. *J. Phys. Chem.* **91**, 4058-62 (1987).

42. Briggs, D. & Grant, J. T. (eds.) *Surface Analysis by Auger and X-ray Photoelectron Spectroscopy* (IM Publications, 2003).

CHAPTER VI

CONCLUDING REMARKS

In recent years, ECL has become a very powerful analytical technique since it is a novel approach to light generation compared to photoluminescence which requires a steady light source. Because no excitation light source is present, ECL is capable of species specific excitation with minimal background signal. However, one major disadvantage to ECL when compared to fluorescence detection is the difficulty to label each analyte with a label capable of emitting at different wavelengths, providing a multiple colorimetric assay. In ECL, $Ru(bpy)_3^2$/TPrA systems is the most sensitive system known so far. ECL detection is often limited to a few widely used $Ru(bpy)_3^{2+}$ type labels, owing to their high ECL efficiencies. Thus, efforts in investigating the ECL mechanism and influencing factors of the $Ru(bpy)_3^{2+}$/TPrA system were important. Additionally, searching for stable and efficient emitting compounds has been a continuous theme in ECL research all over the years.

The work presented in this dissertation demonstrated chloride ion has important effect on the ECL behavior of the $Ru(bpy)_3^{2+}$/ TPrA system at a Au electrode in Chapter II. The ECL was increased at relatively low Cl^- concentrations; but decreased with the further increase of the Cl^- concentration. The commonly used chloride-containing reference electrodes may have significant influence on the ECL behavior in aqueous solution. In chapter III, the ECL behavior of a new label, $[((phen)_2Ru(dpp))_2RhCl_2]^{5+}$, was investigated with DBAE and TPrA as coreactant in organic and aqueous solutions. The limit of detection of ECL intensity of the complex was 1.0 nM using TPrA as coreactant in aqueous medium. The complex could react with calf thymus DNA, which

was monitored with QCM. In Chapter IV, ECL of Qdot 625 was studied in aqueous solutions using TPrA and DBAE as ECL coreactants. The ECL behavior of the Qdot 625 was observed which was strongly dependent on the types and concentrations of ECL coreactants as well as the working electrode material. The sandwich type immunoassay using Qdot as an ECL label was utilized to detect biomolecule CRP successfully. In chapter V, the ECL behavior of $Ru(bpy)_3^{2+}$, DPA, and RUB with DBAE or TPrA as the coreactant was investigated in acetonitrile solution. The ECL maximum emissions at ~630, ~440, and ~560 nm for $Ru(bpy)_3^{2+}$, DPA, and RUB, respectively, were linearly proportional to the concentration of different ECL labels independently in mixed solutions.

In the future, three to five different kinds of sandwich-type PSB<antigen>MB or PSB-dsDNA-MB aggregates, which are modified with three-five different ECL labels and separated magnetically from the solution matrix, could be used for multiplexing of biomolecules after the generation of ECL with a suitable coreactant. These ECL labels can be either hydrophobic (e.g., DPA and RUB) or hydrophilic (e.g., different sized QDs). Also, the ECL measurements can be performed in organic (e.g., MeCN) or aqueous media. Furthermore, ECL behavior of carbon nanotube modified different sizes of QDs should be studied, because this modification may increase the conductivity of the system, hence enhance the ECL signals. Many ECL applications in sensitive biomolecules detection could be realized via the sandwich-type immunoassays described in this dissertation.